Advanced Optics and Lasers
Lecture notes
Summer Semester 2017

Prof. Dr. Roman Schmied
University of Freiburg

July 20, 2017

Contents

Administrative matters

Lecturer: Prof. Dr. Roman Schmied, roman.schmied@unibas.ch, office 402

Tutor: Dr. Aaron LaForge, aaron.laforge@physik.uni-freiburg.de, office 504

Lectures: Wednesdays 08:15 – 10:00 (HS II) and Thursdays 10:15 – 12:00 (HS I)

Tutorials: Thursdays 08:30 – 10:00 (seminar room 5th floor)

Problem sets: handed out on Wednesdays in the lecture and online; solutions to be handed in until the following Wednesday in the lecture

Studienleistung: at least 50% of the points on the problem sets required

Prüfungsleistung: at least 50% of the points on the problem sets required to be eligible for the final oral exam. The final grade will be composed of the grade for the exam (65%) and the grade for the problem sets (35%).

Recommended reading

- W. Lange, *Laserphysik*
- W. Demtröder, *Laserspektroskopie*
- J. Eichler, H. J. Eichler, Springer, *Laser*
- F. K. Kneubühl, M. W. Sigrist, *Laser*
- D. Meschede, *Optik, Licht und Laser*
- C. Rullière, Springer, *Femtosecond laser pulses*

Chapter 1

Properties of Laser Radiation

LASER: **L**ight **A**mplification by **S**timulated **E**mission of **R**adiation
Short definition: Laser = powered macroscopic oscillator for light
Main point: A laser is not just a strong lamp.
Introduction: https://en.wikipedia.org/wiki/Laser

- Excellent directionality of laser beams
  - Weak divergence: Beam diameter $\varnothing \lesssim 1\,\mathrm{cm}$ at a distance $\sim 1\,\mathrm{km}$ possible; shooting a laser beam at the moon for range finding
  - Good focusing ability: $\varnothing_{\mathrm{focus}} \sim \lambda/2$ possible
    Example: HeNe-laser ($\lambda = 632.8\,\mathrm{nm}$), power $P = 1\,\mathrm{mW} \Rightarrow$ intensity $I \sim 10^6\,\mathrm{W/cm^2} \sim 10^7 I_{\mathrm{sun\ on\ earth}}$

Figure 1.1: A laser beam can be well collimated and focused to diffraction-limited spot sizes.

This properties makes laser radiation interesting for many applications in science and industry, see Figure 1.2

- Monochromatic (see Figure 1.3): For a laser operating at $\nu_0 \approx 5 \times 10^{14}\,\mathrm{Hz}$ (yellow), a single-mode, 'continuous wave, cw' laser typically has $\Delta\nu = 1\,\mathrm{MHz}$ ($\Delta\nu < 1\,\mathrm{Hz}$ can be reached) $\Rightarrow \frac{\Delta\nu}{\nu_0} \lesssim 10^{-15}$ (Cs-atom clocks $\sim 10^{-13}$) $\rightarrow$ Application of narrow bandwidth: spectroscopy, laser cooling, metrology.
- High power, *cw*: $\gtrsim 50\,\mathrm{kW}$ (CO_2 laser), pulsed: $\gtrsim 10^{15}\,\mathrm{W}$ (*petawatt laser*, cf. nuclear power plant $\sim 10^9\,\mathrm{W}$ but continuous)
- Coherence: Phase correlation between light waves in longitudinal or transverse directions in the beam. This is the condition for interference. Speckle patterns are due to transverse coherence. $\rightarrow$ Application of coherence: Interferometry, holography, lithography.
- Ultrashort pulses (see Figure 1.7); Example: Ti-sapphire laser, $\lambda = 800\,\mathrm{nm} \Rightarrow T = 2.6 \times 10^{-15}\,\mathrm{s}$; typically $\tau \lesssim 10^{-14}\,\mathrm{s} = 10\,\mathrm{fs}$. With $c = 3 \times 10^8\,\mathrm{m/s} \Rightarrow \ell = c\tau \approx 3\,\mu\mathrm{m}$. Attosecond pulses are possible. $\rightarrow$ Application of ultrashort pulses: Short-time dynamics in atoms (electron motion), molecules (vibrations, rotations), solids (intra-, inter-band relaxation)
- Photon statistics: two-photon correlation function of a laser differs from that of a thermal source $\rightarrow$ A laser is not a collimated narrow-band lamp.

Figure 1.2: Typical applications of lasers for materials processing, medicine, data storage, remote sensing of the atmosphere, which make use of the high directionality of laser light.

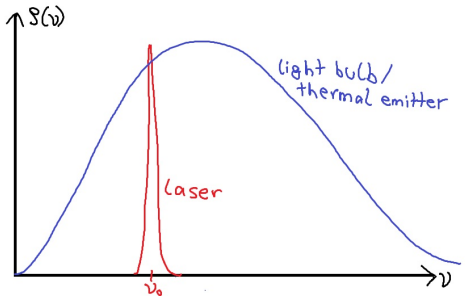

Figure 1.3: Compared to a thermal light source, a laser has a very narrow bandwidth.

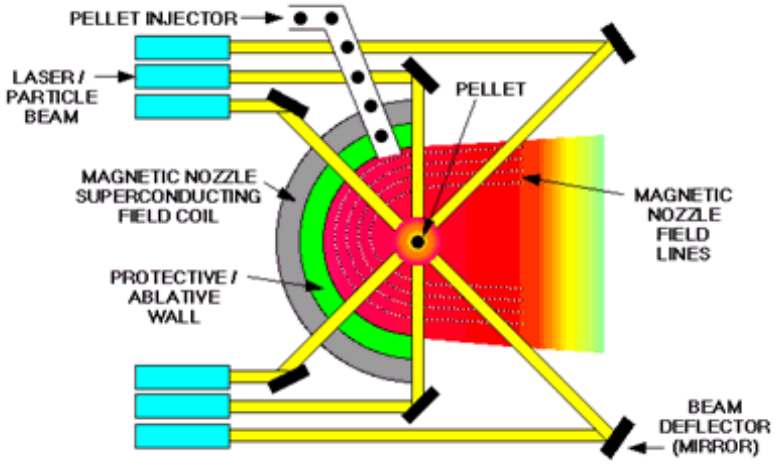

Figure 1.4: Using high-power laser pulses, even nuclear fusion reactions can be initiated.

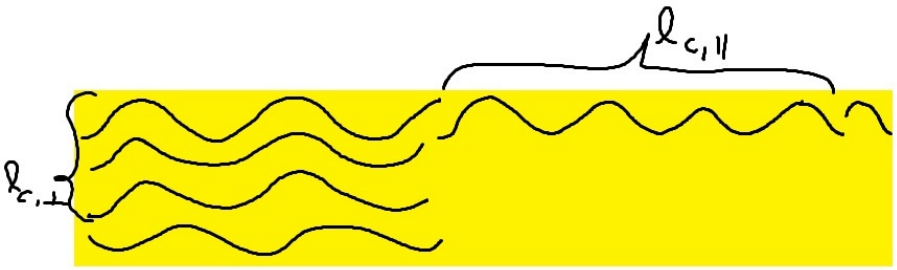

Figure 1.5: A laser beam has large coherence lengths $\ell_{c,\parallel}$ and $\ell_{c,\perp}$.

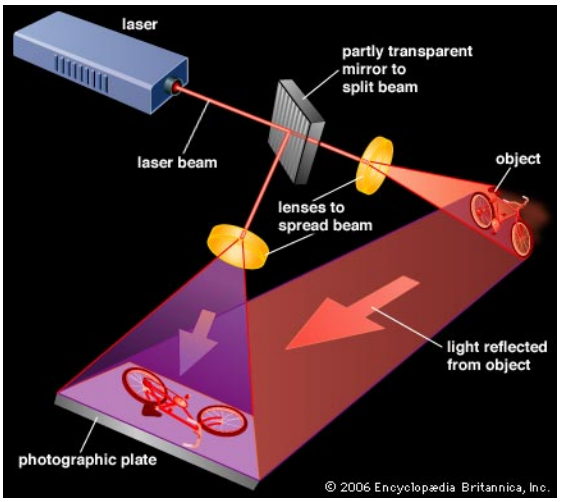

Figure 1.6: Sketch of the working principle of holography using coherence light.

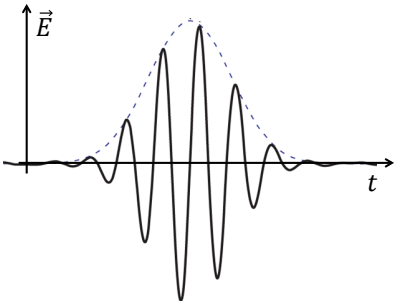

Figure 1.7: Special lasers can emit ultrashort pulses consisting of only a few optical cycles, so called *few cycle pulses*

Chapter 2

Emission & Absorption of light

Schematized atom as multi-level quantum system (see Figure 2.1). Absorption/emission transitions can take place if the resonance condition

$$\Delta E = E_2 - E_1 = h\nu \tag{2.1}$$

is met. There are three elementary processes:

a) Spontaneous emission has a rate (probability per unit time) $W_{\text{sp}} = A_{21}$ (*Einstein-A-coefficient*), $[A] = \text{s}^{-1}$

b) Absorption: $W_{\text{abs}} = B_{12} \cdot \rho$, where B_{12} is the *Einstein-B-coefficient* and $\rho(\nu)$ is the spectral energy density. $[\rho] = \text{J}/(\text{m}^3\text{Hz})$

c) Stimulated (=induced) emission: $W_{\text{stim}} = B_{21} \cdot \rho$

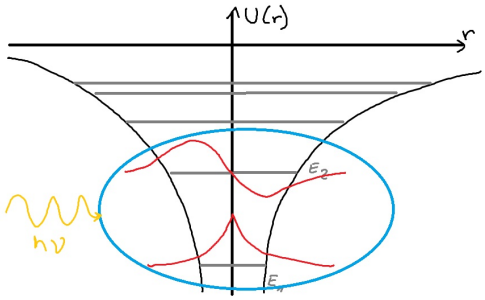

Figure 2.1: The possible energy levels of an electron in the Coulomb potential in an atom are determined by quantum mechanics. In order to understand the process of emission and absorption of light, we focus on any two energy levels (marked with the blue circle) and the transition between them.

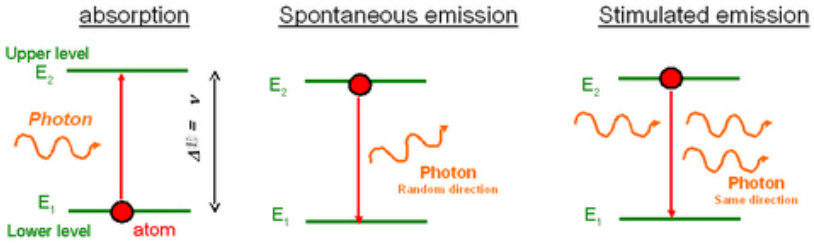

Figure 2.2: The three processes of absorption and emission

In thermodynamic equilibrium the levels are populated according to the Boltzmann distribution,

$$N_i = N \times \frac{g_i e^{-\frac{E_i}{k_B T}}}{Z} \tag{2.2}$$

where N_i is the number of atoms in level E_i, $N = \sum_i N_i$ is the total number of atoms, $Z = \sum_i g_i e^{-\frac{E_i}{k_B T}}$ is the partition function, and g_i is the statistical weight of level E_i due to degeneracy (*e.g.*, a rotational energy level i that has an angular momentum J has $g_i = 2J + 1$).

In a two-level system with levels $|1\rangle$ and $|2\rangle$, $N = N_1(t) + N_2(t)$ is constant and therefore $\dot{N}_1(t) + \dot{N}_2(t) = 0$. The transition rates are

$$\dot{N}_1\Big|_{\text{absorption}} = -B_{12} \cdot \rho \cdot N_1 \qquad \dot{N}_2\Big|_{\text{absorption}} = +B_{12} \cdot \rho \cdot N_1 \tag{2.3a}$$

$$\dot{N}_1\Big|_{\text{spont. em.}} = +A_{21} \cdot N_2 \qquad \dot{N}_2\Big|_{\text{spont. em.}} = -A_{21} \cdot N_2 \tag{2.3b}$$

$$\dot{N}_1\Big|_{\text{stim. em.}} = +B_{21} \cdot \rho \cdot N_2 \qquad \dot{N}_2\Big|_{\text{stim. em.}} = -B_{21} \cdot \rho \cdot N_2 \tag{2.3c}$$

The complete rate equations for the populations of the two levels are therefore

$$\dot{N}_1\Big|_{\text{total}} = -B_{12} \cdot \rho \cdot N_1 + A_{21} \cdot N_2 + B_{21} \cdot \rho \cdot N_2 \tag{2.4a}$$

$$\dot{N}_2\Big|_{\text{total}} = +B_{12} \cdot \rho \cdot N_1 - A_{21} \cdot N_2 - B_{21} \cdot \rho \cdot N_2 \tag{2.4b}$$

Thus, if only spontaneous emission is active ($\rho = 0$),

$$N_2(t) = N_2(0) e^{-A_{21} t}, \tag{2.5}$$

that is after time $t = \tau = 1/A_{21}$ the population in the upper level 2 has decreased by a factor of $1/e = 0.37$.

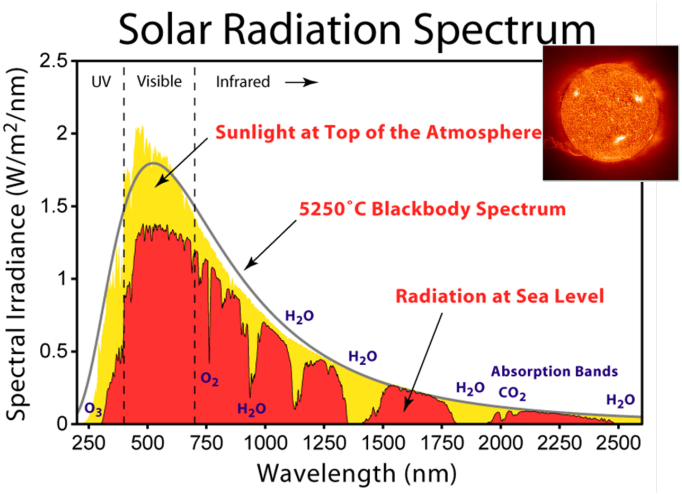

Figure 2.3: Planck's blackbody spectrum at 5250 °C (thick smooth line) in comparison with the spectrum of the sun.

In thermodynamical equilibrium we have $\dot{N}_1\Big|_{\text{total}} = \dot{N}_2\Big|_{\text{total}} = 0$:

$$-B_{12} \cdot \rho \cdot N_1 + A_{21} \cdot N_2 + B_{21} \cdot \rho \cdot N_2 = 0 \quad \Rightarrow \quad \rho = \frac{A_{21} N_2}{N_1 B_{12} - N_2 B_{21}} = \frac{\frac{A_{21}}{B_{21}}}{\frac{N_1}{N_2}\frac{B_{12}}{B_{21}} - 1}. \tag{2.6}$$

With the Boltzmann distribution of N_1 and N_2, Equation (2.2),

$$\frac{N_1}{N_2} = \frac{g_1}{g_2} e^{-(E_1 - E_2)/(k_B T)} \tag{2.7}$$

we get

$$\Rightarrow \rho = \frac{A_{21}}{B_{21}} \times \frac{1}{\frac{B_{12}}{B_{21}}\frac{g_1}{g_2} e^{\frac{E_2-E_1}{k_B T}} - 1}. \tag{2.8}$$

In addition we can use Planck's formula for the spectrum of thermal light,

$$\rho(\nu) = \frac{8\pi h\nu^3}{c^3} \times \frac{1}{e^{\frac{h\nu}{k_B T}} - 1}. \tag{2.9}$$

By comparing the two formulae and using the resonance condition $\Delta E = E_2 - E_1 = h\nu$ we obtain *Einstein's relations*

$$\boxed{B_{12} = \frac{g_2}{g_1} B_{21}} \tag{2.10}$$

and

$$\boxed{\frac{A_{21}}{B_{21}} = \frac{8\pi h\nu^3}{c^3}} \tag{2.11}$$

$\Rightarrow$ The Einstein-coefficients and rates for absorption and stimulated emission are equal (up to g_i)

$\Rightarrow$ Ratio of spontaneous vs. stimulated emission scales as $\propto \nu^3$ and $\propto \rho$, but no dependence on the properties of the transition and of the states involved.

Example: on the surface of the sun ($\nu = 5 \times 10^{14}\,\mathrm{Hz}$, $T = 5250\,^\circ\mathrm{C} = 5523\,\mathrm{K}$),

$$\Rightarrow \frac{\dot{N}_{2,\mathrm{stim}}}{\dot{N}_{2,\mathrm{sp}}} = \frac{1}{e^{\frac{h\nu}{k_B T}} - 1} \sim 0.013 \tag{2.12}$$

Stimulated emission is not important on the sun's surface: almost all the light emitted by the sun comes from spontaneous emission.

How intense must the light field be such that stimulated emission dominates?

$$\begin{aligned} |\dot{N}_{2,\mathrm{stimulated}}| &> |\dot{N}_{2,\mathrm{spontaneous}}| \\ B_{21} \cdot \rho \cdot N_2 &> A_{21} \cdot N_2 \\ \rho &> \frac{A_{21}}{B_{21}} = \frac{8\pi h\nu^3}{c^3} \end{aligned} \tag{2.13}$$

Since $\frac{8\pi h\nu^3}{c^3}$ is the energy-density of electromagnetic modes (number of modes per unit frequency, times photon energy; see Equation (2.9) and problem set 1), the number of photons per electromagnetic mode must therefore be

$$\frac{\rho}{\frac{8\pi h\nu^3}{c^3}} > 1 \tag{2.14}$$

That is, stimulated emission dominates over spontaneous emission if there is more than one photon present per electromagnetic mode. With this observation, we can interpret spontaneous emission as the emission *stimulated by the zero-point fluctuations of the electromagnetic field*. Even with zero photons present, the electromagnertic field (which is a quantum field) fluctuates with an intensity equivalent to one photon per mode. Spontaneous emission is nothing more than the emission stimulated by these "virtual" photons of the electromagnetic field's quantum noise.

Chapter 3

The Laser Principle

3.1 Laser as self-exciting oscillator

In radio frequency (RF) electronics a self-exciting oscillator consists of an amplifier, where a part of the signal from the amplifier is coupled out and another part is fed back to the amplifier via an element causing a phase shift and/or frequency filtering. In optics the analog is a laser with an active medium and a resonator. For a functional laser the following conditions have to be fulfilled:

- amplification > losses (diffraction, outcoupling, etc.)
- $\Delta\varphi \approx n \cdot 2\pi$ with $n = 0, 1, 2, \ldots \Rightarrow$ positive feedback.

For amplification by stimulated emission, the first condition requires that there is an inversion of population: there have to be more atoms in an excited state than in the ground state (per mode): $N_2/g_2 > N_1/g_1$.

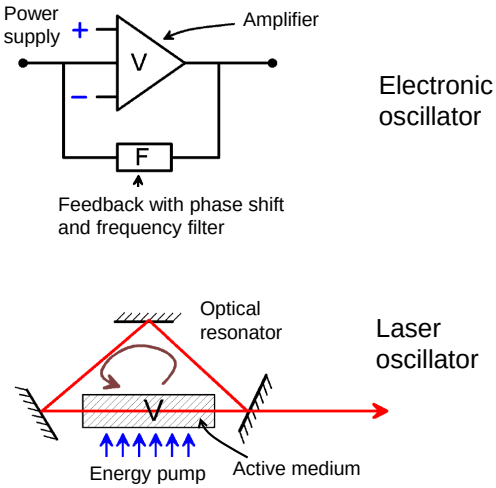

Figure 3.1: Comparison of a self-exciting RF-oscillator (top) with an optical self-exciting oscillator (*i.e.*, laser, bottom)

Toy model

Damped harmonic oscillator with negative damping. The amplitude $x(t)$ satisfies the differential equation

$$\ddot{x}(t) = -kx(t) - \gamma\dot{x}(t), \tag{3.1}$$

where k is the spring constant and γ is the damping. Assuming that $x(t = 0) = 0$ and $x'(t = 0) = v_0$, the solution is

$$x(t) = \frac{v_0}{\Omega}\sin(\Omega t)e^{-\gamma t/2} \tag{3.2}$$

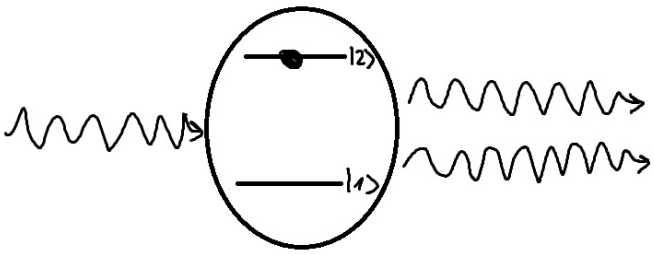

Figure 3.2: Given an atom in the excited state $|2\rangle$, an incoming photon can cause stimulated emission and therefore amplify itself (a second coherent photon is emitted)

with the effective angular frequency $\Omega = \sqrt{k - \gamma^2/4}$ (assuming weak damping: $|\gamma| < 2\sqrt{k}$).

With positive damping ($\gamma > 0$), the amplitude of the oscillation decays exponentially. With negative damping ($\gamma < 0$, anti-damping, amplification), the amplitude of the oscillation grows exponentially.

For laser operation, we need to make sure that the total damping (losses minus amplification) is negative. See Figure 3.4.

3.2 Main components of a laser

Active medium Amplification by inversion, stimulated emission

Energy pump Lamp, other laser, electrical discharge, electrical current, chemical reaction, combustion

Optical resonator Feedback, reduced photon loss

The dynamics of a laser starting to operate is shown in Figure 3.3.

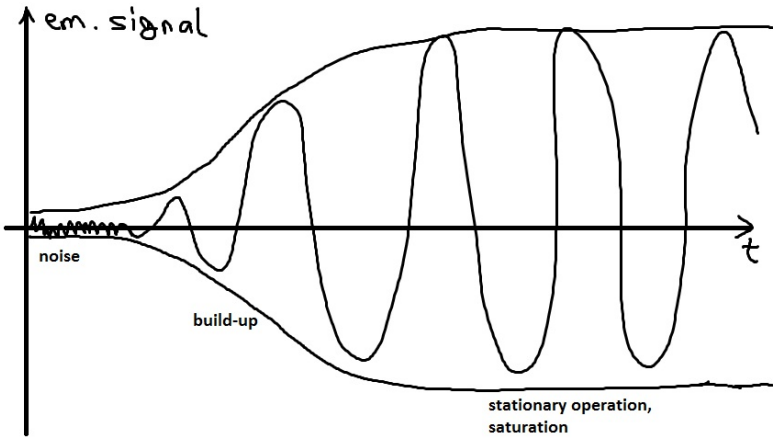

Figure 3.3: Power build-up dynamics of a self-excited oscillator. The exponential increase in the buildup phase corresponds to the toy model with negative damping, Equation (3.2). In stationary operation, the laser mode drains the inversion (losses in Equation (3.6)) until equilibrium between pump power and laser power is established.

3.3 Inversion

Let us assume that we have some process that reliably establishes populations N_1 and N_2. The laser mode shall have an effective mode volume V, an effective linewidth $\Delta\nu$, and contain a time-dependent number $N_{\text{ph}}(t)$ of photons; the spectral energy density of the laser mode is therefore $\rho(t) = \frac{N_{\text{ph}}(t)\cdot h\nu}{V\cdot\Delta\nu}$. The rate at which the number of photons in the laser mode changes is given by the absorption rate and the stimulated emission rate from Equation (2.3), minus a photon loss rate γ:

$$\begin{aligned}\dot{N}_{\text{ph}}\Big|_{\text{total}} &= -B_{12}\cdot\rho\cdot N_1 + B_{21}\cdot\rho\cdot N_2 - \gamma\cdot N_{\text{ph}} \\ &= (B_{21}\cdot N_2 - B_{12}\cdot N_1)\cdot\frac{N_{\text{ph}}\cdot h\nu}{V\cdot\Delta\nu} - \gamma\cdot N_{\text{ph}} \\ &= \left[(B_{21}\cdot N_2 - \frac{g_2}{g_1}B_{21}\cdot N_1)\cdot\frac{h\nu}{V\cdot\Delta\nu} - \gamma\right]\cdot N_{\text{ph}} \\ &= \left[\left(\frac{N_2}{g_2} - \frac{N_1}{g_1}\right)\cdot\frac{B_{21}\cdot g_2\cdot h\nu}{V\cdot\Delta\nu} - \gamma\right]\cdot N_{\text{ph}} \end{aligned} \tag{3.3}$$

The solution of this differential equation is $N_{\text{ph}}(t) = N_{\text{ph}}(0)e^{-\Gamma t}$ with the effective damping rate

$$\Gamma = \gamma - \left(\frac{N_2}{g_2} - \frac{N_1}{g_1}\right)\cdot\frac{B_{21}\cdot g_2\cdot h\nu}{V\cdot\Delta\nu}. \tag{3.4}$$

In order for the laser to generate light, this damping rate must be negative: $\Gamma < 0$, which is the case if

$$\frac{N_2}{g_2} > \frac{N_1}{g_1} + \frac{\gamma\cdot V\cdot\Delta\nu}{B_{21}\cdot g_2\cdot h\nu}. \tag{3.5}$$

This condition is called **inversion**:

$$\boxed{\frac{N_2}{g_2} > \frac{N_1}{g_1} + \text{losses}} \tag{3.6}$$

The inversion condition cannot be fulfilled in thermal equilibrium even in the absence of losses ($\gamma = 0$) since $E_2 > E_1$ (see Equation (2.2)):

$$\frac{N_2/g_2}{N_1/g_1} = e^{-\frac{E_2-E_1}{k_{\text{B}}t}} < 1 \qquad \Rightarrow \qquad \frac{N_2}{g_2} < \frac{N_1}{g_1}. \tag{3.7}$$

Conclusion: a two-level laser cannot operate in thermal equilibrium.

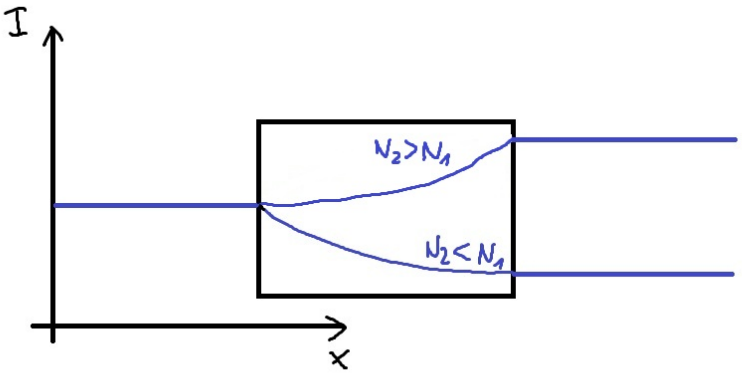

Figure 3.4: Amplification vs. damping of light intensity when propagating through the laser medium (assuming $g_1 = g_2$ for simplicity).

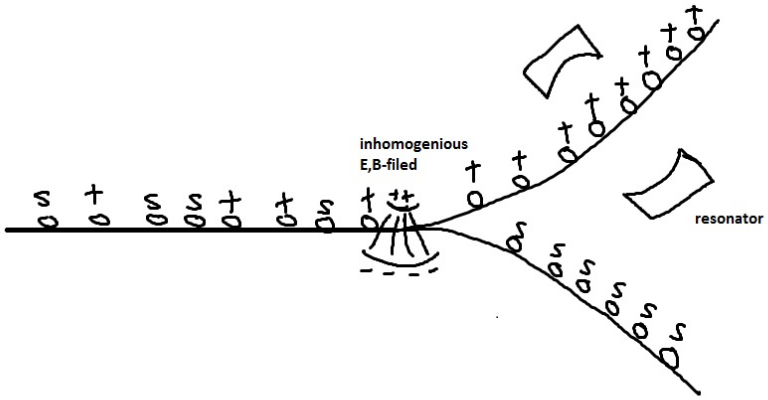

Figure 3.5: Separation of singlet and triplet state by an inhomogeneous magnetic field

Example: At $T = 300\,\mathrm{K}$ we look at the microwave transition of H ($\rightarrow$ maser). Due to the hyperfine structure the $1^2S_{1/2}$ electronic groundstate is split in two states: $F = 1$ (parallel spins of electron and proton; $g_2 = 3$) and $F = 0$ (anti-parallel spins; $g_1 = 1$), where the energy gap $E_2 - E_1$ between these states is responsible for the 21 cm-line ($\nu = 1.42\,\mathrm{GHz}$). In this system, we find that $\frac{N_2/g_2}{N_1/g_1} = 0.93$: the populations are almost equal, but not inversion. However, a hydrogen maser can be realized as shown in Figure 3.5 by spatially separating the beam into the two spin components.

The upper state $F = 1$ has a lifetime $\tau(|1\rangle) \approx 1\,\mathrm{s} \Rightarrow \delta\omega \approx 1\,\mathrm{Hz}$. $\Rightarrow$ good for frequency calibration with $\sim 10^{-9}$ precision, H-masers are used as a cheap alternative to Cs atomic clocks as a frequency standard.

3.3.1 Pumping in a two-level system

Can we establish inversion with an optical process that pumps atoms from $|1\rangle$ to $|2\rangle$ until $N_2/g_2 > N_1/g_1$? Assuming a constant spectral density ρ_{pump} of the pump field, the rate equations for the populations (see Equation (2.4)) in equilibrium, assuming no laser action ($N_{\mathrm{ph}} = 0$),

$$\dot{N}_1\Big|_{\mathrm{total}} = -B_{12} \cdot \rho_{\mathrm{pump}} \cdot N_1 + A_{21} \cdot N_2 + B_{21} \cdot \rho_{\mathrm{pump}} \cdot N_2 = 0 \tag{3.8a}$$

$$\dot{N}_2\Big|_{\mathrm{total}} = +B_{12} \cdot \rho_{\mathrm{pump}} \cdot N_1 - A_{21} \cdot N_2 - B_{21} \cdot \rho_{\mathrm{pump}} \cdot N_2 = 0 \tag{3.8b}$$

with the solution (assuming $N_1 + N_2 = N$)

$$N_1 = N \cdot \frac{1 + \frac{B_{21}}{A_{21}}\rho_{\mathrm{pump}}}{1 + \frac{B_{21}+B_{12}}{A_{21}}\rho_{\mathrm{pump}}} \overset{\rho_{\mathrm{pump}}\to\infty}{\longrightarrow} \frac{B_{21}}{B_{21} + B_{12}} = \frac{g_1}{g_1 + g_2} \tag{3.9a}$$

$$N_2 = N - N_1 \overset{\rho_{\mathrm{pump}}\to\infty}{\longrightarrow} \frac{B_{12}}{B_{21} + B_{12}} = \frac{g_2}{g_1 + g_2} \tag{3.9b}$$

For any finite pumping rate we have $\frac{N_2}{g_2} < \frac{N_1}{g_1}$; only in the limit of infinite pumping rate $\rho_{\mathrm{pump}} \to \infty$ we find $\frac{N_2}{g_2} = \frac{N_1}{g_1}$. There is no pumping rate for which inversion ($\frac{N_2}{g_2} > \frac{N_1}{g_1}$) is established.

3.4 3-level laser

Idea:

"Trap" population in state $|2\rangle$ by uncoupling the $|1\rangle \leftrightarrow |2\rangle$ transition from the pump process. In this way, stimulated transitions out of $|2\rangle$ (Equation (3.8)b) are avoided. This is achieved by populating $|2\rangle$ via an additional level $|3\rangle$ by means of a fast, irreversible relaxation process.

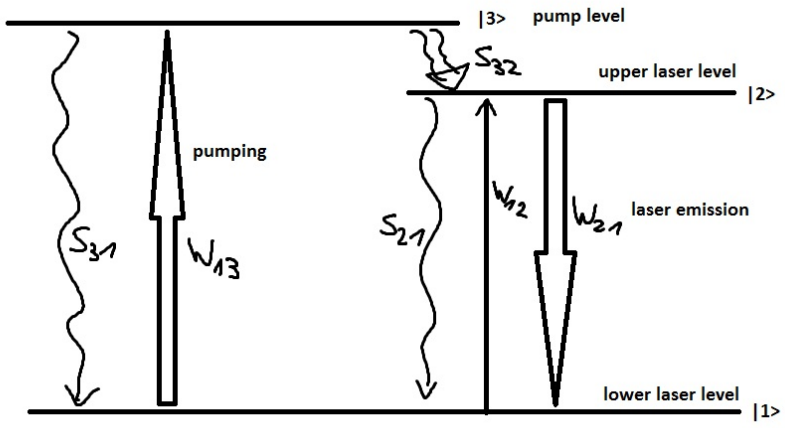

Figure 3.6: Working scheme of a 3-level laser

Wanted:

- $S_{32} \gg S_{31}$: Efficient decay into $|2\rangle$, faster than stimulated emission back into $|1\rangle$
- $S_{32} \gg S_{21}$: Efficient build-up of inversion in $|2\rangle$
- $W_{13} \gg S_{21}$: fast pumping such that $\frac{N_1}{N_2+N_3} < 50\%$

$\Rightarrow$ strong pumping is required, which is a disadvantage.

In free atoms 3-level lasers are hardly possible since if $|1\rangle \rightarrow |3\rangle$ and $|3\rangle \rightarrow |2\rangle$ are allowed, then $|2\rangle \rightarrow |1\rangle$ is forbidden due to selection rules.

$\Rightarrow$ selection rules do not hold strictly in crystals, liquids, ..., *e.g.*, ruby laser (first laser, Th. Maiman, 1960). The ruby laser is based on Al_2O_3 doped with $\leqslant 0.1\%$ Cr^+.

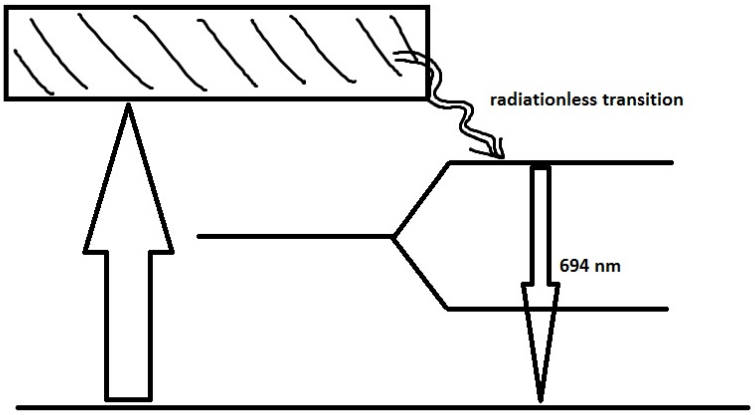

Figure 3.7: Scheme of a ruby laser. The pump level $|3\rangle$ is a broad band of overlapping levels.

3.5 4-level laser

For a 4-level laser as shown in Figure 3.8 we want the following properties:

- $S_{32} \gg S_{30}$: Fast transition into $|2\rangle$ to avoid stimulated emission from the pump ($|3\rangle \rightarrow |0\rangle$)

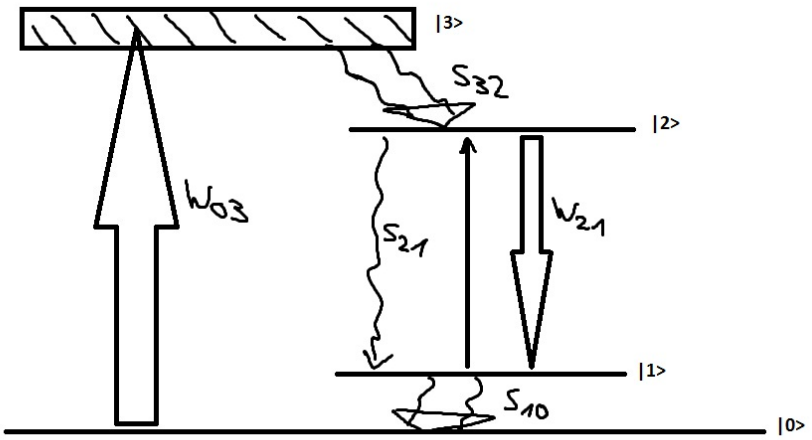

Figure 3.8: 4-level laser scheme

- $S_{10} \gg S_{21}$: Fast depletion of $|1\rangle$ to avoid re-absorption of laser photons ($|1\rangle \rightarrow |2\rangle$)
- Condition: $E_1 - E_0 \gg k_B T$ to avoid thermal buildup of population in $|1\rangle$

$\Rightarrow$ Inversion even if $W_{03} < S_{21}$
$\Rightarrow$ Only a small part of population must be in $|2\rangle$ to fulfill Equation (3.6) For stationary operation the condition

$$S_{10} > S_{21} + W_{21} \tag{3.10}$$

must be fulfilled.

Almost all lasers are 4-level lasers.

3.6 Rate equations

$\rightarrow$ Simplified, but quantitative description of laser activity:

Assumptions:

- Only one mode contributes to the laser activity (all photons have $h\nu$). Only average energy density $\bar{\rho}$ is considered. The total photon density (photons per unit volume) is

$$p = \frac{1}{h\nu} \int \rho(\nu')\mathrm{d}\nu' = \frac{\bar{\rho} \cdot \Delta\nu}{h\nu} \tag{3.11}$$

  with $\Delta\nu$ the laser line width.
- Only one polarization
- Neglect spatial mode structure (see chapter 7)
- The active medium is represented by the population densities n_i (atoms per unit volume)

3.6.1 3-level system

see Figure 3.6. General rate equations for the three levels:

$$\dot{n}_1 = -W_{12} \cdot n_1 - W_{13} \cdot n_1 + W_{21} \cdot n_2 + W_{31} \cdot n_3 + S_{21} \cdot n_2 + S_{31} \cdot n_3 \tag{3.12a}$$
$$\dot{n}_2 = -W_{21} \cdot n_2 - W_{23} \cdot n_2 + W_{12} \cdot n_1 + W_{32} \cdot n_3 + S_{32} \cdot n_3 - S_{21} \cdot n_2 \tag{3.12b}$$
$$\dot{n}_3 = -W_{31} \cdot n_3 - W_{32} \cdot n_3 + W_{13} \cdot n_1 + W_{23} \cdot n_2 - S_{31} \cdot n_3 - S_{32} \cdot n_3 \tag{3.12c}$$

with $n_1 + n_2 + n_3 = n$. Absorption and stimulated emission rates are related to the corresponding photon density: $W_{ij} = B_{ij} h\nu p_{ij} = \sigma_{ij} \cdot c \cdot p_{ij}$ where σ_{ij} is the cross section for the process. We assume that $p_{13} = p_{31} = p_{\text{pump}}$, $p_{23} = p_{32} = 0$ (non-radiative decay), and $p_{12} = p_{21} = p_{\text{laser}}$.

Optical spontaneous emission rates are $S_{ij} = A_{ij}$; but S_{32} is non-radiative.

With these substitutions, the rate equations for the levels are

$$\dot{n}_1 = -(\sigma_{12} p_{\text{laser}} + \sigma_{13} p_{\text{pump}}) \cdot c \cdot n_1 + \sigma_{21} p_{\text{laser}} \cdot c \cdot n_2 + \sigma_{31} p_{\text{pump}} \cdot c \cdot n_3 + S_{21} \cdot n_2 + S_{31} \cdot n_3 \quad (3.13)\text{a}$$

$$\dot{n}_2 = -\sigma_{21} p_{\text{laser}} \cdot c \cdot n_2 + \sigma_{12} p_{\text{laser}} \cdot c \cdot n_1 + S_{32} \cdot n_3 - S_{21} \cdot n_2 \quad (3.13)\text{b}$$

$$\dot{n}_3 = -\sigma_{31} p_{\text{pump}} \cdot c \cdot n_3 + \sigma_{13} p_{\text{pump}} \cdot c \cdot n_1 - S_{31} \cdot n_3 - S_{32} \cdot n_3 \quad (3.13)\text{c}$$

To solve these coupled differential equations, we make two simplifying assumptions:

1. We assume that the level dynamics are very fast compared to the photon dynamics (see below), so that the level populations are always in equilibrium: $\dot{n}_1 = \dot{n}_2 = \dot{n}_3 = 0$. This allows us to solve Equation (3.13) for n_1, n_2, and n_3 as functions of p_{pump} and p_{laser}; the level populations follow the slower photon populations adiabatically. These functions are rather complicated.

2. We assume that $S_{32} \to \infty$, that is, a very fast non-radiative decay of the excited state. This assumption simplifies the steady-state populations to

$$n_1 = n \cdot \frac{c p_{\text{laser}} \sigma_{21} + S_{21}}{c p_{\text{laser}} (\sigma_{12} + \sigma_{21}) + c p_{\text{pump}} \sigma_{13} + S_{21}} \quad (3.14)\text{a}$$

$$n_2 = n \cdot \frac{c p_{\text{laser}} \sigma_{12} + c p_{\text{pump}} \sigma_{13}}{c p_{\text{laser}} (\sigma_{12} + \sigma_{21}) + c p_{\text{pump}} \sigma_{13} + S_{21}} \quad (3.14)\text{b}$$

$$n_3 = 0 \quad (3.14)\text{c}$$

See below for a brief discussion of the branching ratio in the case of a finite S_{32}.

We define the inversion as $I = n_2 - n_1$, in terms of which we have $n_1 = (n - I)/2$ and $n_2 = (n + I)/2$. At equilibrium,

$$I = n \cdot \frac{c p_{\text{laser}} (\sigma_{12} - \sigma_{21}) + c p_{\text{pump}} \sigma_{13} - S_{21}}{c p_{\text{laser}} (\sigma_{12} + \sigma_{21}) + c p_{\text{pump}} \sigma_{13} + S_{21}} \quad (3.15)$$

The rate equation for the laser photon number is, from Equation (3.13)b,

$$\dot{p}_{\text{laser}} = (\sigma_{21} n_2 - \sigma_{12} n_1) c p_{\text{laser}} - \gamma p_{\text{laser}} = -\Gamma p_{\text{laser}} \quad (3.16)$$

similar to Equation (3.3), with the effective damping

$$\Gamma = \gamma - (\sigma_{21} - \sigma_{12}) \frac{nc}{2} - (\sigma_{21} + \sigma_{12}) \frac{Ic}{2}. \quad (3.17)$$

γ summarizes the total photon losses (see section 3.7); we call $\tau_{\text{ph}} = 1/\gamma$ the *photon lifetime* in the cavity.

There are two steady-state solutions ($\dot{p}_{\text{laser}} = 0$) for Equation (3.16):

1. $p_{\text{laser}}(t) = 0$ is always a solution, independently of the pump intensity p_{pump};

2. $I = I_{\text{th}}$: if the inversion is equal to the threshold inversion

$$I_{\text{th}} = n \cdot \frac{\sigma_{12} - \sigma_{21}}{\sigma_{12} + \sigma_{21}} + \frac{2\gamma}{c(\sigma_{12} + \sigma_{21})} \quad (3.18)$$

then the system is in a steady state and the effective damping vanishes ($\Gamma = 0$). Solving $I = I_{\text{th}}$ with Equation (3.15) for the equilibrium laser photon density, we find

$$p_{\text{laser}} = p_{\text{pump}} \times \frac{\sigma_{13}(cn\sigma_{21} - \gamma)}{\gamma(\sigma_{12} + \sigma_{21})} - \frac{S_{21}(cn\sigma_{12} + \gamma)}{c\gamma(\sigma_{12} + \sigma_{21})} \quad (3.19)$$

Physically this situation can only occur when $p_{\text{laser}} > 0$, which means that a pump power larger than the *threshold pump power*

$$p_{\text{pump}} > p_{\text{th}} = \frac{S_{21}(cn\sigma_{12} + \gamma)}{c\sigma_{13}(cn\sigma_{21} - \gamma)} \quad (3.20)$$

is required.

We can therefore distinguish the following regimes of the laser:

below threshold: For $p_{\text{pump}} < p_{\text{th}}$, only the solution $p_{\text{laser}}(t) = 0$ is stable. The inversion is

$$I = n \cdot \frac{c p_{\text{pump}} \sigma_{13} - S_{21}}{c p_{\text{pump}} \sigma_{13} + S_{21}} \tag{3.21}$$

and grows with the pump power.

above threshold: For $p_{\text{pump}} > p_{\text{th}}$, the physically relevant (stable) solution is Equation (3.19), which we can write as

$$p_{\text{laser}} = n \cdot \frac{S_{21}}{\gamma} \cdot \frac{p_{\text{pump}} - p_{\text{th}}}{p_{\text{sat}}} \tag{3.22}$$

with the saturation photon density

$$p_{\text{sat}} = \frac{n S_{21}(\sigma_{12} + \sigma_{21})}{\sigma_{13}(nc\sigma_{21} - \gamma)}. \tag{3.23}$$

The inversion is pegged at $I = I_{\text{th}}$.

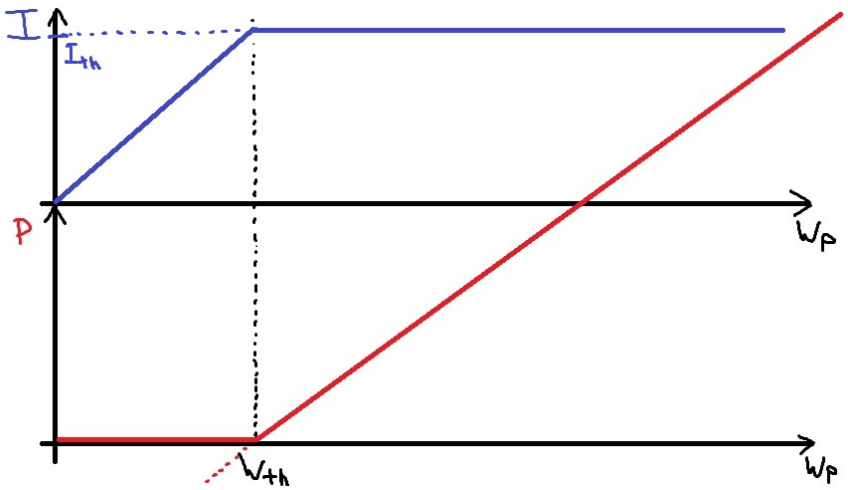

Figure 3.9: Inversion I and photon density p in a cw laser as functions of W_{pulse}

Figure 3.9 shows these steady-state regimes schematically.

instantaneous gain

For a time-dependent study of the differential Equation (3.13), assume that the laser power p_{laser} differs from the steady-state solution Equation (3.22). The instantaneous inversion is given by Equation (3.15), which allows us to evaluate the instantaneous effective damping of Equation (3.17):

$$\begin{aligned}\Gamma &= \gamma - (\sigma_{21} - \sigma_{12})\frac{nc}{2} - (\sigma_{21} + \sigma_{12})\frac{c}{2}\left[n \cdot \frac{c p_{\text{laser}}(\sigma_{12} - \sigma_{21}) + c p_{\text{pump}} \sigma_{13} - S_{21}}{c p_{\text{laser}}(\sigma_{12} + \sigma_{21}) + c p_{\text{pump}} \sigma_{13} + S_{21}}\right] \\ &= \gamma - n \cdot c \cdot \frac{c\sigma_{13}\sigma_{21} p_{\text{pump}} - S_{21}\sigma_{12}}{c p_{\text{laser}}(\sigma_{12} + \sigma_{21}) + c p_{\text{pump}} \sigma_{13} + S_{21}}\end{aligned} \tag{3.24}$$

We see that the instantaneous gain $g = -\Gamma$ is largest for $p_{\text{laser}} = 0$ and decreases to zero as p_{laser} reaches the equilibrium value given in Equation (3.22). The resulting non-linear dynamics for $p_{\text{laser}}(t)$ is quite complex.

For very large pump intensities $p_{\text{pump}} \to \infty$, the instantaneous damping rate is

$$\Gamma_\infty = \lim_{p_{\text{pump}} \to \infty} \Gamma = \gamma - cn\sigma_{21} = \gamma - g_0 \tag{3.25}$$

independent of the laser photon density p_{laser}; we have defined $g_0 = cn\sigma_{21}$ as the *asymptotic gain* of the laser (the maximum possible rate of laser photon gain in the active medium, assuming full inversion). As a result, for very large pump intensities the laser build-up proceeds exponentially, $p_{\text{laser}}(t) = p_{\text{laser}}(0)e^{-\Gamma_\infty t}$ with $\Gamma_\infty < 0$.

For finite pump intensities $p_{\text{pump}} > p_{\text{th}}$, the small-signal damping rate for $p_{\text{laser}} \approx 0$ is

$$\Gamma_0 = \gamma - n \cdot c \cdot \frac{c\sigma_{13}\sigma_{21}p_{\text{pump}} - S_{21}\sigma_{12}}{cp_{\text{pump}}\sigma_{13} + S_{21}} = \Gamma_\infty \cdot \left(1 - \frac{1}{1 + \frac{p_{\text{pump}} - p_{\text{th}}}{p_{\text{sat}}}}\right) \tag{3.26}$$

Equation (3.26) still leads to exponential amplification $e^{-\Gamma_0 t}$ of small light fields, for example in the beginning of the laser build-up process.

$$\begin{aligned}
p_{\text{pump}} &= p_{\text{th}} && \Rightarrow \Gamma_0 = 0 \\
p_{\text{pump}} &= p_{\text{th}} + p_{\text{sat}} && \Rightarrow \Gamma_0 = \frac{1}{2}\Gamma_\infty \\
p_{\text{pump}} &= p_{\text{th}} + 2p_{\text{sat}} && \Rightarrow \Gamma_0 = \frac{2}{3}\Gamma_\infty \\
p_{\text{pump}} &\to \infty && \Rightarrow \Gamma_0 = \Gamma_\infty
\end{aligned} \tag{3.27}$$

branching ratio

More generally, S_{32} is finite (but large) and the above limits apply only approximately. In particular, we call the *branching ratio* the probability that atoms excited into $|3\rangle$ decay non-radiatively into $|2\rangle$,

$$\eta = \frac{S_{32}}{S_{31} + S_{32} + W_{31} + W_{32}} = \frac{S_{32}}{S_{31} + S_{32} + \sigma_{31}cp_{\text{pump}}}. \tag{3.28}$$

For $S_{32} \mapsto \infty$ this branching ratio becomes 1, *i.e.*, all atoms decay non-radiatively from $|3\rangle$ to $|2\rangle$. The assumption $\eta \approx 1$ can be relaxed in a more detailed discussion.

3.6.2 4-level system

For the 4-level system, an additional level $|0\rangle$ drains the population from $|1\rangle$ non-radiatively, such that $n_1 \approx 0$ at all times, and σ_{12} can be neglected (no re-absorption of laser light).

See Figure 3.8: the general rate equations for the level populations are, similiar to Equation (3.12),

$$\dot{n}_i = -\sum_{j\neq i} W_{ij}n_i + \sum_{j\neq i} W_{ji}n_j - \sum_{j<i} S_{ij}n_i + \sum_{j>i} S_{ji}n_j \tag{3.29a}$$

$$\sum_i n_i = n \tag{3.29b}$$

with $i, j \in \{1, 2, 3, 4\}$. Within the adiabatic approximation $\dot{n}_1 = \dot{n}_2 = \dot{n}_3 = \dot{n}_4 = 0$ and assuming again $S_{32} \to \infty$ and $S_{10} \to \infty$, the equilibrium populations are

$$n_0 = n \cdot \frac{cp_{\text{laser}}\sigma_{21} + S_{21}}{cp_{\text{laser}}\sigma_{21} + cp_{\text{pump}}\sigma_{03} + S_{21}} \tag{3.30a}$$

$$n_1 = 0 \tag{3.30b}$$

$$n_2 = n \cdot \frac{cp_{\text{pump}}\sigma_{03}}{cp_{\text{laser}}\sigma_{21} + cp_{\text{pump}}\sigma_{03} + S_{21}} \tag{3.30c}$$

$$n_3 = 0 \tag{3.30d}$$

Comparing this solution to Equation (3.14), we see that the expressions for the three-level laser (subsection 3.6.1) remain valid for four-level lasers if we make the following substitutions:

	3-level laser	4-level laser
reservoir population	n_1	n_0
pump cross section	σ_{13}	σ_{03}
effective laser re-absorption cross section	σ_{12}	0

The inversion in the four-level laser is always positive,

$$I = n_2 - n_1 = n_2 \tag{3.31}$$

The pump threshold of Equation (3.20) becomes

$$p_{\text{pump}} > p_{\text{th}} = \frac{S_{21}\gamma}{c\sigma_{03}(cn\sigma_{21} - \gamma)}, \tag{3.32}$$

which tends to be much lower that the threshold in three-level lasers. Notably it goes to zero in the absence of losses ($\gamma \to 0$), which is not the case for the three-level laser. This behavior is what makes four-level laser an attractive option for building real lasers.

3.7 Output power of a laser

p_{pump}, p_{laser}, and I are not directly accessible in experiments → connection with output power and pump power.

The laser-mode energy inside the resonator is given by

$$E_{\text{laser}} = p_{\text{laser}} \cdot h\nu_{21} \cdot V \tag{3.33}$$

where V is the resonator volume.

The photon losses in the laser photon rate Equation (3.16) are $\gamma = \gamma_{\text{out}} + \gamma_{\text{loss}}$, where

- $\gamma_{\text{out}} = T/\tau_{\text{rt}}$ is the rate of power loss through the output coupling mirror; T is the transmittance of the output coupler and τ_{rt} is the round-trip time of the laser resonator, often $\tau_{\text{rt}} = 2d/c$ for a resonator length d
- γ_{loss} are unwanted 'bad' losses: scattering, absorption (other that W_{12}), diffraction at optical elements, spontaneous emission, etc.

We want to minimize γ_{loss} and optimize γ_{out}.

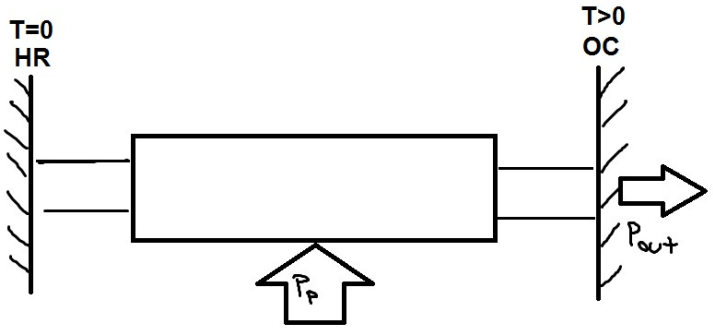

Figure 3.10: A laser with one highly reflecting mirror (HR) and one output coupling mirror (OC) with $T > 0$.

Since Equation (3.16) describes a total laser photon loss rate $\dot{p}_{\text{loss}} = \gamma \cdot p_{\text{laser}}$, the total laser power energy rate loss is $\dot{E}_{\text{loss}} = \gamma \cdot p_{\text{laser}} \cdot h\nu_{21} \cdot V$ (see Equation (3.33)). The fraction of this energy loss that goes into laser output power is $\gamma_{\text{out}}/(\gamma_{\text{out}} + \gamma_{\text{loss}}) = \gamma_{\text{out}}/\gamma$, and hence the output power of the laser is

$$P_{\text{out}} = \frac{\gamma_{\text{out}}}{\gamma}\dot{E}_{\text{loss}} = \gamma_{\text{out}} \cdot p_{\text{laser}} \cdot h\nu_{21} \cdot V. \tag{3.34}$$

Inserting the steady-state solution of Equation (3.22) gives

$$P_{\text{out}} = \frac{\gamma_{\text{out}}}{\gamma} \cdot n \cdot S_{21} \cdot \frac{p_{\text{pump}} - p_{\text{th}}}{p_{\text{sat}}} \cdot h\nu_{21} \cdot V. \tag{3.35}$$

The pump power P_{pump} is assumed to traverse the entire gain medium. We assume that the gain medium has an area A and a length ℓ (and thus a volume $V = A \cdot \ell$). The number of photons entering the gain medium per unit time is $\mathrm{d}N_{\text{pump}}/\mathrm{d}t = P_{\text{pump}}/(h\nu_{\text{pump}})$. These phonons remain within the gain medium for a time $\Delta t_{\text{pump}} = \ell/c$, so that at any given moment there are $N_{\text{pump}} = \Delta t_{\text{pump}} \cdot \mathrm{d}N_{\text{pump}}/\mathrm{d}t = P_{\text{pump}} \cdot \frac{\ell}{ch\nu_{\text{pump}}}$ pump-beam photons within the gain medium. The density of pump photons is therefore

$$p_{\text{pump}} = \frac{N_{\text{pump}}}{V} = P_{\text{pump}} \cdot \frac{1}{ch\nu_{\text{pump}}A}. \tag{3.36}$$

The narrower we focus the pump beam, the smaller A (the effective pump beam area) becomes and the larger the density of pump photons.

With the analogous definitions

$$\begin{aligned} p_{\text{th}} &= P_{\text{th}} \cdot \frac{1}{ch\nu_{\text{pump}}A} & p_{\text{sat}} &= P_{\text{sat}} \cdot \frac{1}{ch\nu_{\text{pump}}A} \\ \Rightarrow P_{\text{th}} &= A \cdot h\nu_{\text{pump}} \cdot \frac{S_{21}}{\sigma_{13}} \cdot \frac{\sigma_{12} + \frac{\gamma}{nc}}{\sigma_{21} - \frac{\gamma}{nc}} & \Rightarrow P_{\text{sat}} &= A \cdot h\nu_{\text{pump}} \cdot \frac{S_{21}}{\sigma_{13}} \cdot \frac{\sigma_{12} + \sigma_{21}}{\sigma_{21} - \frac{\gamma}{nc}} \end{aligned} \tag{3.37}$$

Equation (3.35) becomes

$$\begin{aligned} P_{\text{out}} &= \frac{\gamma_{\text{out}}}{\gamma} \cdot n \cdot S_{21} \cdot \frac{P_{\text{pump}} - P_{\text{th}}}{P_{\text{sat}}} \cdot h\nu_{21} \cdot V \\ &= \sigma_{\text{s}} \cdot (P_{\text{pump}} - P_{\text{th}}). \end{aligned} \tag{3.38}$$

σ_{s} is called the *slope efficiency* (Figure 3.11):

$$\begin{aligned} \sigma_{\text{s}} &= \frac{\gamma_{\text{out}}}{\gamma} \cdot n \cdot S_{21} \cdot \frac{h\nu_{21} \cdot V}{A \cdot h\nu_{\text{pump}} \cdot \frac{S_{21}}{\sigma_{13}} \cdot \frac{\sigma_{12}+\sigma_{21}}{\sigma_{21}-\frac{\gamma}{nc}}} \\ &= \underbrace{n\ell\sigma_{13}}_{\text{pump absorption probability}} \cdot \underbrace{\frac{h\nu_{\text{laser}}}{h\nu_{\text{pump}}}}_{\text{quantum efficiency}} \cdot \underbrace{\frac{\sigma_{21}}{\sigma_{21}+\sigma_{12}}}_{\text{laser re-absorption loss}} \cdot \underbrace{\underbrace{\frac{\gamma_{\text{out}}}{\gamma_{\text{out}}+\gamma_{\text{loss}}}}_{\text{branching ratio}} \cdot \underbrace{\left(1 - \frac{\gamma_{\text{out}}+\gamma_{\text{loss}}}{g_0}\right)}_{\text{effective amplification}}}_{\text{outcoupling efficiency } \eta_K} \end{aligned} \tag{3.39}$$

where we have substituted $\gamma = \gamma_{\text{out}} + \gamma_{\text{loss}}$ and $\nu_{21} = \nu_{\text{laser}}$, and recall the definition of the asymptotic gain $g_0 = cn\sigma_{21}$ (see Equation (3.25)).

- the pump absorption probability $n\ell\sigma_{13}$ specifies the probability that a pump photon is absorbed in the gain medium instead of passing through unabsorbed
- the quantum efficiency $\nu_{\text{laser}}/\nu_{\text{pump}}$ specifies what fraction of the energy of a pump photon ends up in a laser photon (the rest is dissipated non-radiatively through S_{32})
- the re-absorption factor $\sigma_{21}/(\sigma_{21} + \sigma_{12})$ describes the importance of laser-light re-absorption (via σ_{12}) in equilibrium; in the four-level laser, this factor is 1 since there is no re-absorption
- the branching ratio $\frac{\gamma_{\text{out}}}{\gamma_{\text{out}}+\gamma_{\text{loss}}}$ specifies the fraction of the lost laser-mode photons that end up in the laser beam instead of being absorbed or scattered into other directions

How should we choose the transmittivity T of the output coupler? We know that there is no laser output for both $T = 0$ (the output coupler lets no light pass through) and $T = 1$ (too much loss → sub-threshold); the maximum laser output power must be somewhere in-between.

We first express the γ_{out}-dependent part η_K of the slope efficiency (*i.e.*, the outcoupling efficiency) in terms of the output coupler transmissivity T,

$$\eta_K = \frac{\gamma_{\text{out}}}{\gamma_{\text{out}} + \gamma_{\text{loss}}} \cdot \left(1 - \frac{\gamma_{\text{out}} + \gamma_{\text{loss}}}{g_0}\right) = \frac{T/\tau_{\text{rt}}}{T/\tau_{\text{rt}} + \gamma_{\text{loss}}} \cdot \left(1 - \frac{T/\tau_{\text{rt}} + \gamma_{\text{loss}}}{g_0}\right) = \frac{T}{T+L} \cdot \left(1 - \frac{T+L}{G_0}\right) \tag{3.40}$$

where $L = \gamma_{\text{loss}}\tau_{\text{rt}}$ is the *round-trip loss* and $G_0 = g_0\tau_{\text{rt}}$ is the *round-trip gain* of the laser resonator. We maximize this η_K with respect to T:

$$\frac{\mathrm{d}\eta_K}{\mathrm{d}T} = 0 \qquad \Rightarrow T_{\text{opt}} = \sqrt{G_0 L} - L \tag{3.41}$$

(This is only valid if $0 < L < G_0$ so that the system operates as a laser: more gain than losses). The maximized slope efficiency is (setting $T = T_{\text{opt}}$ in Equation (3.39))

$$\eta_{K,\text{opt}} = 1 + \frac{L}{G_0} - 2\sqrt{\frac{L}{G_0}} = 1 + \frac{\gamma_{\text{loss}}}{g_0} - 2\sqrt{\frac{\gamma_{\text{loss}}}{g_0}} \tag{3.42}$$

In the limit of small losses $L \ll G_0$, the maximized slope efficiency transmission factor is

$$\eta_{K,\text{opt}} \approx 1 - 2\sqrt{\frac{L}{G_0}} \tag{3.43}$$

reached for an output coupler with transmissivity

$$T_{\text{opt}} \approx \sqrt{G_0 L} \tag{3.44}$$

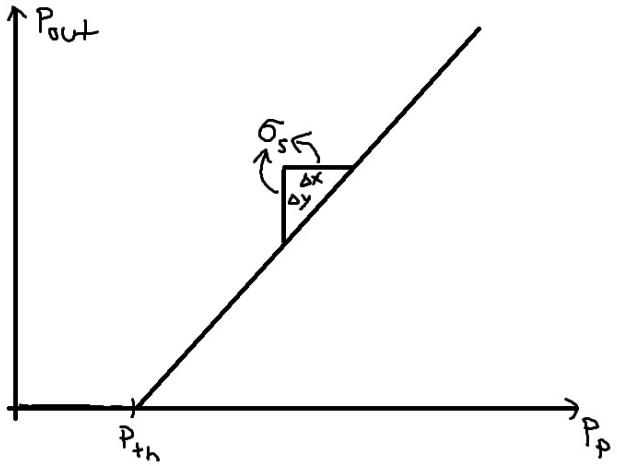

Figure 3.11: Graphical illustration of the meaning of the slope efficiency σ_s.

So we find the result that the outcoupling efficiency is maximum at one value of the output coupler transmission T_{opt}, for given round-trip gain G_0 and round-trip losses L. Interestingly, in the ideal case that $L \to 0$ we find that the situation where η_K is maximum shifts to $T_{\text{opt}} \to 0$, which seems paradoxical. But this just means that the intra-resonator light intensity grows to infinity, which is unrealistic: in a more realistic treatment, η_K and σ_s drop off due to non-linear effects at high intra-resonator powers.

The non-linear decrease of η_K with increasing bad losses L highlights the importance to keep L low in order to obtain high laser output powers. In practice this means that all surfaces of optical elements have to be extremely clean to avoid light scattering and absorption.

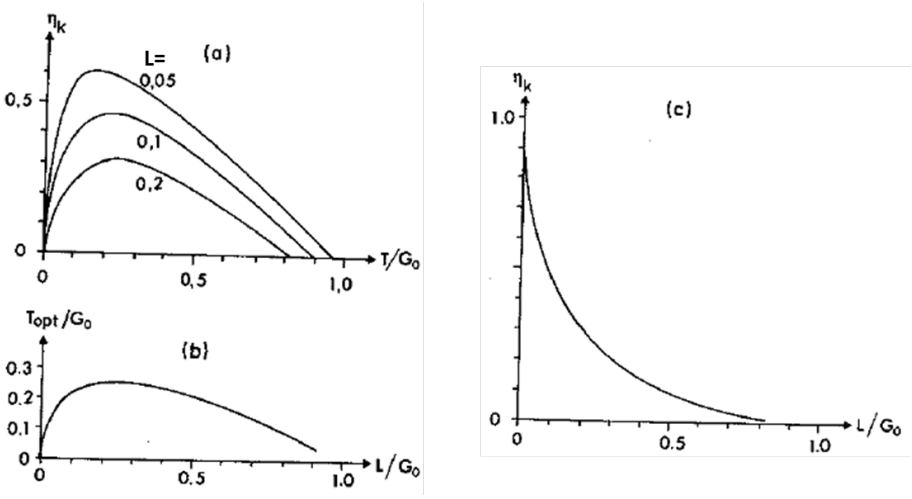

Figure 3.12: η_K and T_{opt} as functions of the mirror transmission T and the "bad" losses L.

Chapter 4

Line widths

4.1 Homogeneous line broadening

Homogeneous line broadening can be observed if all particles of an ensemble feature the same line width and position, e. g. due to spontaneous emission (excited-state lifetime broadening due to the time-energy uncertainty principle).

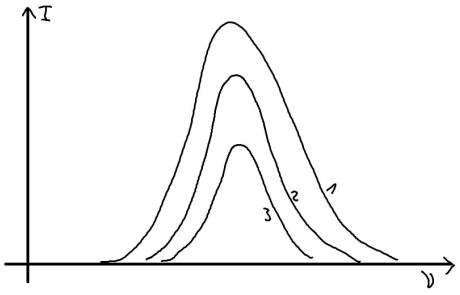

Figure 4.1: Homogeneous broadening is the intrinsic width of absorption/emission lines common to all particles of the same species. It is observed only if all particles are unperturbed by other mechanisms that shift or broaden their absorption/emission on a particle-by-particle (inhomogeneous) basis.

4.1.1 Natural line broadening

For an optical transition between two energy states with a photon of frequency ν_0 in an atom the condition

$$E_2 - E_1 = h\nu_0 \tag{4.1}$$

has to be met. Due to Heisenberg's Uncertainty Relation (HUR, $\Delta E \cdot \Delta t \gtrsim \hbar/2$) the energy levels are not completely sharp, but diffuse, which leads to broadening of the spectral line. Given that

$$A_{21} = \frac{1}{\tau}, \tag{4.2}$$

where τ is the average ($1/e$-) lifetime of an excited state, we can apply the HUR to find the line width,

$$\Delta\nu = \frac{1}{\tau}. \tag{4.3}$$

Here, $\Delta\nu$ is the full width at half maximum value (FWHM).

In a simple classical model the valence electron bound to an atom is described by a damped harmonic oscillator,

$$\ddot{x} + \gamma\dot{x} + \omega_0^2 x = 0. \tag{4.4}$$

For $x(0) = 0$ and $\dot{x}(0) = v_0$ we find the solution

$$x(t) = \frac{v_0}{\Omega} \exp\left(-\frac{\gamma}{2}t\right) \cdot \sin(\Omega t) \tag{4.5}$$

with

$$\Omega = \sqrt{\omega_0^2 - \left(\frac{\gamma}{2}\right)^2}. \tag{4.6}$$

The amplitude of $|x(t)|^2$ decays to x_0/e after a lifetime $\tau = 1/\gamma$.

Fourier-transform:

$$\tilde{x}(\omega) = \int_0^\infty x(t) e^{i\omega t} dt = \frac{v_0}{\omega_0^2 - \omega^2 - i\gamma\omega} \tag{4.7}$$

The spectral intensity $I(\omega) = |\tilde{x}(\omega)|^2$ describes two Lorentzian curves centered at $\pm\sqrt{\omega_0^2 - \gamma^2/2}$ and with FWHM $\Delta\omega = \gamma + \mathcal{O}(\gamma^3/\omega_0^2)$. Thus, for $\gamma \ll \omega_0$, $\Delta\omega \cdot \tau = 1$. The FWHM natural linewidth is the reciprocal of the natural lifetime: $\Delta\omega = 1/\tau = A_{21}$.

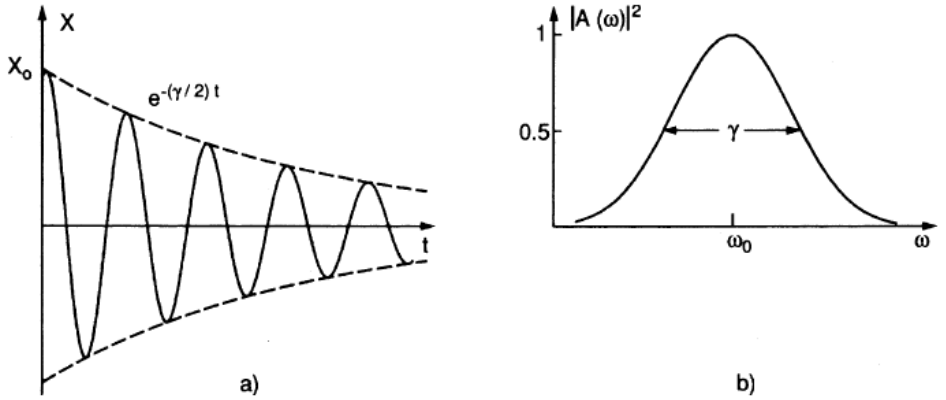

Fig. 3.2. (**a**) Damped oscillation: (**b**) the frequency distribution $A(\omega)$ of the amplitudes obtained by the Fourier transform of $x(t)$ yields the intensity profile $I(\omega - \omega_0) \propto |A(\omega)|^2$

Figure 4.2: From Demtröder "Laser spectroscopy".

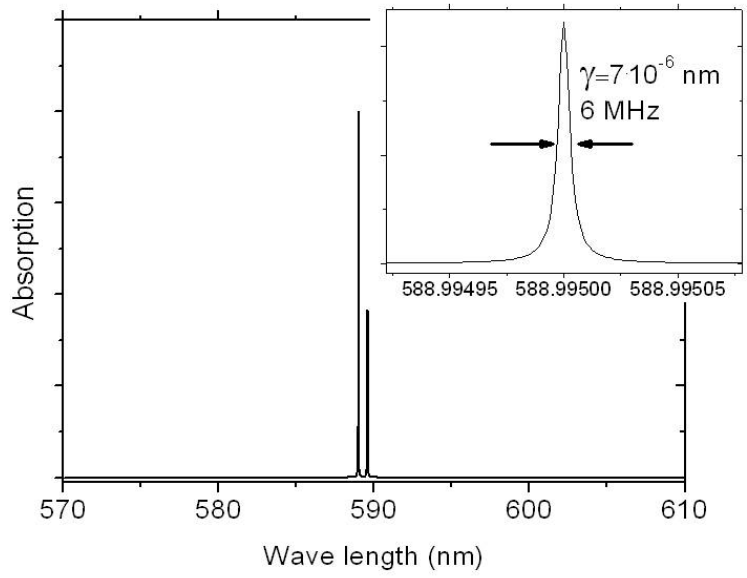

Figure 4.3: Na D1 and D2-lines which are lifetime broadened.

Examples

- Na transition from $3P_{3/2}$ (2^{nd} excited state) to $3S_{1/2}$ (ground state) has $\lambda = 589\,\text{nm}$ and $\nu_0 = 5 \times 10^{14}\,\text{Hz}$ with an average life time $\tau \approx 16\,\text{ns}$, which lead to

$$\Delta\nu \approx 10\,\text{MHz}, \qquad \frac{\Delta\nu}{\nu} \approx 2.0 \times 10^{-8}. \tag{4.8}$$

- H transition from $2S_{1/2} \rightarrow 1S_{1/2}$ has $\lambda = 121\,\text{nm}$, $\nu_0 = 2 \times 10^{15}\,\text{Hz}$, and $\tau = 1\,\text{s}$ (forbidden transition). For this transition one finds

$$\Delta\nu = 0.16\,\text{Hz}, \qquad \frac{\Delta\nu}{\nu} = 6 \times 10^{-17}. \tag{4.9}$$

- CO_2: vibrational transitions of molecules with $\lambda = 10.6\,\mu\text{m}$, $\nu_0 = 3 \times 10^{13}\,\text{Hz}$, and $\tau \approx 1\,\text{ms}$:

$$\Delta\nu = 159\,\text{Hz}, \qquad \frac{\Delta\nu}{\nu} = 6 \times 10^{-12}. \tag{4.10}$$

4.1.2 Saturation broadening

Artificial shortening of the lifetime by stimulated emission due to the presence of electromagnetic waves leads to a broadening of the linewidth (cf. HUR). The spectral line profile stays Lorentzian.

$$\Rightarrow \Delta\omega_S = \Delta_\omega \sqrt{1 + S_0} \tag{4.11}$$

with the saturation parameter

$$S_0 = \frac{I}{I_{\text{sat}}} = \frac{B_{21}\rho}{A_{21}}, \tag{4.12}$$

where I is the light intensity.

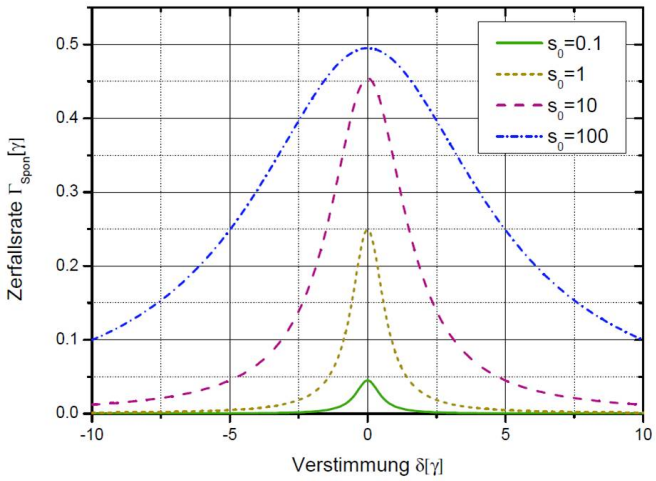

Figure 4.4: Spectral line broadened by saturation broadening.

4.1.3 Collisional broadening (pressure broadening)

A collision (scattering event) between a de-excited atom and an excited atom can have two effects. If the collision is inelastic, the excited atom changes its internal state, for instance it can be de-excited into its

ground state. This process only occurs in 'hard collisions' which are quite rare. More frequently, the atoms scatter elastically, which leads to 'scrambling' of the atomic oscillation phase, see Figure 4.5 (random collisional phase shifts). If we assume that these phase shifts occur completely randomly, this leads to an exponentially damped oscillation amplitude when summing over many contributing atoms. Equivalently we could consider one atom which scatters many times during the spectroscopic measurement. Since this process is the same for all atoms, collisional broadening is homogeneous. We already know that the Fourier transform of an exponentially damped sinusoidal oscillation is a Lorentzian function (see Equation (4.7)). The width of this function can be estimated by the collision rate

$$\gamma_s = \langle n \cdot \sigma(v_{\text{rel}}) \cdot v_{\text{rel}} \rangle \approx n\sigma \langle v_{\text{rel}} \rangle, \tag{4.13}$$

Here, n denotes the density of particles, which usually can be obtained from the ideal gas law, $n = N/V = p/(k_B T)$, where p is the gas pressure. σ is the (velocity-independent) scattering cross section, which can be calculated, *e.g.*, using the simple 'hard spheres' model, $\sigma = \pi(R_1 + R_2)^2$ where R_1 and R_2 denote the radii of the active atom and of the collision partner, respectively. The mean relative velocity $\langle v_{\text{rel}} \rangle = \sqrt{\frac{8k_B T}{\pi}\left(\frac{1}{m_1} + \frac{1}{m_2}\right)}$ is obtained from kinetic gas theory.

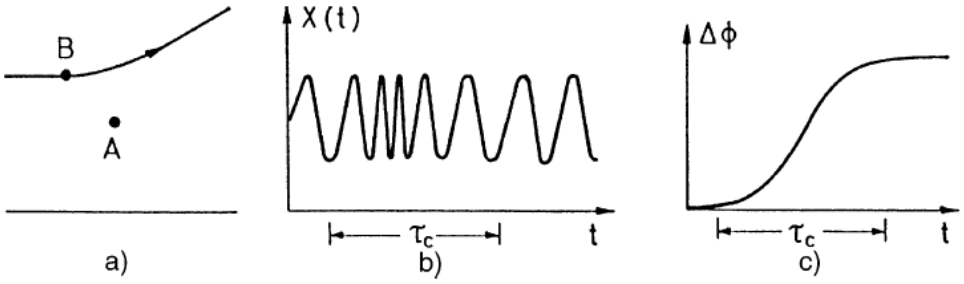

Figure 4.5: a) Phenomenological model for the collision of an optically active atom A with another particle B. Due to the interaction between particles during the collision, the oscillation frequency transiently changes b), which results in a collisional phase shift c). From Demtröder "Laser spectroscopy".

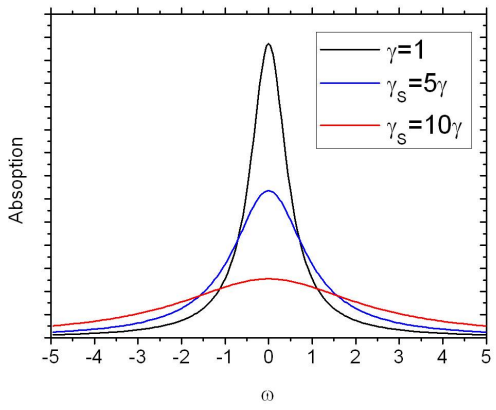

Figure 4.6: Spectral line broadened by collisional broadening.

4.2 Inhomogeneous line broadening – Doppler effect

Due to thermal motion, every particle has a different velocity relatively to the observer and therefore absorbs/emits at a slightly different frequency/wavelength due to the Doppler effect. This is called Doppler

broadening, which is an inhomogeneous effect since it affects every atom differently.

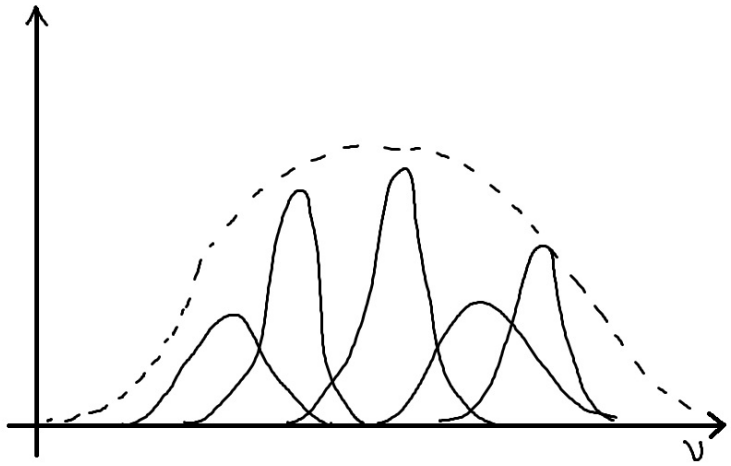

Figure 4.7: Inhomogeneous line broadening due to Doppler shifts

Given a particle moving with velocity $\vec{v}$, the wavelength of a wave emitted by the particle in its direction of motion has a shorter wavelength than a wave emitted in the opposite direction. For $\|v\| \ll c$ (non-relativistic) one finds

$$\omega = \omega_0 + \vec{k} \cdot \vec{v} \tag{4.14}$$

with the wave vector $\vec{k}$ parallel to the Poynting vector (photon emission direction) and

$$\|\vec{k}\| = \frac{2\pi}{\lambda} = \frac{\omega_0}{c} \tag{4.15}$$

In the rest frame we get

$$\omega = \omega_0 + \vec{k} \cdot \vec{v} = \omega_0 \left(1 + \frac{v_\parallel}{c}\right) \tag{4.16}$$

where $v_\parallel$ is the component of the velocity parallel to the wave direction $\vec{k}$.

In a thermal gas the velocities along a single coordinate (here, along the wave propagation direction) are distributed according to a Maxwell–Boltzmann distribution,

$$n(v_\parallel) = n_0 \sqrt{\frac{m}{2\pi k_\mathrm{B} T}} \exp\left[-\frac{m v_\parallel^2}{2 k_\mathrm{B} T}\right] \tag{4.17}$$

such that

- $\int_{-\infty}^{\infty} n(v_\parallel) \mathrm{d}v_\parallel = n_0$ (normalization)
- $\langle v_\parallel \rangle = \frac{1}{n_0} \int_{-\infty}^{\infty} v_\parallel \cdot n(v_\parallel) \mathrm{d}v_\parallel = 0$ (inversion symmetry)
- $\langle v_\parallel^2 \rangle = \frac{1}{n_0} \int_{-\infty}^{\infty} v_\parallel^2 \cdot n(v_\parallel) \mathrm{d}v_\parallel = \frac{k_\mathrm{B} T}{m}$ (equipartition theorem: $\langle \frac{1}{2} m v_\parallel^2 \rangle = \frac{1}{2} k_\mathrm{B} T$ for every particle)

This distributioncan be converted into the intensity distribution of emitted (or absorbed) light as a function of angular frequency $I(\omega) \propto n[c(\omega - \omega_0)/\omega_0]$ using Equation (4.16),

$$I(\omega) = I_0 \exp\left[-\frac{mc^2}{2 k_\mathrm{B} T} \left(\frac{\omega - \omega_0}{\omega_0}\right)^2\right] \tag{4.18}$$

which is a Gaussian function centered at $\omega = \omega_0$ with FWHM

$$\Delta\omega = \frac{\omega_0}{c} \sqrt{8 \ln(2) \frac{k_\mathrm{B} T}{m}}. \tag{4.19}$$

Example: Na at $T = 500\,\mathrm{K}$ (see Equation (4.8)): The mass of Na is $m_\mathrm{Na} = 23\,\mathrm{u}$, which leads to

$$\Delta\nu_\mathrm{Doppler} = \frac{\Delta\omega_\mathrm{Doppler}}{2\pi} = \frac{1}{\lambda} \sqrt{8 \ln(2) \frac{k_\mathrm{B} T}{m}} = 1.7\,\mathrm{GHz}. \tag{4.20}$$

4.3 Combination of homogeneous and inhomogeneous broadening: Voigt profile

Line broadening is a mixture of homogeneous and inhomogeneous broadenings → convolution of Gaussian $G(\omega)$ and Lorentzian $L(\omega)$ distributions:

$$I(\omega) = \int_0^\infty G(\omega')L(\omega - \omega')\mathrm{d}\omega' \tag{4.21}$$

⇒ Voigt-profile, see Figure 4.8.

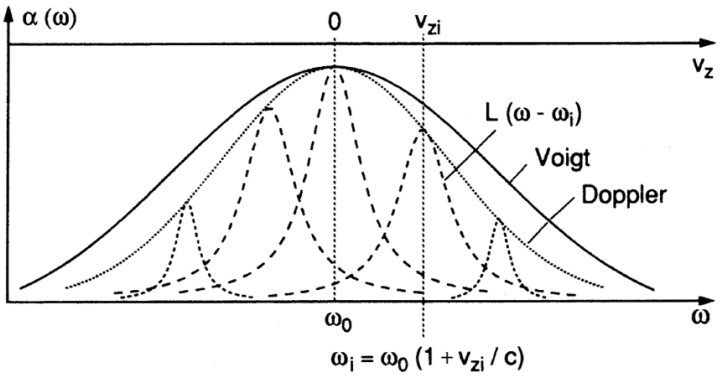

Fig. 3.9. Voigt profile as a convolution of Lorentzian line shapes $L(\omega_0 - \omega_i)$ of molecules with different velocity components v_{zi} and central absorption frequencies $\omega_i = \omega_0(1 + v_{zi}/c)$

Figure 4.8: From Demtröder "Laser spectroscopy".

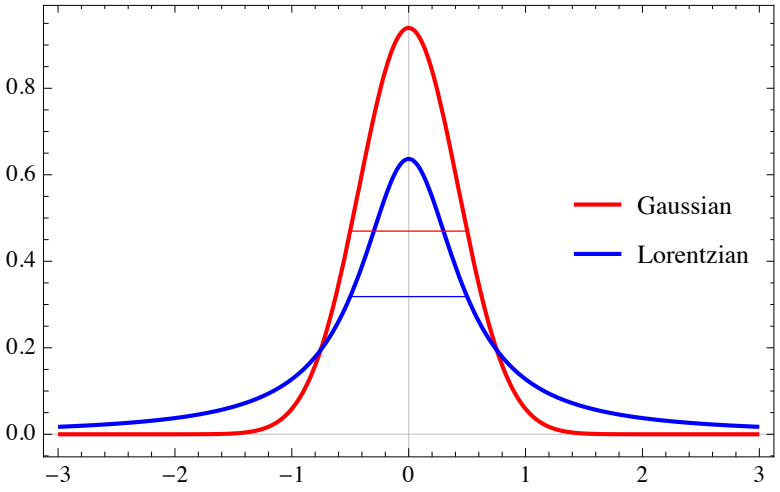

Figure 4.9: Comparison of a Gaussian $G(x) = \sqrt{\frac{4\ln(2)}{\pi}}e^{-4\ln(2)x^2}$ and a Lorentzian $L(x) = \frac{2/\pi}{1+4x^2}$ distribution, both with unit areas and unit FWHMs (thin horizontal lines). The Lorentzian has much broader wings; the Gaussian is more peaked.

4.4 Line broadening in liquids and solids

In condensed systems (liquids and solids), the environment of every particle is different. Since the spectrum of a particle is very sensitive to the particle's environment (Stark and Zeeman shifts; Pauli exclusion), this leads to inhomogeneous broadening.

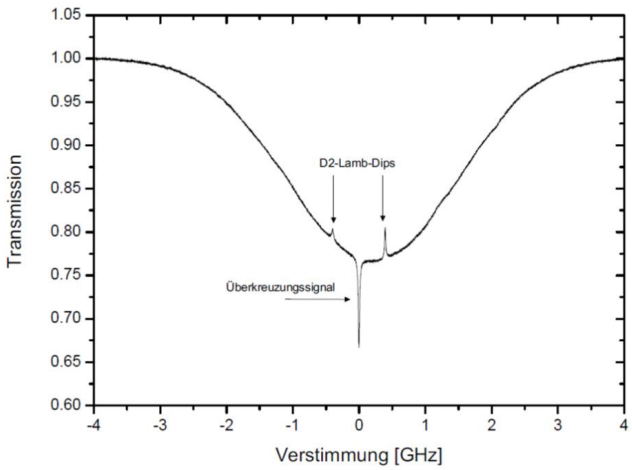

Figure 4.10: Experimentally recorded Doppler-free spectra of Li atoms in dilute Li vapor. The broad minimum shows the Doppler-broadened absorption peak. The narrow maxima are the Doppler-free atomic lines. The trick is to use two counter-propagating laser beams.

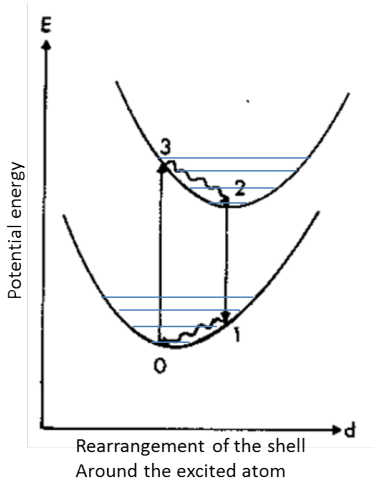

Figure 4.11: Generalized level scheme for vibronic transitions in atoms or molecules coupled to an environment. Upon laser excitation, the system first relaxes down into the well of the excited state potential, which is associated with a changing of the local environment of the excited atom and simultaneous emission of phonons.

In general, condensed systems support elastic waves (phonons), which are coupled to the electronic, vibrational, and rotational degrees of freedom of dissolved molecules. During every excitation and emission event, both in the upper and lower levels, rapid thermalization takes place by restructuring the immediate solvent environment of the particle and by emitting phonons (Figure 4.11), similar to the scheme of a 4-level laser (Figure 3.8).

4.4.1 Liquids

In a liquid, there is an infinite number of ways a particle's environment could be structured, due to the continuous nature of the configuration space. As a result, spectra of molecules dissolved in liquids have extremely broad features and usually do not show any fine structure. See Figure 4.12 for an example.

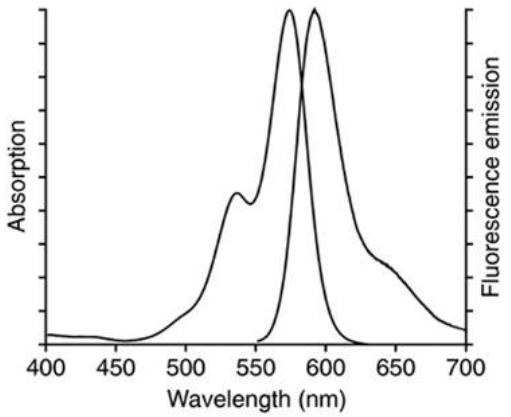

Figure 4.12: Absorption and emission lines of the dye molecule Rhodamine 6G dissolved in ethanol. The absorption takes place at shorter wavelengths (higher energies) than the emission, corresponding to the scheme of Figure 4.11.

4.4.2 Solids

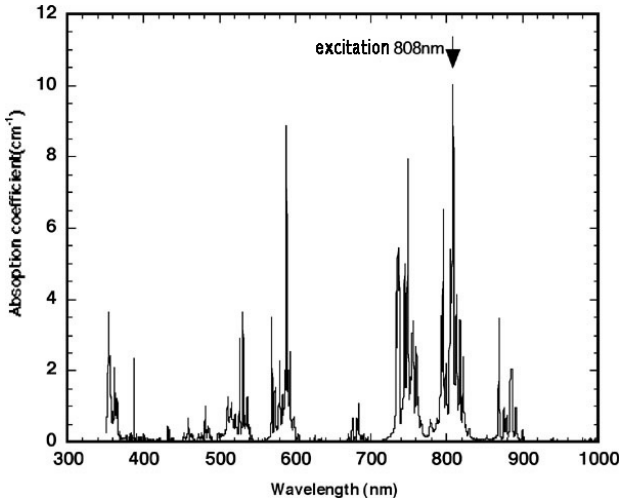

Figure 4.13: Absorption lines of Nd^{3+} ions in an Yttrium Aluminum Garnet (YAG, $Y_3Al_5O_{12}$) crystal. A 4-level laser based on this system (a Nd:YAG laser) is usually pumped with monochromatic light at the most intense absorption line around 808 nm, and emits laser light around 1064 nm.

Particles "dissolved" in solids (crystals) also experience a variety of different environments; however, not a continuum as in liquids. The environment (crystal field) of a particle depends on its position and orientation within the unit cell, as well as on neighboring lattice defects and impurities. In general, the spectra of such particles still feature rather sharp lines and structures (Figure 4.13), albeit much broader than gas-phase (individual) particles.

4.5 Spectral hole burning

Spectral hole burning appears in inhomogeneously broadened gain media. For every frequency there is an independent level of inversion $I(\nu)$ and an independent effective gain $G(\nu)$. When the laser puts out light, the effective gain is depressed to match the effective losses ($G = L$ and thus $\Gamma = 0$ in steady state); for

an inhomogeneously broadened medium, this leads to a structured gain profile as in Figure 4.14 (3). The gain profile develops "spectral holes".

Compare this to the homogeneously broadened case, Figure 4.14 (2), where laser operation depresses the entire gain profile homogeneously.

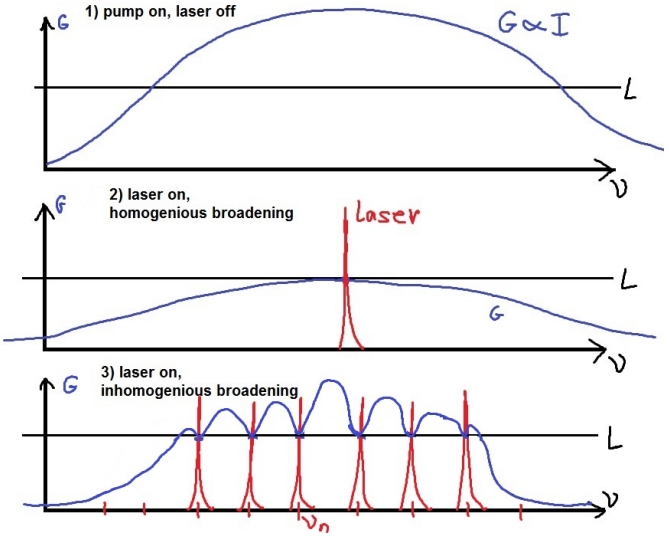

Figure 4.14: Laser spectrum for three cases: (1) pump on, but laser off; (2) laser on with homogeneous broadening of $G(\nu)$; (3) laser on with inhomogeneous broadening of $G(\nu)$. The regions of gain > losses in case 3 are due to the fact that the resonator only supports specific frequency modes; not all frequencies can lase.

More generally, spectral hole burning refers to the situation where a strong light field (in the above case, the laser field) saturates the absorption of a medium at a certain wavelength, so that a weaker probe-light field cannot be absorbed as well at the same wavelength.

4.6 Spatial hole burning

See Figure 4.15: In a linear resonator, interference of counter-propagating waves leads to a standing-wave pattern which excludes some spatial regions of the active medium from participating in the laser amplification process. Solution: Ring resonators ⇒ traveling wave.

More generally, spatial hole burning refers to the situation where a strong light field (in the above case, the laser field) saturates the absorption of a medium at a certain point in space, so that a weaker probe-light field cannot be absorbed as well at the same point in space.

4.7 Laser output line width

The Schawlow–Townes limit gives the ultimate lower limit on the linewidth of a cw laser:

$$\frac{\Delta\nu_{\text{laser}}}{\nu_{\text{laser}}} \geqslant \frac{\pi h(\Delta\nu_0)^2}{P_{\text{laser}}}, \tag{4.22}$$

where $\Delta\nu_0 = \tau_{\text{ph}}^{-1}$ is the FWHM resonator linewidth (see section 6.1) and $\Delta\nu_{\text{laser}}$ is the smallest possible linewidth (FWHM) of the laser output.

The derivation of this formula is quite involved (even Schawlow and Townes got it wrong by a factor of two in the original publication) and is usually done in terms of a random walk of the phase of the electromagnetic field in the resonator. See any good book on lasers for more details.

The reason for the Schawlow–Townes limit is the influence of spontaneous emission into the laser mode: every spontaneously emitted photon has a random phase with respect to the laser light, and adding it to the light in the resonator gives rise to a slight random phase shift (→ random walk). The more

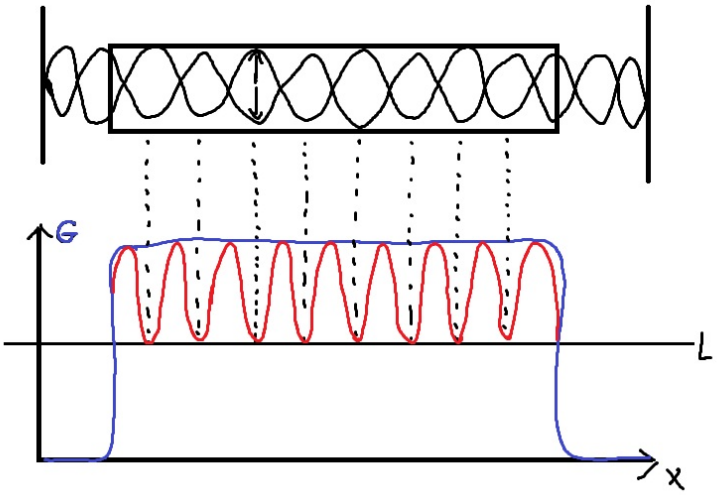

Figure 4.15: blue: Gain profile without the effect of spatial hole burning, red: Gain profile with spatial hole burning. Due to the boundary conditions for the electro-magnetic field inside the resonator, a standing-wave pattern develops, which has peaks (laser gain through stimulated emission) and nodes (no stimulated emission, zero electric-field amplitude). See chapter 6.

light there is in the resonator (the larger P_{out}), the smaller this influence becomes. On the other hand, a larger resonator linewidth $\Delta\nu_0$ gives a larger laser linewidth because a larger photon loss rate $\Delta\nu_0$ yields a larger ratio of $P_{\text{out}}/E_{\text{resonator}}$, thus amplifying the influence of resonator phase fluctuations on output phase fluctuations.

Examples

- HeNe laser: $\lambda = 632.8\,\text{nm}$, $P_{\text{out}} = 1\,\text{mW}$, $L = 0.5\,\text{m}$, $R = 1 - T = 98\%$
  $\Rightarrow \Delta\nu_0 = \frac{1-R}{\pi\sqrt{R}} \cdot \frac{c}{2L} = 1.9\,\text{MHz}$ (photon lifetime $\tau_{\text{ph}} = 1/\Delta\nu_0 = 0.52\,\mu\text{s}$) and $\Delta\nu_{\text{laser}} \geqslant \frac{\pi h\nu(\Delta\nu_0)^2}{P_{\text{laser}}} = \frac{hc^3(1-R)^2}{4\pi\lambda L^2 P_{\text{laser}} R} = 3.7\,\text{mHz}$ (coherence time $T_{\text{coh}} = 1/\Delta\nu_{\text{laser}} \leqslant 273\,\text{s}$, coherence length $\ell_{\text{coh}} = c \cdot T_{\text{coh}} \leqslant 0.55\,\text{au}$ [astronomical units]).
  In practical systems, unless extreme care is taken, this Schawlow–Townes limit is overwhelmed by technical noise, *e.g.*, thermal drifts.

- Diode laser: $\lambda = 632.8\,\text{nm}$, $P_{\text{out}} = 1\,\text{mW}$, $L = 0.5\,\text{mm}$, $R = 30\%$
  $\Rightarrow \Delta\nu_0 = 122\,\text{GHz}$ (photon lifetime $\tau_{\text{ph}} = 8.2\,\text{ps}$) and $\Delta\nu_{\text{laser}} \geqslant 15\,\text{MHz}$ (coherence time $T_{\text{coh}} \leqslant 68\,\text{ns}$, coherence length $\ell_{\text{coh}} \leqslant 20\,\text{m}$).
  This is a significant limit.

So the Schawlow–Townes limit can actually become relevant, but only for lasers with high gain (small output coupler reflectivity R) and short resonators, such as diode lasers.

Chapter 5

Coherence and Interference

5.1 Interference

Given two one-dimensional plane waves along the x-axis, with equal frequencies and wavelengths but different phases:

$$\begin{aligned} E_1(x,t) &= A_1 e^{\mathrm{i}(kx-\omega t+\varphi_1)} \\ E_2(x,t) &= A_2 e^{\mathrm{i}(kx-\omega t+\varphi_2)}, \end{aligned} \tag{5.1}$$

assuming $A_1, A_2 \in \mathbb{R}$. These waves interfere according to the superposition principle. The total amplitude is

$$E_{\text{sum}} = E_1 + E_2. \tag{5.2}$$

For electro-magnetic waves one usually cannot observe the electric field due to the high frequency. A more easily measurable quantity is the square of the absolute value of the wave amplitude, the intensity I:

$$\begin{aligned} I = |E_{\text{sum}}|^2 &= E_{\text{sum}} \cdot E_{\text{sum}}^* = (E_1+E_2)(E_1+E_2)^* \\ &= |E_1|^2 + |E_2|^2 + E_1E_2^* + E_2E_1^* \\ &= |E_1|^2 + |E_2|^2 + 2\Re(E_1E_2^*) \\ &= A_1^2 + A_2^2 + 2\Re[A_1 e^{\mathrm{i}(kx-\omega t+\varphi_1)} A_2 e^{-\mathrm{i}(kx-\omega t+\varphi_2)}] \\ &= A_1^2 + A_2^2 + 2A_1A_2\Re[e^{\mathrm{i}(\varphi_1-\varphi_2)}] \\ &= A_1^2 + A_2^2 + 2A_1A_2\cos(\varphi_1-\varphi_2), \end{aligned} \tag{5.3}$$

where $\Re$ is the real part. We obtain an interference maximum (intensity maximum) if

$$\Delta\varphi = \varphi_1 - \varphi_2 = n \cdot 2\pi \tag{5.4}$$

with $n \in \mathbb{Z}$.

For two waves propagating in opposite directions,

$$\begin{aligned} E_1(x,t) &= A_1 e^{\mathrm{i}(kx-\omega t+\varphi_1)} \\ E_2(x,t) &= A_2 e^{\mathrm{i}(-kx-\omega t+\varphi_2)}, \end{aligned} \tag{5.5}$$

the intensity is given by

$$\begin{aligned} I &= A_1^2 + A_2^2 + 2\Re[A_1 e^{\mathrm{i}(kx-\omega t+\varphi_1)} A_2 e^{-\mathrm{i}(-kx-\omega t+\varphi_2)}] \\ &= A_1^2 + A_2^2 + 2A_1A_2\Re[e^{\mathrm{i}(2kx+\varphi_1-\varphi_2)}] \\ &= A_1^2 + A_2^2 + 2A_1A_2\cos(2kx+\varphi_1-\varphi_2), \end{aligned} \tag{5.6}$$

Therefore we obtain a maximum of intensity for

$$2kx = n \cdot 2\pi - (\varphi_1 - \varphi_2) \tag{5.7}$$

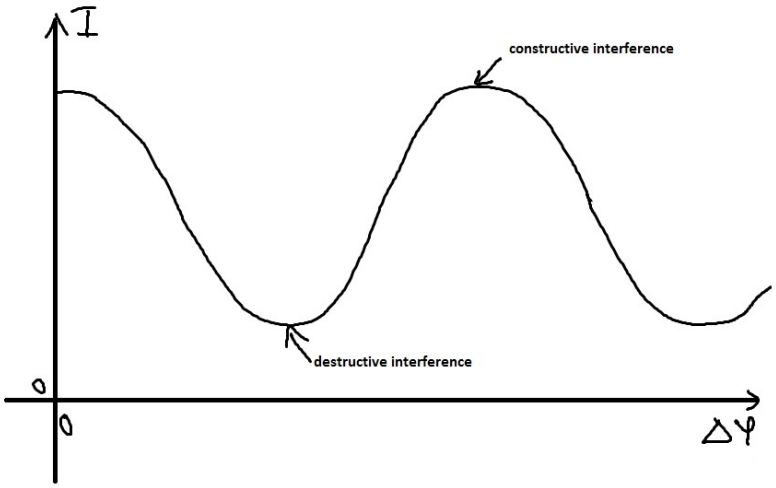

Figure 5.1: Intensity of two waves with amplitudes A_1 and A_2 propagating in the same direction as a function of their phase difference $\Delta\varphi$. Zero intensity at a destructive interference minimum can only be achieved if $\Delta\varphi = (2n+1)\pi$ and $A_1 = A_2$

with $n \in \mathbb{Z}$. Considering that $k = \frac{2\pi}{\lambda}$ we can see that the distance between two consecutive interference maxima is

$$\Delta x = \frac{\lambda}{2}. \tag{5.8}$$

The resulting wave has a constant amplitude for a fixed coordinate in space. Such a wave is called a *standing wave*.

Now we consider the case of two waves with different frequencies,

$$\begin{aligned} B_1 &= A_1 e^{\mathrm{i}(k_1 x - \omega_1 t + \varphi_1)} \\ B_2 &= A_2 e^{\mathrm{i}(k_2 x - \omega_2 t + \varphi_2)} \end{aligned} \tag{5.9}$$

The intensity is then given by

$$I = A_1^2 + A_2^2 + 2A_1 A_2 \cos[(k_1 - k_2)x - (\omega_1 - \omega_2)t + \varphi_1 - \varphi_2] \tag{5.10}$$

At a fixed point x in space, the intensity oscillates in time, with a time

$$\Delta t = \frac{2\pi}{|\omega_1 - \omega_2|} \tag{5.11}$$

between intensity maxima. The associated angular frequency $\Delta\omega = \omega_1 - \omega_2$ is called a *beat note*. For a polychromatic light field, which consists of many frequency components, there are many beat notes with random phases, which in total cause the interference trace to be damped exponentially.

5.2 Coherence

There are two types of coherence: temporal and spatial coherence.

5.2.1 Temporal Coherence

Consider a Michelson–Morley interferometer with variable distances x_1 and x_2 between the mirrors and the beam splitter (see Figure 5.4). The length difference Δx between the two light paths to the screen is

$$\Delta x = 2(x_2 - x_1), \tag{5.12}$$

corresponding to a runtime difference $\Delta t = \Delta x / c$ in the two arms of the interferometer.

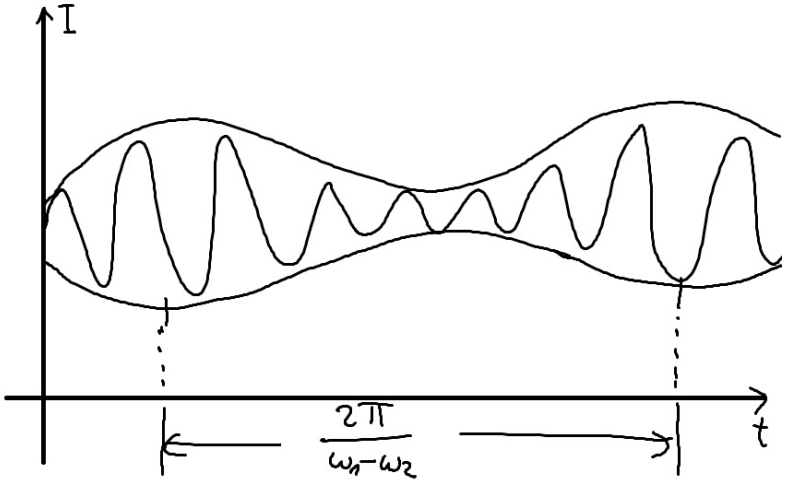

Figure 5.2: Temporal variation of the intensity of two interfering waves with different frequencies

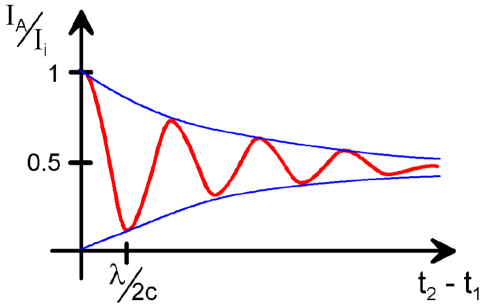

Figure 5.3: Exponentially damped interferogram measured for partially coherent, chaotic light.

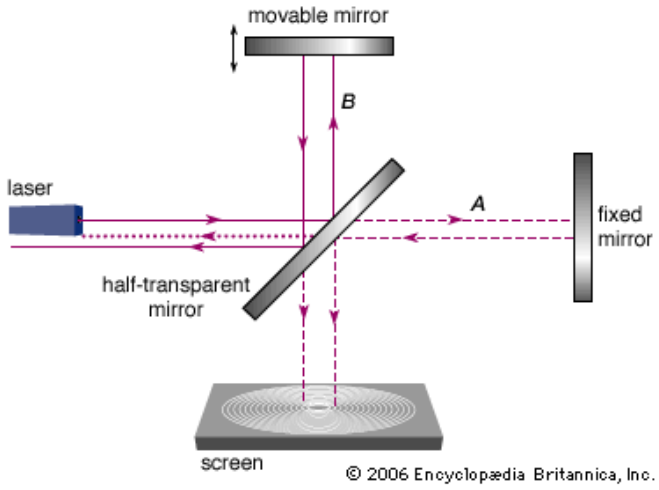

Figure 5.4: Schematic representation of a Michelson–Morley interferometer.

We assume that the laser beam consists not just of a single frequency, but of a superposition of many frequencies (that are usually all very close together, see section 4.7). We call $\Delta\omega = 2\pi \cdot \Delta\nu$ the frequency spread.

Over the runtime difference Δt of the interferometer, the different frequencies of the laser beam accumulate phase differences $\Delta\varphi = \Delta\omega \cdot \Delta t$. The interferometer only operates with good contrast if

$|\Delta\varphi| < \pi$; otherwise, the interference fringes are washed out due to the many beat nodes (see section 5.1):

$$|\Delta\varphi| < \pi \qquad \Rightarrow |\Delta x| < \frac{c}{2\Delta\nu} = \pi \cdot \ell_C \tag{5.13}$$

in terms of the *coherence length*

$$\ell_C = \frac{c}{2\pi\Delta\nu} = \frac{c}{\Delta\omega} \tag{5.14}$$

and the *coherence time*

$$T_C = \frac{\ell_C}{c} = \frac{1}{\Delta\omega}. \tag{5.15}$$

We see that the frequency spread $\Delta\omega$ of a laser gives a maximum on the temporal and spatial extents over which interference can take place.

examples

spectrally filtered lamp:

$$\begin{aligned} \lambda &= 546\,\text{nm} \\ \Delta\nu &= 640\,\text{MHz} \\ \ell_C &= 7.5\,\text{cm} \end{aligned} \tag{5.16}$$

laser:

$$\begin{aligned} \lambda &= 632\,\text{nm} \\ \Delta\nu &= 1\,\text{MHz} \\ \ell_C &= 48\,\text{m} \end{aligned} \tag{5.17}$$

5.2.2 Spatial Coherence

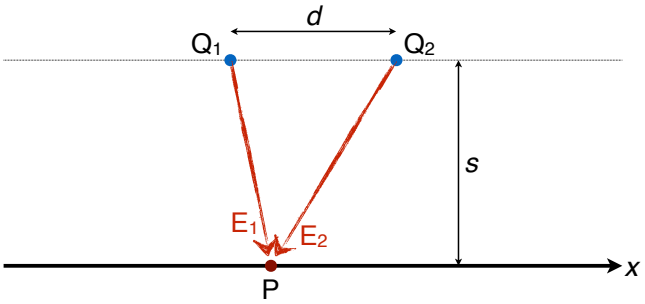

Figure 5.5: Two light sources Q_1 and Q_2 separated by a distance d, shedding coherent light onto a screen at distance s.

Consider two light sources of the same color, separated by a distance d, illuminating a screen that is placed at a distance s (see Figure 5.5). A point P on the screen sees two interfering light fields, as in section 5.1:

$$\begin{aligned} E_1(P,t) &= A_1 e^{i(k\cdot\overline{Q_1P}-\omega t+\varphi_1)} \\ E_2(P,t) &= A_2 e^{i(k\cdot\overline{Q_2P}-\omega t+\varphi_2)} \end{aligned} \tag{5.18}$$

with the distances $\overline{Q_1P} = \sqrt{s^2+(x+d/2)^2}$ and $\overline{Q_2P} = \sqrt{s^2+(x-d/2)^2}$. The intensity of the total field is therefore

$$\begin{aligned} I(x,t) = |E_1+E_2|^2 &= A_1^2 + A_2^2 + 2A_1A_2\cos\left[k\left(\sqrt{s^2+(x+d/2)^2}-\sqrt{s^2+(x-d/2)^2}\right)+\Delta\varphi\right] \\ &\approx A_1^2 + A_2^2 + 2A_1A_2\cos\left[\frac{2kx}{\sqrt{1+(2s/d)^2}}+\Delta\varphi\right] \text{ for small } |x|. \end{aligned} \tag{5.19}$$

Around the center of the interference pattern (small $|x|$), the interference maxima are spaced by $\frac{2k\cdot\Delta x}{\sqrt{1+(2s/d)^2}} = 2\pi$, or

$$\Delta x = \frac{\pi}{k}\sqrt{1+(2s/d)^2} \approx \frac{2\pi s}{kd} = \frac{\lambda s}{d} \tag{5.20}$$

assuming $s \gg d$.

The position of the central interference maxima depend on the relative phase of the two sources,

$$x_n \approx n\cdot\Delta x - \frac{s}{kd}\cdot\Delta\varphi = \frac{\lambda s}{d}\cdot\left(n - \frac{\Delta\varphi}{2\pi}\right) \tag{5.21}$$

under the same assumptions as above. If the relative phases of the two sources fluctuate in time, that is, if $\Delta\varphi$ is not fixed, then the entire interference pattern fluctuates in space (shifts around at random); integrating over time, the interference pattern is thus washed out.

The two sources at Q_1 and Q_2 are usually derived from the same oscillator (*i.e.*, laser), prototypically in Young's double-slit experiment. The question of the stability of their relative phase $\Delta\varphi$, that is, their phase coherence, is thus a question of how to split a laser beam into two spatially separated beams without destroying their coherence. We will return to this point in more detail in chapter 7.

5.2.3 Washing out interference fringes

Assume we are observing a function $f(x,\varphi) = \cos(kx+\varphi)$, similar to Equation (5.10) and Equation (5.19). Now assume that the phase φ is not sharply defined but fluctuates around a mean value $\bar{\varphi}$ with a standard deviation σ, so that the probability of having a given value φ is

$$p(\varphi) = \frac{e^{-\frac{(\varphi-\bar{\varphi})^2}{2\sigma^2}}}{\sigma\sqrt{2\pi}}. \tag{5.22}$$

The expectation value of the function f is therefore

$$\begin{aligned}\langle f(x)\rangle &= \int_{-\infty}^{\infty} f(x,\varphi)p(\varphi)\mathrm{d}\varphi = \int_{-\infty}^{\infty}\cos(kx+\varphi)\frac{e^{-\frac{(\varphi-\bar{\varphi})^2}{2\sigma^2}}}{\sigma\sqrt{2\pi}}\mathrm{d}\varphi = e^{-\frac{1}{2}\sigma^2}\cdot\cos(kx+\bar{\varphi})\\ &= e^{-\frac{1}{2}\sigma^2}\cdot f(x,\bar{\varphi}).\end{aligned} \tag{5.23}$$

This means that the contrast of the interference fringe f is damped by the factor $e^{-\frac{1}{2}\sigma^2}$ in the presence of phase fluctuations.

Chapter 6

Optical resonators

6.1 Simplest type: Fabry-Pérot interferometer

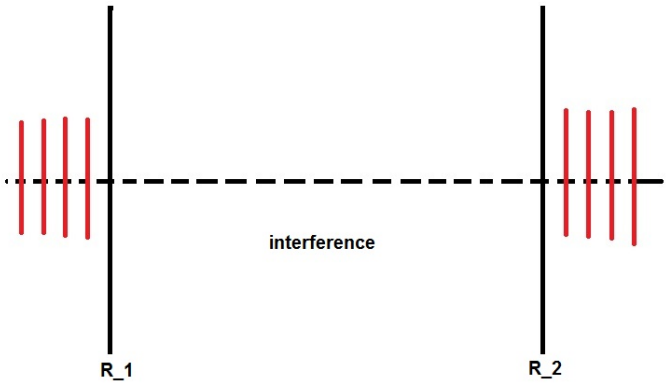

Figure 6.1: scheme of a Fabry-Pérot inferferometer.

The Fabry-Pérot interferometer consists of two planar mirrors of finite reflectivity R_1 and R_2. We assume that their transmission is given by

$$T_i = 1 - R_i \tag{6.1}$$

where T and R refer to the intensity; this assumes that $T_i + R_i = 1$, *i.e.*, that there are no other losses. For the electric field, the transmission and reflection coefficients are

$$t_i = \sqrt{T_i} \qquad\qquad r_i = \sqrt{R_i} \tag{6.2}$$

respectively. More generally, t_i and r_i can be complex (to describe phase shifts during the reflection), and we define $T_i = |t_i|^2$ and $R_i = |r_i|^2$.

We use a one-dimensional approximation: the light waves are assumed to be perfect plane waves, extending infinitely in the plane parallel to the propagation direction (the z axis); and the mirrors are infinitely large and planar. The electric field of the wave coming from the left in Figure 6.1 is then given by

$$E_{\text{in}} = E \cdot e^{i(kz-\omega t)}, \tag{6.3}$$

the field entering the resonator through the left mirror is

$$E_0 = t_1 \cdot E_{\text{in}}, \tag{6.4}$$

the field after one round trip through the resonator is

$$E_1 = E_0 \cdot e^{\mathrm{i}kL} \cdot r_2 \cdot e^{\mathrm{i}kL} \cdot r_1 = E_0 \cdot r_1 r_2 e^{2\mathrm{i}kL} \tag{6.5}$$

where L is the effective distance between the mirrors. After n double reflections on the mirrors (n round trips) the electric field is

$$E_n = E_0 \cdot \left(r_1 r_2 e^{2ikL}\right)^n \tag{6.6}$$

The total electrical field in the resonator is sum of all of these contributions,

$$E_{\text{int}} = \sum_{n=0}^{\infty} E_n = t_1 E_{\text{in}} \frac{1}{1 - r_1 r_2 e^{2ikL}} \tag{6.7}$$

The wave going out of the right mirror, leaving the resonator, is

$$E_{\text{out}} = E_{\text{int}} \cdot e^{ikL} \cdot t_2 = E_{\text{in}} \frac{t_1 t_2 e^{ikL}}{1 - r_1 r_2 e^{2ikL}}. \tag{6.8}$$

The total transmission through the two-mirror setup is

$$T_{\text{FP}} = \left|\frac{E_{\text{out}}}{E_{\text{in}}}\right|^2 = \frac{T_1 T_2}{1 + R_1 R_2 - 2\Re(r_1 r_2 e^{2ikL})} \tag{6.9}$$

and, assuming $r_i \in \mathbb{R}$,

$$T_{\text{FP}} = \frac{T_1 T_2}{1 + R_1 R_2 - 2\sqrt{R_1 R_2}\cos(2kL)} = \frac{(1 - R_1)(1 - R_2)}{1 + R_1 R_2 - 2\sqrt{R_1 R_2}\cos(2kL)}. \tag{6.10}$$

For $R_1 = R_2 = R$:

$$\begin{aligned} T_{\text{FP}} &= \frac{(1-R)^2}{1 + R^2 - 2R\cos(2kL)} \\ &= \frac{(1-R)^2}{1 + R^2 - 2R\left[1 - 2\sin^2(kL)\right]} \\ &= \frac{1}{1 + \frac{4R}{(1-R)^2}\sin^2(kL)} \qquad \text{Airy function} \end{aligned} \tag{6.11}$$

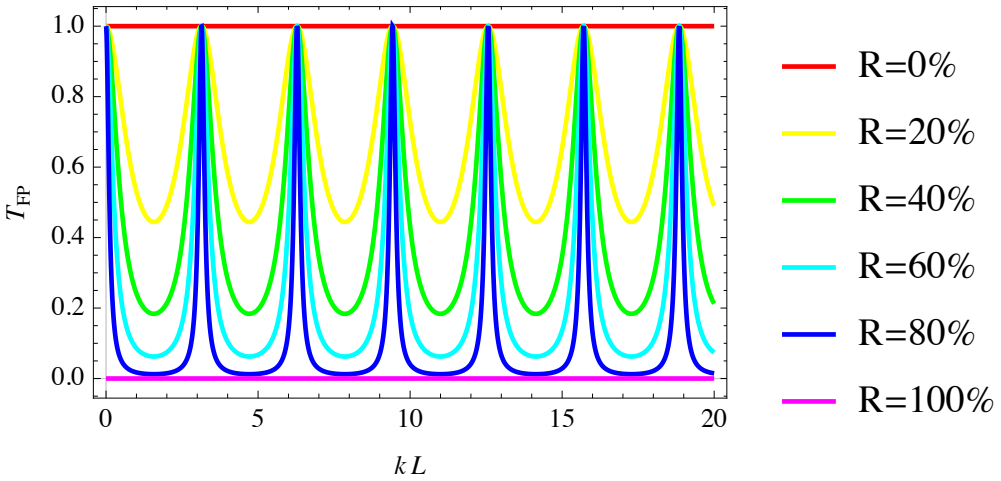

Figure 6.2: The transmission T_{FP} of the Fabry-Pérot interferometer as a function of the scaled frequency kL for various values of the reflectivity R of the mirrors.

We find that there is total transmission on resonance (only for $R_1 = R_2 = R$) due to destructive interference of the light going back out of the resonator and the part of the incoming wave that is immediately reflected without entering the resonator. On resonance, $kL = n\pi$ ($n \in \mathbb{Z}$) and therefore $\sin(kL) = 0$ and $T_{\text{FP}} = 1$:

$$\Rightarrow \lambda_n = \frac{2L}{n} \qquad \nu_n = \frac{c}{2L} \cdot n \qquad n \sim 10^6 \text{ (typically)} \tag{6.12}$$

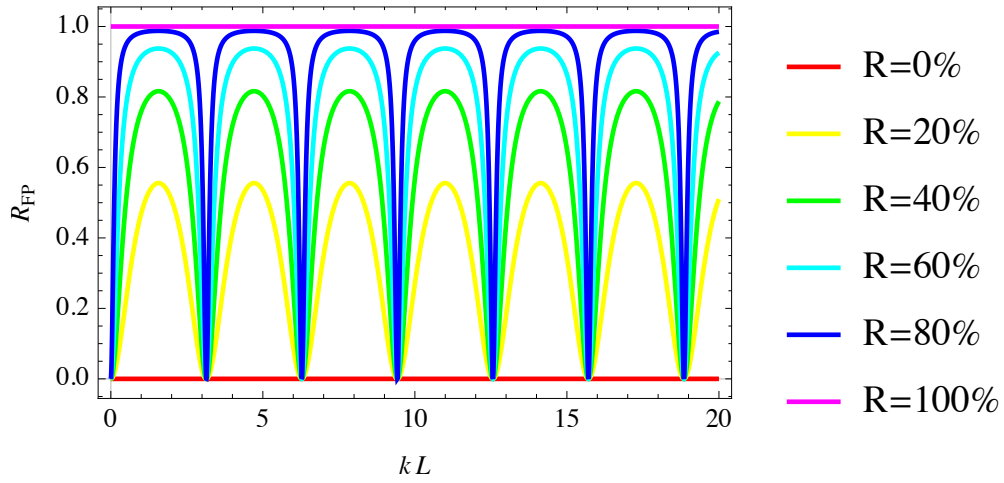

Figure 6.3: The reflection $R_{FP} = 1 - T_{FP}$ of the Fabry-Pérot interferometer as a function of the scaled frequency kL for various values of the reflectivity R of the mirrors.

The distance between the resonances is

$$\Delta\nu = \nu_{n+1} - \nu_n = \frac{c}{2L} \qquad \text{free spectral range (FSR)} \tag{6.13}$$

Resonance shape:

(i) $R_i \ll 1$, *e.g.*, a glass plate ('étalon')

$$T_{FP} \approx 1 - 4R\sin^2(kL) \tag{6.14}$$

The transmission is only lightly modulated in frequency.

(ii) $R_i \approx 1$: With

$$\begin{aligned}\sin(kL) &= \sin\left(\frac{2\pi\nu}{c}\cdot L\right)\\ &= \sin\left(\pi\frac{\nu}{\Delta\nu}\right)\\ &= \sin\left(\pi\frac{\nu-\nu_n}{\Delta\nu} + n\pi\right)\\ &= (-1)^n \sin\left(\pi\frac{\nu-\nu_n}{\Delta\nu}\right)\end{aligned} \tag{6.15}$$

since $\sin(\alpha + n\pi) = \sin(\alpha)\cos(n\pi) + \cos(\alpha)\sin(n\pi) = (-1)^n\sin(\alpha)$.

For $|\nu - \nu_n| \ll \Delta\nu$ we can apply the small-angle approximation:

$$\sin(kL) \approx \pi\frac{\nu-\nu_n}{\Delta\nu} \tag{6.16}$$

$$\Rightarrow T_{FP} \approx \frac{1}{1 + \frac{4R\pi^2}{(1-R)^2}\left(\frac{\nu-\nu_n}{\Delta\nu}\right)^2} = \frac{1}{1 + \left(\frac{\nu-\nu_n}{\Delta\nu_{res}/2}\right)^2} \qquad \text{Lorentzian curve} \tag{6.17}$$

$$\Delta\nu_{res} = \frac{1-R}{\pi\sqrt{R}}\cdot\Delta\nu = \frac{1-R}{\pi\sqrt{R}}\cdot\frac{c}{2L} = \text{FWHM of resonance} \tag{6.18}$$

We define the *finesse*

$$\mathcal{F} = \frac{\Delta\nu}{\Delta\nu_{res}} = \frac{\pi\sqrt{R}}{T} = \frac{\pi\sqrt{R}}{1-R} \tag{6.19}$$

the *quality factor*

$$Q = \frac{\nu}{\Delta\nu_{\text{res}}} = n \cdot \mathcal{F} \tag{6.20}$$

and the *resonance enhancement*

$$U = \frac{I_{\text{int}}}{I_{\text{in}}} = \frac{1}{T} = \frac{1}{1-R} = \frac{\mathcal{F}}{\pi\sqrt{R}} \tag{6.21}$$

The photon life time inside the resonator is given by

$$\tau_{\text{ph}} = \frac{1}{\Delta\nu_{\text{res}}} = \frac{2\pi\sqrt{R}}{1-R} \cdot \frac{L}{c} = \frac{\pi\sqrt{R}}{1-R} \cdot \tau_R = \mathcal{F} \cdot \tau_R \tag{6.22}$$

where $\tau_R = 2L/c$ is the-round trip time of a photon in the resonator.

Example: $L = 5\,\text{cm}$, $R = 98\%$, $\lambda = 632.8\,\text{nm} \Rightarrow \nu = 4.7 \times 10^{14}\,\text{Hz}$, $\Delta\nu = 3\,\text{GHz}$, $\Delta\nu_{\text{res}} = 19\,\text{MHz}$, $\mathcal{F} = 156$, $n = 1.6 \times 10^5$, $Q = 2.5 \times 10^7$, $\tau_R = 0.33\,\text{ns}$, $\tau_{\text{ph}} = 52\,\text{ns}$, $U = 50$.

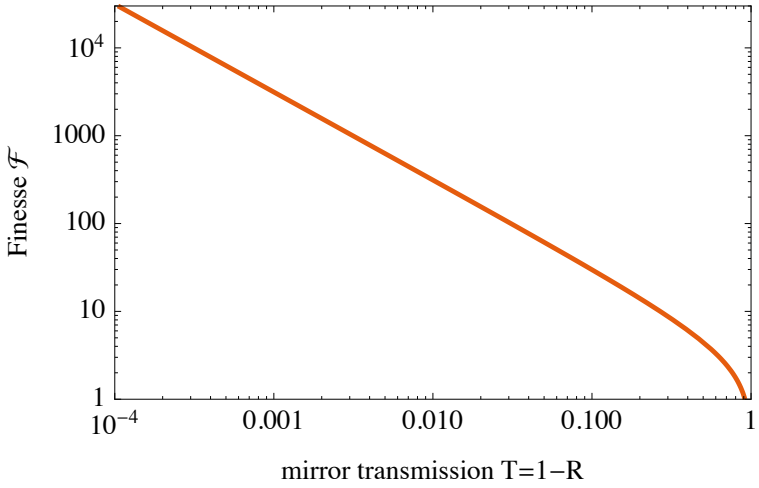

Figure 6.4: Finesse $\mathcal{F}$ of a lossless Fabry-Pérot interferometer, Equation (6.19), as a function of the mirror transmission $T = 1 - R$.

6.2 Resonator stability

Is the Fabry-Pérot resonator stable? See Figure 6.5.

6.2.1 Ray optics with ABCD matrices

In this section we find a simple method for describing the propagation of classical light rays (no diffraction, no interference) in the paraxial approximation.

Definition: Light ray

See Figure 6.6: we define a light ray by its distance $r(z)$ from the resonator axis and by the slope, assuming that it always remains in a single plane containing the z-axis. At any given z coordinate, the ray is thus described by the tuple

$$\vec{r}(z) = \begin{pmatrix} r(z) \\ r'(z) = \frac{\mathrm{d}r(z)}{\mathrm{d}z} \end{pmatrix} \tag{6.23}$$

If we know the description at one z-coordinate, how do we calculate the resulting description at some other z-coordinate?

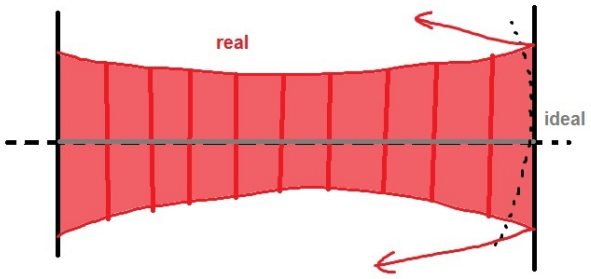

Figure 6.5: A real wave is not stable in a FP-resonator. Solution: one mirror has to be curved

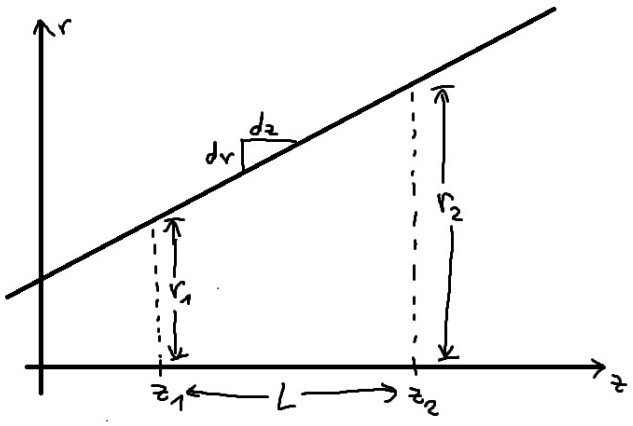

Figure 6.6: Definition of a classical light ray.

(i) Propagation in homogeneous medium (vacuum, air, etc.) from z_1 to z_2:

$$\begin{aligned} r_2' &= r_1' \\ r_2 &= r_1 + r_1'(z_2 - z_1) = r_1 + r_1' L \\ \Rightarrow \vec{r}_2 &= \begin{pmatrix} 1 & L \\ 0 & 1 \end{pmatrix} \cdot \vec{r}_1 \end{aligned} \tag{6.24}$$

Thus we can describe a propagation by a distance L by multiplication with a 2×2 matrix $\hat{M} = \begin{pmatrix} 1 & L \\ 0 & 1 \end{pmatrix}$.

(ii) Planar interface (air/glass) perpendicular to the z-axis:
With the paraxial approximation for small angles $\sin(\theta) \approx \tan(\theta)$ we obtain with Snell's law

$$n_1 \tan(\theta_1) \approx n_2 \tan(\theta_2) \tag{6.25}$$

At the interface:

$$\begin{aligned} r_1 &= r_2 \text{ (the ray does not move laterally during the transition through the interface)} \\ n_1 r_1' &\approx n_2 r_2' \text{ (Snell's law)} \\ \Rightarrow \vec{r}_2 &= \begin{pmatrix} 1 & 0 \\ 0 & n_1/n_2 \end{pmatrix} \cdot \vec{r}_1 \end{aligned} \tag{6.26}$$

Thus we can describe the transition from a medium with refractive index n_1 into a medium with refractive index n_2 by multiplication with a 2×2 matrix $\hat{M} = \begin{pmatrix} 1 & 0 \\ 0 & n_1/n_2 \end{pmatrix}$.

(iii) Thin lens with focal length f perpendicular to the z-axis:
We have $r_1 = r_2$. Using $1/f = 1/g + 1/b$ we obtain

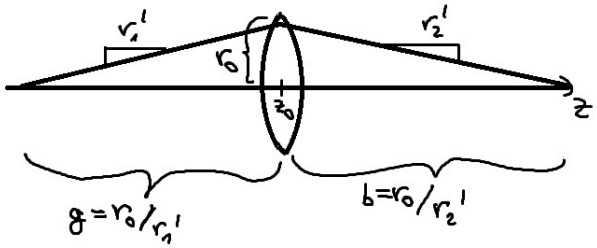

Figure 6.7: A thin lens

$$\begin{aligned} r_1 &= r_2 = r_0 \text{ (the ray does not move laterally during the passage through the thin lens)} \\ \frac{1}{f} &= \frac{1}{r_1/r_1'} + \frac{1}{-r_2/r_2'} = \frac{r_1'}{r_1} - \frac{r_2'}{r_2} \text{ (imaging)} \\ \Rightarrow \vec{r}_2 &= \begin{pmatrix} 1 & 0 \\ -1/f & 1 \end{pmatrix} \cdot \vec{r}_1 \end{aligned} \tag{6.27}$$

Thus we can describe the transition through a thin lens with focal length f by multiplication with a 2×2 matrix $\hat{M} = \begin{pmatrix} 1 & 0 \\ -1/f & 1 \end{pmatrix}$.

(iv) Spherical mirror of radius R: equivalent to a lens of focal length $f = R/2$
planar mirror: $R = \infty$; convex mirror: $R < 0$; concave mirror: $R > 0$

$$\hat{M} = \begin{pmatrix} 1 & 0 \\ -2/R & 1 \end{pmatrix} \tag{6.28}$$

In this way, each optical element can be assigned a ray matrix ("ABCD matrix") $\hat{M} = \left(\begin{smallmatrix} A & B \\ C & D \end{smallmatrix}\right)$. The combination of n optical elements $\hat{M}_1$, $\hat{M}_2$, ..., $\hat{M}_n$ can then be described by

$$\hat{M}_{\text{total}} = \hat{M}_n \cdots \hat{M}_2 \cdot \hat{M}_1, \tag{6.29}$$

assuming that the light ray traverses them in increasing order (first element 1 corresponding to $\hat{M}_1$, etc.).

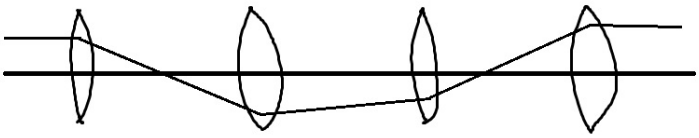

Figure 6.8: A resonator can be represented by lenses separated by the resonator length L.

6.2.2 Resonator stability

In order to investigate the stability of a simple resonator constructed from two curved mirrors (radii R_1 and R_2) spaced by L, we define the round-trip ABCD matrix through the following sequence: start after the first mirror, go to the second mirror, then reflect off of the second mirror, then go to back to the first mirror, and finally reflect off of the first mirror:

$$\begin{aligned}\hat{M}_{\mathrm{RT}} &= \begin{pmatrix} 1 & 0 \\ -\frac{2}{R_1} & 1 \end{pmatrix} \cdot \begin{pmatrix} 1 & L \\ 0 & 1 \end{pmatrix} \cdot \begin{pmatrix} 1 & 0 \\ -\frac{2}{R_2} & 1 \end{pmatrix} \cdot \begin{pmatrix} 1 & L \\ 0 & 1 \end{pmatrix} = \begin{pmatrix} 1-\frac{2L}{R_2} & 2L\left(1-\frac{L}{R_2}\right) \\ \frac{2(2L-R_1-R_2)}{R_1R_2} & \frac{4L^2-2(R_1+2R_2)L+R_1R_2}{R_1R_2} \end{pmatrix} \\ &= \begin{pmatrix} 2g_2-1 & 2g_2L \\ \frac{g_1(4g_2-2)-2g_2}{L} & (4g_1-2)g_2-1 \end{pmatrix} \end{aligned} \tag{6.30}$$

with the dimensionless quantities $g_i = 1 - \frac{L}{R_i}$.

For stability we need to ask: Does the ray stay in the resonator after $n \to \infty$ round-trips? That is,

$$\vec{r}_\infty = \lim_{n\to\infty} \hat{M}_{\mathrm{RT}}^n \cdot \vec{r}_0 \tag{6.31}$$

must not diverge for a stable resonator. For this we look for stable eigenvectors and eigenvalues ($\to$ resonator modes):

$$\hat{M}_{\mathrm{RT}} \cdot \vec{r}_e = \lambda \vec{r}_e \text{ with } |\lambda| \leqslant 1 \text{ for stability} \tag{6.32}$$

The eigenvalues of $\hat{M}_{\mathrm{RT}}$ are

$$\lambda_\pm = 2g_1g_2 - 1 \pm 2\sqrt{g_1g_2(g_1g_2-1)} \tag{6.33}$$

The condition that simultaneously $|\lambda_+| \leqslant 1$ and $|\lambda_-| \leqslant 1$ is only satisfied if

$$\boxed{0 \leqslant g_1g_2 \leqslant 1} \tag{6.34}$$

in which case the eigenvalues are complex-valued, $\lambda_\pm = 2g_1g_2 - 1 \pm 2\mathrm{i}\sqrt{g_1g_2(1-g_1g_2)}$, with $|\lambda_\pm| = 1$. Figure 6.9 shows the different regimes for (g_1, g_2) in which the resonator is stable.

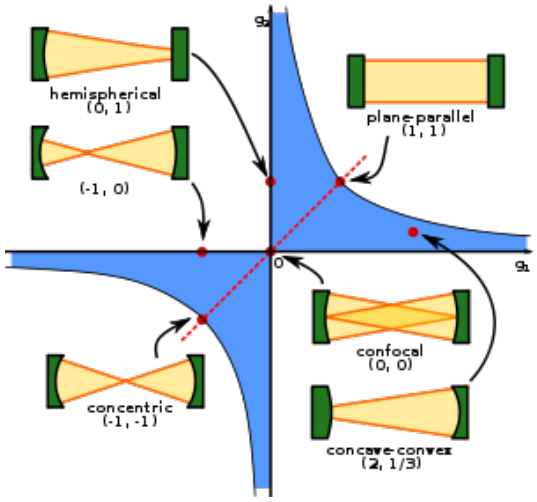

Figure 6.9: Stability diagram: A resonator is stable if it is in the blue-shaded region; it is only marginally stable on the edges of this region. For $g_1 = g_2 = 0$ the resonator is *confocal* ($R_1 = R_2 = L$), for $g_1 = g_2 = 1$ it is a Fabry-Pérot resonator (plane mirrors, $R_1 = R_2 = \infty$), and for $g_1 = g_2 = -1$ the resonator is *concentric* ($R_1 = R_2 = L/2$).

Chapter 7

Laser modes

7.1 Diffraction losses

Diffraction at finite-size mirrors is a cavity loss process: the photons in the resonator are scattered (diffracted) at the mirror edges and leave the resonator.

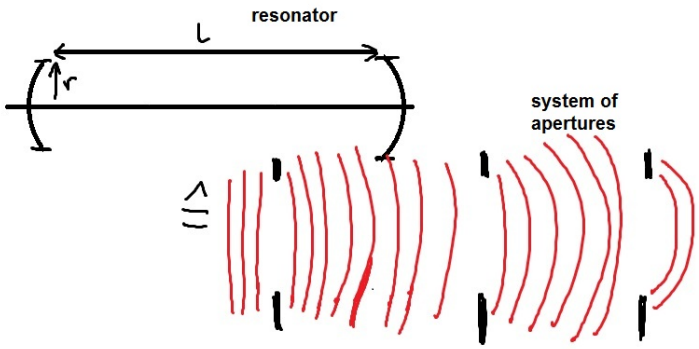

Figure 7.1: A resonator with finite-size mirrors can be treated like a system of apertures, separated by the resonator length L. Diffraction occurs at every aperture.

Fresnel number:

The Fresnel number is defined as

$$N = \frac{r^2}{\lambda L} \tag{7.1}$$

where r is the radius of the apertures/mirrors (assumed both equal) and L the distance between them. For $N \gg 1$ diffraction losses are small (see Figure 7.2 and subsection 7.2.1).

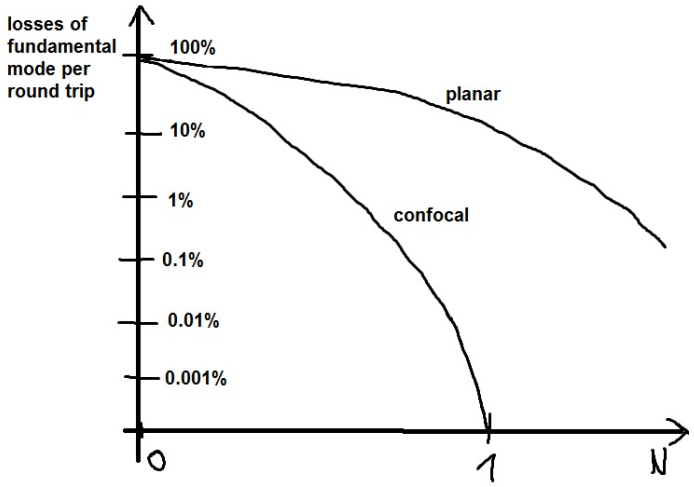

Figure 7.2: Losses of the fundamental mode per round trip as a function of the Fresnel number N for a confocal and a planar resonator

7.2 Paraxial wave equation

Maxwell (vacuum):

$$\vec{\nabla} \times \vec{E} = -\frac{\partial \vec{B}}{\partial t} \tag{7.2a}$$

$$\vec{\nabla} \cdot \vec{E} = 0 \text{ (no charges)} \tag{7.2b}$$

$$\vec{\nabla} \times \vec{B} = \mu_0 \epsilon_0 \frac{\partial \vec{E}}{\partial t} = \frac{1}{c^2} \frac{\partial \vec{E}}{\partial t} \text{ (no currents)} \tag{7.2c}$$

$$\vec{\nabla} \cdot \vec{B} = 0 \tag{7.2d}$$

(remember that $c = 1/\sqrt{\mu_0 \epsilon_0}$), from which follows using Equation (7.2)a and Equation (7.2)c,

$$\vec{\nabla} \times (\vec{\nabla} \times \vec{E}) = -\vec{\nabla} \times \frac{\partial \vec{B}}{\partial t} = -\frac{\partial}{\partial t} \vec{\nabla} \times \vec{B} = -\frac{1}{c^2} \frac{\partial}{\partial t} \frac{\partial E}{\partial t} = -\frac{1}{c^2} \frac{\partial^2 \vec{E}}{\partial t^2} \tag{7.3}$$

Remember that $\vec{\nabla} \times (\vec{\nabla} \times \vec{E}) = \vec{\nabla}(\vec{\nabla} \cdot \vec{E}) - \Delta \vec{E} = -\Delta \vec{E}$ using Equation (7.2)b, with the Laplacian $\Delta = \frac{\partial}{\partial x^2} + \frac{\partial}{\partial y^2} + \frac{\partial}{\partial z^2}$. From this we find

$$\boxed{\Delta \vec{E} - \frac{1}{c^2} \frac{\partial^2}{\partial t^2} \vec{E} = 0} \qquad \text{wave equation} \tag{7.4}$$

In what follows we discuss monochromatic waves: $\vec{E}(\vec{r}, t) = \vec{\mathcal{E}}(\vec{r}) e^{-i\omega t}$

$$\Rightarrow \Delta \vec{\mathcal{E}}(\vec{r}) + k^2 \vec{\mathcal{E}}(\vec{r}) = 0, \qquad k = \frac{\omega}{c} = \frac{2\pi}{\lambda} \qquad \text{Helmholtz equation} \tag{7.5}$$

This equation is to be interpreted for each component of the vector $\vec{\mathcal{E}}$ separately. Some well-known solutions are

$$\vec{\mathcal{E}}(\vec{r}) = \vec{\mathcal{E}}_0 \cdot e^{i\vec{k} \cdot \vec{r}} \qquad \text{plane wave}$$

$$\vec{\mathcal{E}}(\vec{r}) = \vec{A} \cdot \frac{e^{ikr}}{r} \qquad \text{spherical wave} \tag{7.6}$$

with $\|\vec{k}\| = k$ and $\|\vec{r}\| = r$.

For a wave passing an aperture that lies in a plane orthogonal to the z-axis, and propagating approximately along the z-axis, we adopt the following Ansatz:

$$\mathcal{E}(\vec{r}) = \psi(\vec{r}) e^{-ikz}. \tag{7.7}$$

Here, $\mathcal{E}$ stands for any of the three components of the field, which all satisfy Equation (7.5). We assume that $\psi(\vec{r})$ depends only weakly on z on the wavelength scale λ: this is the *paraxial approximation*:

$$\lambda \left|\frac{\partial \psi}{\partial z}\right| \ll |\psi| \Leftrightarrow \left|\frac{\partial \psi}{\partial z}\right| \ll k|\psi| \tag{7.8a}$$

$$\lambda^2 \left|\frac{\partial^2 \psi}{\partial z^2}\right| \ll |\psi| \Leftrightarrow \left|\frac{\partial^2 \psi}{\partial z^2}\right| \ll k^2|\psi| \tag{7.8b}$$

Starting from the Helmholtz Equation (7.5)

$$\begin{aligned} \Delta\mathcal{E} + k^2\mathcal{E} &= 0 \\ \left(\frac{\partial}{\partial x^2} + \frac{\partial}{\partial y^2} + \frac{\partial}{\partial z^2}\right)\psi e^{-ikz} + k^2\psi e^{-ikz} &= 0 \\ \left(\frac{\partial^2 \psi}{\partial x^2} + \frac{\partial^2 \psi}{\partial y^2} + \frac{\partial^2 \psi}{\partial z^2} - 2ik\frac{\partial \psi}{\partial z}\right) e^{-ikz} &= 0 \end{aligned} \tag{7.9}$$

and neglecting the third term in the parenthesis because $\left|\frac{\partial^2 \psi}{\partial z^2}\right| \ll \left|\frac{\partial^2 \psi}{\partial x^2} + \frac{\partial^2 \psi}{\partial y^2}\right|$ gives the

$$\boxed{\Delta_T \psi = 2ik\frac{\partial \psi}{\partial z}} \qquad \text{paraxial wave equation} \tag{7.10}$$

in terms of the transverse Laplacian $\Delta_T = \frac{\partial^2}{\partial x^2} + \frac{\partial^2}{\partial y^2}$ (Cartesian coordinates) or $\Delta_T = \frac{\partial^2}{\partial r^2} + \frac{1}{r}\frac{\partial}{\partial r} + \frac{1}{r^2}\frac{\partial^2}{\partial \phi^2}$ (cylindrical coordinates).

7.2.1 Fresnel diffraction

If the Fresnel number, Equation (7.1), is large ($N \gg 1$), the paraxial wave Equation (7.10) is a very good approximation. In general, knowing any component of the electric field $\mathcal{E}(x, y, z_0)$ in a plane $z = z_0$ then allows us to propagate this component to another plane z with the Fresnel diffraction integral

$$\mathcal{E}(x, y, z) = \frac{e^{ik(z-z_0)}}{i\lambda(z - z_0)} \iint_{-\infty}^{\infty} dx' dy' \mathcal{E}(x', y', z_0) e^{\frac{ik}{2(z-z_0)}[(x-x')^2+(y-y')^2]} \tag{7.11}$$

which is an exact solution of the paraxial wave equation.

For example, if we insert a square aperture into a beam path, what does the beam look like a certain distance after the aperture?

7.3 Gaussian beam

The general solution of the paraxial wave equation, Equation (7.11), is cumbersome in practice and maladapted to the description of optical resonators.

A more specialized solution of the paraxial wave Equation (7.10) is the *Gaussian beam*

$$\boxed{\vec{\mathcal{E}}(r, z) = E_0 \hat{x} \frac{w_0}{w(z)} e^{-\frac{r^2}{w^2(z)}} e^{-i\left(kz + \frac{kr^2}{2R(z)} - \varphi(z)\right)}} \tag{7.12}$$

assuming that the beam is polarized along the x-axis (using the unit vector $\hat{x}$).

- $r = \sqrt{x^2 + y^2}$ and z are the radial and axial coordinates
- $w(z)$ is the *beam waist* at which the beam intensity has dropped to $1/e^2$ of the value on-axis ($r = 0$)
- $R(z)$ is the *radius of curvature* of the wave fronts, see Figure 7.4
- $\varphi(z)$ is the *Gouy phase* that slightly modifies the plane-wave propagation phase kz

- The magnetic field is
$$\vec{\mathcal{B}}(r,z) = -\frac{\mathrm{i}}{\omega}\vec{\nabla}\times\vec{\mathcal{E}} \tag{7.13}$$
satisfying Equation (7.2)a: $\vec{\nabla}\times(\vec{\mathcal{E}}e^{-\mathrm{i}\omega t}) = -\frac{\partial}{\partial t}(\vec{\mathcal{B}}e^{-\mathrm{i}\omega t})$. It has components in the y and z direction (mostly along y); but zero component in the x direction.
- The Poynting vector, describing the direction of propagation of the light energy, is
$$\vec{S}(r,z) = \frac{1}{\mu_0}\vec{E}^*\times\vec{B} = \frac{1}{\mu_0}\vec{\mathcal{E}}^*\times\vec{\mathcal{B}}. \tag{7.14}$$
It has components in the y and z direction (mostly along z); but zero component in the x direction.

Inserting Equation (7.12) into Equation (7.10) (not forgetting Equation (7.7)) gives the differential equations for $w(z)$, $R(z)$, and $\varphi(z)$, with the solutions

$$w(z) = w_0\sqrt{1+\left(\frac{z}{z_0}\right)^2} \tag{7.15a}$$
$$R(z) = z\left[1+\left(\frac{z_0}{z}\right)^2\right] \tag{7.15b}$$
$$\varphi(z) = \arctan\left(\frac{z}{z_0}\right) \tag{7.15c}$$

where $z_0 = \frac{kw_0^2}{2} = \frac{\pi w_0^2}{\lambda}$ is the *Rayleigh range*, and $z = 0$ is the point where the beam has minimal waist (*i.e.*, the beam focus).

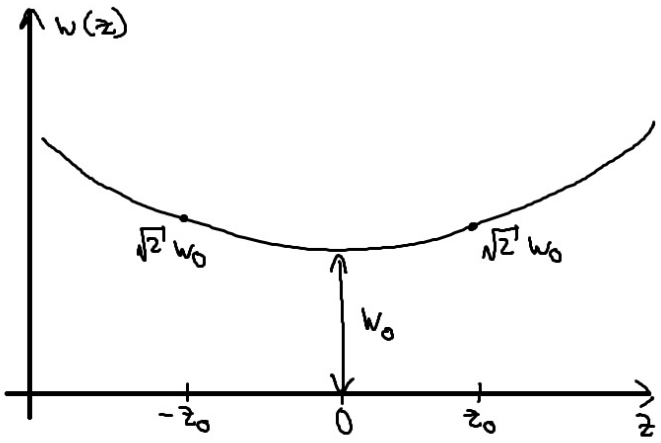

Figure 7.3: The beam waist $w(z)$, Equation (7.15)a, as a function of z

- The paraxial approximation requires that $z_0 \gg w_0 \gg \lambda$
- Gaussian profile gives the minimum beam divergence in the far field.
- Only parameters are λ, w_0

7.3.1 Far-field limit

In the far field, when $|z| \gg z_0$, the beam parameters of Equation (7.15) are approximately

$$w(z) \approx w_0\frac{|z|}{z_0} \tag{7.16a}$$
$$R(z) \approx z \tag{7.16b}$$
$$\varphi(z) \approx \frac{\pi}{2}\,\mathrm{sign}(z) \tag{7.16c}$$

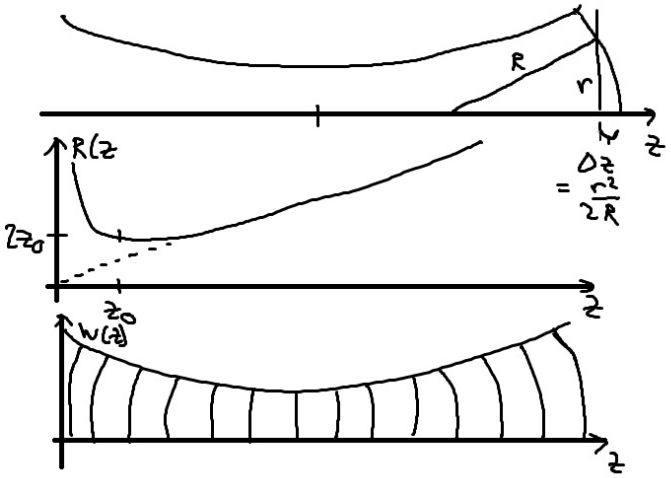

Figure 7.4: Wavefronts of a Gaussian beam. At the waist of the beam ($z = 0$) the radius of curvature $R(z)$, Equation (7.15)b, diverges.

From Equation (7.16)a the far-field divergence half-angle is

$$\tan(\alpha) = \lim_{z\to\infty} \frac{\mathrm{d}w(z)}{\mathrm{d}z} = \frac{w_0}{z_0} = \frac{w_0}{\frac{\pi w_0^2}{\lambda}} = \frac{\lambda}{\pi w_0}. \tag{7.17}$$

We can therefore relate the beam parameters to the far-field divergence half-angle α:

$$w_0 = \frac{\lambda}{\pi \tan(\alpha)} \tag{7.18)a}$$

$$z_0 = \frac{\lambda}{\pi \tan^2(\alpha)} \tag{7.18)b}$$

The Gaussian beam deviates from a classical ray description in a volume around the focus that is described by the longitudinal size z_0 and the transverse size w_0. In the classical ray limit $\lambda \to 0$ this volume shrinks to zero.

We note that the *numerical aperture* of the Gaussian beam is

$$\mathrm{NA} = \sin(\alpha) = \frac{\tan(\alpha)}{\sqrt{1+\tan^2(\alpha)}} = \frac{\lambda}{\sqrt{\lambda^2 + \pi^2 w_0^2}}. \tag{7.19}$$

7.4 Propagation of Gaussian beams

We define the *complex beam parameter* $q(z)$ with

$$\frac{1}{q(z)} = \frac{1}{R(z)} - \mathrm{i}\frac{\lambda}{\pi w^2(z)} \tag{7.20}$$

remembering that both $R(z)$ and $w(z)$ are real-valued. Given a beam parameter q, we calculate the beam waist and the wavefront curvature with

$$w = \sqrt{-\frac{\lambda}{\pi \cdot \Im(1/q)}} \tag{7.21)a}$$

$$R = \frac{1}{\Re(1/q)} \tag{7.21)b}$$

Naturally, a parameter q is only physically meaningful if both $R \in \mathbb{R}$ and $w \in \mathbb{R}$, which means that we must have $\Im(1/q) \leqslant 0$ for physically meaningful Gaussian beams.

7.4.1 Free-space propagation

Using Equation (7.15),

$$q(z) = \left[\frac{1}{z\left[1+\left(\frac{z_0}{z}\right)^2\right]} - \mathrm{i}\frac{\lambda}{\pi w_0^2\left[1+\left(\frac{z}{z_0}\right)^2\right]} \right]^{-1} = z + \mathrm{i}z_0. \tag{7.22}$$

The free-space propagation of a Gaussian beam from a position z_1 to a position z_2 can therefore be done through the complex beam parameter: noticing that $q(z_1) = z_1 + \mathrm{i}z_0$ and $q(z_2) = z_2 + \mathrm{i}z_0$, we find that $q(z_1) - z_1 = q(z_2) - z_2 = \mathrm{i}z_0$ and therefore

$$q(z_2) = q(z_1) + z_2 - z_1. \tag{7.23}$$

Propagation in free space over a distance L is therefore done with

$$\boxed{q_2 = q_1 + L = \frac{1 \cdot q_1 + L}{0 \cdot q_1 + 1}} \tag{7.24}$$

where $q_i = q(z_i)$.

7.4.2 Thin lens

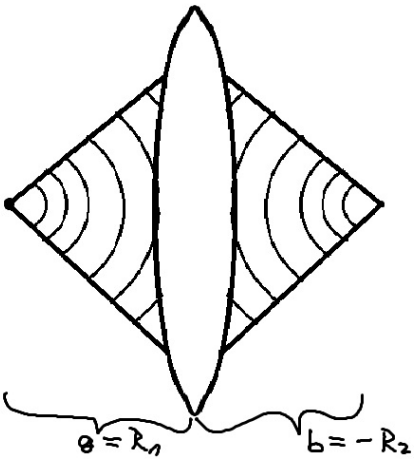

Figure 7.5: Wavefronts of a spherical wave passing through a thin lens

A thin lens affects only the radius of curvature of the beam, not its waist (Figure 7.5):

$$\begin{aligned} \frac{1}{R_1} - \frac{1}{R_2} &= \frac{1}{f} & w_1 &= w_2 \\ \Re(1/q_1) - \Re(1/q_2) &= \frac{1}{f} & \Im(1/q_1) &= \Im(1/q_2) \\ \Re(\frac{1}{q_1} - \frac{1}{q_2}) &= \frac{1}{f} & \Im(\frac{1}{q_1} - \frac{1}{q_2}) &= 0 \end{aligned} \tag{7.25}$$

These are all satisfied if $\frac{1}{q_1} - \frac{1}{q_2} = \frac{1}{f}$, and hence

$$\boxed{q_2 = \frac{f q_1}{f - q_1} = \frac{1 \cdot q_1 + 0}{-\frac{1}{f} \cdot q_1 + 1}} \tag{7.26}$$

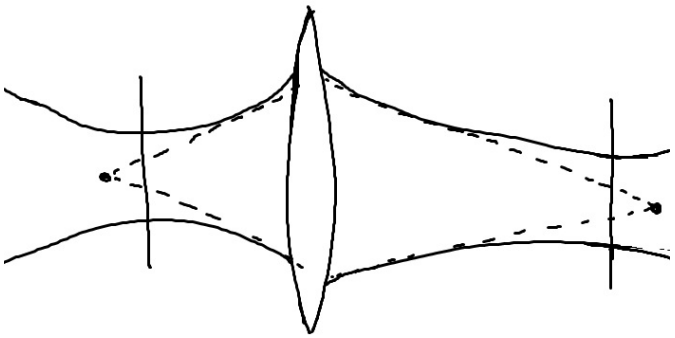

Figure 7.6: In general the position of the waist of a Gaussian beam is not at the same position as the focus in ray optics!

7.4.3 ABCD matrices

Comparing Equation (7.24) and Equation (7.26) with Equation (6.24) and Equation (6.27), we notice that the classical ray propagation with an $\left(\begin{smallmatrix} A & B \\ C & D \end{smallmatrix}\right)$ matrix corresponds to a Gaussian beam propagation

$$q_2 = \frac{A \cdot q_1 + B}{C \cdot q_1 + D} \tag{7.27}$$

This transformation equation defines the connection between ray optics and Gaussian beam optics. Everything in subsection 6.2.1 thus remains valid. In particular, two optical elements can still be described by the product of their ABCD matrices. Consider a first optical element described by $\hat{M}_1 = \left(\begin{smallmatrix} A_1 & B_1 \\ C_1 & D_1 \end{smallmatrix}\right)$ followed by a second optical element $\hat{M}_2 = \left(\begin{smallmatrix} A_2 & B_2 \\ C_2 & D_2 \end{smallmatrix}\right)$. In ray optics, combination of these two elements is described by the matrix

$$\hat{M} = \begin{pmatrix} A & B \\ C & D \end{pmatrix} = \begin{pmatrix} A_2 & B_2 \\ C_2 & D_2 \end{pmatrix} \cdot \begin{pmatrix} A_1 & B_1 \\ C_1 & D_1 \end{pmatrix} = \begin{pmatrix} A_1A_2 + C_1B_2 & B_1A_2 + D_1B_2 \\ A_1C_2 + C_1D_2 & B_1C_2 + D_1D_2 \end{pmatrix} \tag{7.28}$$

In Gaussian beam optics, the propagation through these elements proceeds as

$$\begin{aligned} q_2 &= \frac{A_1 q_1 + B_1}{C_1 q_1 + D_1} \\ q_3 &= \frac{A_2 q_2 + B_2}{C_2 q_2 + D_2} = \frac{A_2 \cdot \frac{A_1 q_1 + B_1}{C_1 q_1 + D_1} + B_2}{C_2 \cdot \frac{A_1 q_1 + B_1}{C_1 q_1 + D_1} + D_2} = \frac{A_2(A_1 q_1 + B_1) + B_2(C_1 q_1 + D_1)}{C_2(A_1 q_1 + B_1) + D_2(C_1 q_1 + D_1)} \\ &= \frac{(A_1A_2 + C_1B_2)q_1 + (B_1A_2 + D_1B_2)}{(A_1C_2 + C_1D_2)q_1 + (B_1C_2 + D_1D_2)}, \end{aligned} \tag{7.29}$$

which is precisely the expression expected from Equation (7.28).

7.5 Resonator modes for Gaussian beams

As in subsection 6.2.2 we construct a resonator from two curved mirrors with radii R_1 and R_2, spaced by a distance L, and define $g_i = 1 - \frac{L}{R_i}$. The cavity ABCD matrix of Equation (6.30) must now satisfy the eigenvalue equation

$$q = \frac{A \cdot q + B}{C \cdot q + D} \tag{7.30}$$

so that q is the resonator eigen-mode. This quadratic equation has two solutions (two modes),

$$q_\pm = \frac{A - D \pm \sqrt{(A-D)^2 + 4BC}}{2C} = L \cdot \frac{(1-g_1)g_2 \pm \sqrt{g_1 g_2 (g_1 g_2 - 1)}}{2g_1 g_2 - g_1 - g_2} \tag{7.31}$$

These solutions are physically relevant only if $\Im(1/q) < 0$ according to Equation (7.21)a. Since $1/q_\pm = \frac{(g_1-1)g_2 \pm \sqrt{g_1 g_2 (g_1 g_2 - 1)}}{g_2 L}$, this can have a negative imaginary part only if $g_1 g_2 (g_1 g_2 - 1) \leqslant 0$, *i.e.*, if $0 \leqslant g_1 g_2 \leqslant 1$. We see that the stability criterion of Equation (6.34) is unchanged: it is valid for both ray optics and Gaussian optics. The relevant cavity mode is thus

$$\hat{q} = \begin{cases} L \cdot \frac{(1-g_1)g_2 + \mathrm{i}\sqrt{g_1 g_2 (1-g_1 g_2)}}{2g_1 g_2 - g_1 - g_2} & \text{if } g1, g2 < 0 \\ L \cdot \frac{(1-g_1)g_2 - \mathrm{i}\sqrt{g_1 g_2 (1-g_1 g_2)}}{2g_1 g_2 - g_1 - g_2} & \text{if } g1, g2 > 0 \end{cases} \tag{7.32}$$

Remember how we had defined the cavity ABCD matrix in subsection 6.2.2: the resonator mode $\hat{q}$ first propagates from mirror 1 to mirror 2. This allows us to find the position of the beam focus in the cavity: propagating a distance z away from mirror 1, the beam parameter is, according to Equation (7.24),

$$\hat{q}(z) = \hat{q} + z \tag{7.33}$$

The focus is the place z_{focus} where $\hat{q}(z_{\text{focus}})$ is purely imaginary, so that the beam waist is minimized and the wavefront curvature radius diverges (Equation (7.21)). Using Equation (7.32) we find that the focus is at a distance

$$z_{\text{focus}} = -L \cdot \frac{(1-g_1)g_2}{2g_1 g_2 - g_1 - g_2} \tag{7.34}$$

from the first mirror. At the focus, the beam parameter is

$$\hat{q}_{\text{focus}} = \mathrm{i}\frac{L\sqrt{g_1 g_2 (1-g_1 g_2)}}{|2g_1 g_2 - g_1 - g_2|} = \mathrm{i}\frac{\pi w_0^2}{\lambda}, \tag{7.35}$$

from which we determine the focal waist and the Rayleigh range

$$w_0 = \sqrt{\frac{\lambda L \sqrt{g_1 g_2 (1-g_1 g_2)}}{\pi |2g_1 g_2 - g_1 - g_2|}} \tag{7.36a}$$

$$z_0 = \frac{\pi w_0^2}{\lambda} = L \cdot \frac{\sqrt{g_1 g_2 (1-g_1 g_2)}}{|2g_1 g_2 - g_1 - g_2|} \tag{7.36b}$$

Relative to this focus, the first mirror is located at position $z_1 = -z_{\text{focus}} = -L \cdot \frac{(g_1-1)g_2}{2g_1 g_2 - g_1 - g_2}$, and the second mirror at $z_2 = z_1 + L = L \cdot \frac{(g_2-1)g_1}{2g_1 g_2 - g_1 - g_2}$.

See Equation (7.12): the total phase of a propagating Gaussian beam on the axis ($r = 0$) is given by

$$\vartheta(z) = kz - \varphi(z) = kz - \arctan\left(\frac{z}{z_0}\right) \tag{7.37}$$

where kz is the phase of a plane wave and $\arctan \frac{z}{z_0}$ the Gouy phase. In a resonator, the phase accumulated between the left mirror (at $z = z_1$) and the right mirror (at $z = z_2$) must be an integer multiple of π:

$$\vartheta(z_2) - \vartheta(z_1) = \ell \cdot \pi \qquad \text{with } \ell \in \mathbb{Z} \tag{7.38}$$

With the above expressions for z_1 and z_2 this condition becomes, after some trigonometric magic,

$$\begin{aligned} k(z_2 - z_1) - \arctan\left(\frac{z_2}{z_0}\right) + \arctan\left(\frac{z_1}{z_0}\right) &= \ell \cdot \pi \\ \Rightarrow kL - \arctan\left(\frac{L \cdot \frac{(g_2-1)g_1}{2g_1 g_2 - g_1 - g_2}}{L \cdot \frac{\sqrt{g_1 g_2 (1-g_1 g_2)}}{|2g_1 g_2 - g_1 - g_2|}}\right) + \arctan\left(\frac{-L \cdot \frac{(g_1-1)g_2}{2g_1 g_2 - g_1 - g_2}}{L \cdot \frac{\sqrt{g_1 g_2 (1-g_1 g_2)}}{|2g_1 g_2 - g_1 - g_2|}}\right) &= \ell \cdot \pi \\ \Rightarrow kL - \left(\frac{\pi}{2} \mp \arcsin\sqrt{g_1 g_2}\right) &= \ell \cdot \pi \\ \Rightarrow kL = (\ell + \frac{1}{2}) \cdot \pi \mp \arcsin\sqrt{g_1 g_2} & \\ \Rightarrow \nu_\ell = \frac{c}{2L}\left[\ell + \frac{1}{\pi}\left(\frac{\pi}{2} \mp \arcsin\sqrt{g_1 g_2}\right)\right] & \end{aligned} \tag{7.39}$$

where the upper sign stands for $g_1, g_2 > 0$ and the lower sign for $g_1, g_2 < 0$. These are the frequencies of the modes of the resonator. Note that the frequency spacing $\Delta\nu = \frac{c}{2L}$ is the same as for the Fabry-Pérot resonator.

7.6 Transverse modes

A complete set of solutions for the paraxial wave equation for a stable resonator is given by the Hermite–Gauss modes for $(m, n) \in \mathbb{N}_0^2$:

$$\psi_{mn}(x, y, z) = \psi_0 \frac{w_0}{w(z)} H_m\left(\frac{x\sqrt{2}}{w(z)}\right) H_n\left(\frac{y\sqrt{2}}{w(z)}\right) \cdot e^{-\frac{r^2}{w^2(z)}} e^{-i\left(\frac{kr^2}{2R(z)} + \varphi(z)\right)} \tag{7.40}$$

with $r = \sqrt{x^2 + y^2}$. Here, $w(z)$ and $R(z)$ are the same as before, but the Gouy phase is now

$$\varphi(z) = (m + n + 1) \arctan\left(\frac{z}{z_0}\right). \tag{7.41}$$

The first Hermite polynomials are

$$\begin{aligned} H_0(x) &= 1 \\ H_1(x) &= 2x \\ H_2(x) &= 4x^2 - 2 \\ H_3(x) &= 8x^3 - 12x. \end{aligned} \tag{7.42}$$

- Same wave front curvature as for Gaussian beams → the stability condition of resonators is independent of m, n.
- The transverse dimension increases with $m, n \to$ higher diffraction losses. Specifically, the root-mean-square beam diameters scale as $\sqrt{\langle x^2 \rangle} \propto \sqrt{1 + 2m}$ and $\sqrt{\langle y^2 \rangle} \propto \sqrt{1 + 2n}$.
- m, n indicate the number of node lines in x and y direction.

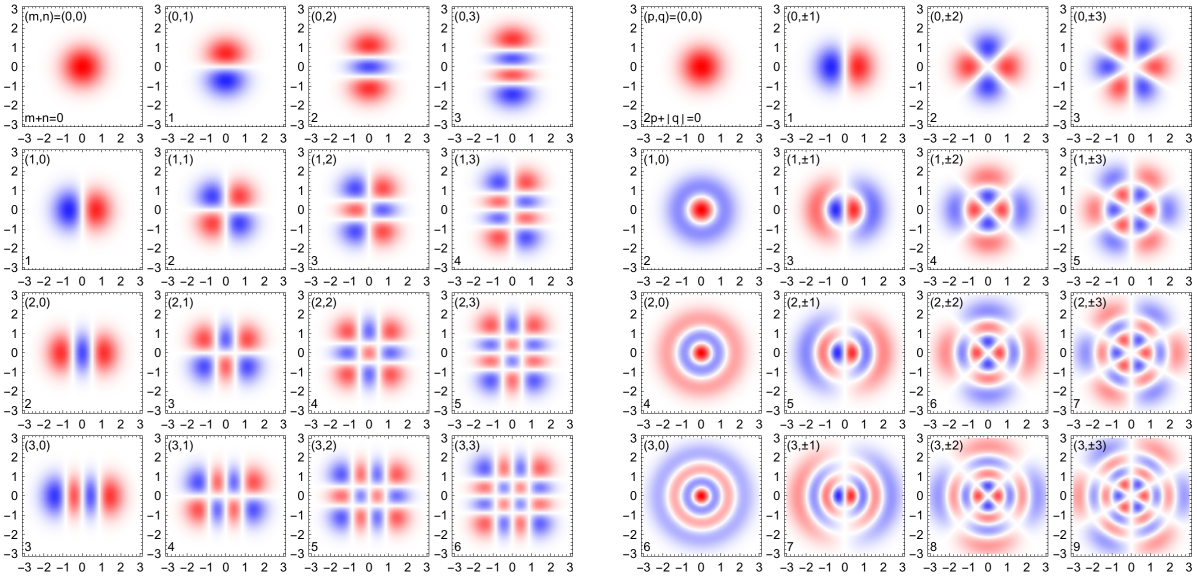

Figure 7.7: A few low-order transverse modes: Hermite–Gauss (left, Equation (7.40)) and Laguerre–Gauss (right, Equation (7.47)) modes. Red and blue regions have opposite sign. The scaled coordinates are $x/w(z)$ and $y/w(z)$. Degenerate Hermite–Gauss modes (with equal $m+n$) can be combined into degenerate Laguerre–Gauss modes (with equal $2p + |q|$) and vice-versa, since they have the same frequency (see Equation (7.43) and Equation (7.50)). Note that for the Laguerre–Gauss modes with $q \neq 0$ there are two degenerate solutions; we have only plotted their real-valued symmetric combination $\psi_{p,-q}(r, \phi) + \psi_{p,q}(r, \phi)$, whereas the other solution is found by a rotation around the center.

- Resonance frequencies:

$$\begin{aligned}\nu_{\ell mn} &= \frac{c}{2L}\left[\ell + \frac{m+n+1}{\pi}\left(\frac{\pi}{2} \mp \arcsin\sqrt{g_1 g_2}\right)\right] \\ &= \ell \cdot \underbrace{\frac{c}{2L}}_{\Delta\nu_{\text{FSR}}} + (m+n+1)\cdot \underbrace{\frac{c}{2\pi L}\left(\frac{\pi}{2} \mp \arcsin\sqrt{g_1 g_2}\right)}_{\Delta\nu_{\text{Gouy}}}\end{aligned} \tag{7.43}$$

Examples:

- Planar FP resonator ($g_1 = g_2 = 1$):

$$\nu_{\ell mn} = \frac{c}{2L}\cdot\ell \qquad \text{(degeneracy!)} \tag{7.44}$$

- confocal ($g_1 = g_2 = 0$)

$$\begin{aligned}\nu_{\ell mn} &= \frac{c}{2L}\left[\ell + \frac{m+n+1}{2}\right] && \text{for a beam exactly on the axis} \\ \nu_{\ell mn} &= \frac{c}{4L}\left[\ell + \frac{m+n+1}{2}\right] && \text{for a beam with transverse displacement, requiring} \\ & && \text{two round-trips until overlapping the initial position}\end{aligned} \tag{7.45}$$

- concentric ($g_1 = g_2 = -1$)

$$\nu_{\ell mn} = \frac{c}{2L}(\ell + m + n + 1) \tag{7.46}$$

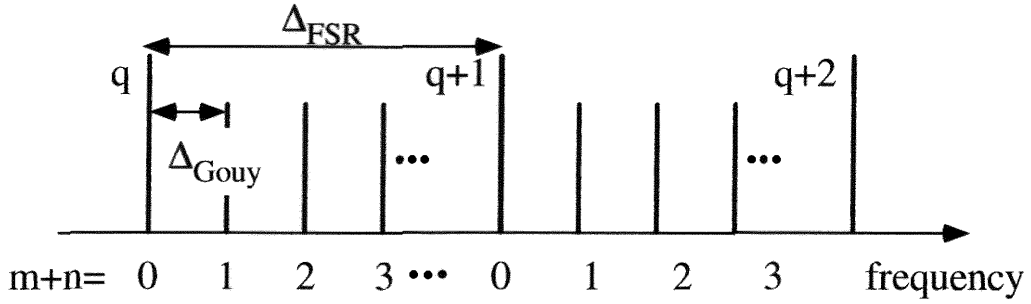

Figure 7.8: Transmission spectrum of a concentric resonator for transverse Hermite–Gauss modes, see Equation (7.43). For Laguerre–Gauss modes, replace $m+n$ with $2p+|q|$, see Equation (7.50).

For a completely cylindrically symmetric resonator the Laguerre–Gauss modes are more useful. Example: doughnut mode (see Figure 7.7). For this, degenerate modes of Equation (7.40) are added to form the cylindrically symmetric modes for $p \in \mathbb{N}_0$ and $q \in \mathbb{Z}$:

$$\psi_{pq}(r,\phi,z) = \psi_0 \frac{w_0}{w(z)}\left(\frac{r\sqrt{2}}{w(z)}\right)^{|q|} L_p^{|q|}\left(\frac{2r^2}{w^2(z)}\right)\cdot e^{-\frac{r^2}{w^2(z)}} e^{-\mathrm{i}\left(q\phi + \frac{kr^2}{2R(z)} + \varphi(z)\right)}. \tag{7.47}$$

where L_p^a are generalized Laguerre polynomials:

$$\begin{aligned}L_0^a(x) &= 1 \\ L_1^a(x) &= 1 + a - x \\ L_2^a(x) &= \frac{a^2 + 3a + 2 - 2(a+2)x + x^2}{2} \\ L_3^a(x) &= \frac{a^3 + 6a^2 + 11a + 6 - 3(a^2 + 5a + 6)x + 3(a+3)x^2 - x^3}{6}\end{aligned} \tag{7.48}$$

- The Gouy phase is now

$$\varphi(z) = (2p + |q| + 1) \arctan\left(\frac{z}{z_0}\right) \tag{7.49}$$

- The transverse dimension increases with p and q → higher diffraction losses. Specifically, the root-mean-square beam diameter scales as $\sqrt{\langle r^2 \rangle} \propto \sqrt{1 + 2p + |q|}$.
- p indicates the number of radial node lines
- q indicates the azimuthal dependence $e^{-\mathrm{i}q\phi}$: $|q|$ azimuthal node lines in the real-valued combinations $(\psi_{p,q} + \psi_{p,-q})/\sqrt{2}$ and $(\psi_{p,q} - \psi_{p,-q})/(\mathrm{i}\sqrt{2})$.
- Resonance frequencies: comparing Equation (7.41) with Equation (7.49),

$$\nu_{\ell pq} = \frac{c}{2L}\left[\ell + \frac{2p + |q| + 1}{\pi}\left(\frac{\pi}{2} \mp \arcsin\sqrt{g_1 g_2}\right)\right] \tag{7.50}$$

7.7 Mode selection

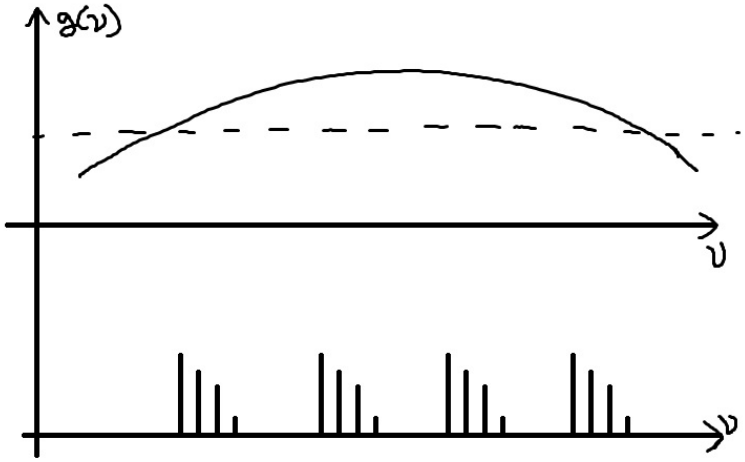

Figure 7.9: Without mode selection a laser can operate on several longitudinal ℓ and transverse (m, n) modes at the same time.

A laser resonator can operate (lase) on many modes, with frequencies given in Equation (7.43) or Equation (7.50). How can we ensure that the laser puts out a monochromatic light beam, originating from only a single optical mode?

An optical mode can only generate laser light if its gain is larger than its losses (chapter 3). In order to select one particular optical mode, we therefore need to (i) maximize its gain and (ii) minimize its losses, while for all other modes we (i) minimize the gain and (ii) maximize the losses. A combination of gain and loss modulations is usually sufficient to limit lasing operation to a single optical mode.

The gain profile of most laser media has a strong wavelength dependence. For example, Nd:YAG crystals only provide significant gain around wavelengths of 1064 nm; helium-neon gas only has gain around 632.8 nm. Usually, no further gain modulation is added to the laser.

The remaining mode selection tries to minimize the loss of the desired mode while maximizing the losses of all other modes, with the goal of having only one single mode whose loss is smaller than its gain.

Specific loss-modulation techniques are:

1. Get rid of higher transverse modes by introducing losses for these modes. The easiest way to do so is to place an aperture into the beam, since higher-order transverse modes have a larger radius than the $(m, n) = (0, 0)$ mode (see above).

2. Selection of one polarization out of two per mode. This can for example be achieved by the shape of the active medium: inclined facets can allow one polarization to pass without attenuation (Brewster's angle), while the other polarization is (partly) reflected out of the resonator. Due to mode-competition, the wrong polarization mode dies out. Any birefringent effect can be used to this end.

3. Longitudinal mode selection: Rough (laser line): Gratings (*e.g.*, CO_2 laser, semiconductor laser), prisms (Ar^+ laser).

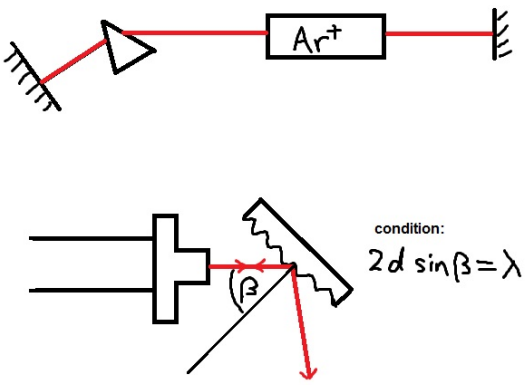

Figure 7.10: Methods of longitudinal mode selection: With a prism (top) and a grating (bottom), only a narrow frequency range is back-reflected into the resonator; "wrong" frequencies refracted out of the beam path and thus experience higher loss.

Another possibility for a rough selection is a birefringent (Lyot) filter (= adjustable λ-phase plate + polarizer). This gives transmission:

$$T(\lambda) = T_0 \cos^2\left(\frac{\pi \Delta n L}{\lambda}\right). \tag{7.51}$$

With these methods we can limit the spectral width down to $\sim 1\,\mathrm{nm}$

4. Longitudinal mode selection: Fine selection
Introduce an intra-cavity étalon (low-finesse Fabry-Pérot interferometer = glass plate, see section 6.1), which has 100% transmission for resonant frequencies and higher loss for all other frequencies. This allows to reduce the spectral width of the laser to $\sim 1\,\mathrm{MHz}$.

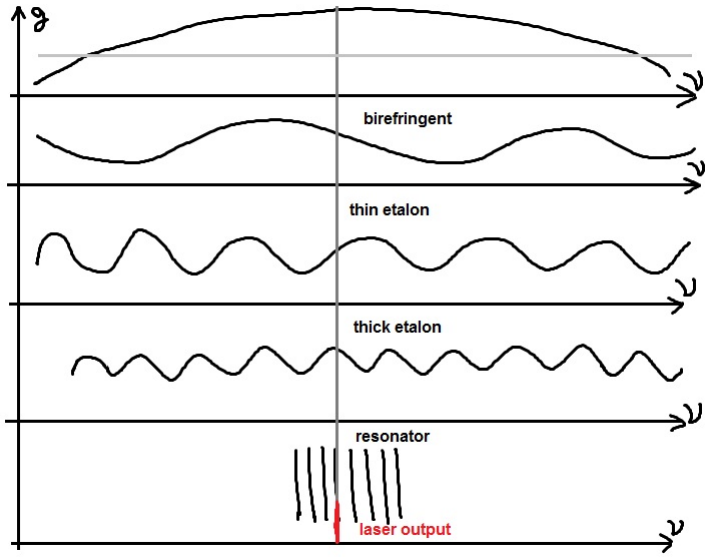

Figure 7.11: Combination of all longitudinal mode selective elements. The losses of all modes except one are increased above their respective gain.

Chapter 8

Short laser pulses

Recall: for a 4-level laser, the differential equations for the inversion density $I = n_2$ and the laser-mode photon density p_{laser} are (from Equation (3.13)b and Equation (3.16), using the translation table on page 17)

$$\dot{n}_2(t) = -[c\sigma_{21}p_{\text{laser}}(t) + S_{21}]n_2(t) + W_{\text{pump}}[n - n_2(t)] \tag{8.1a}$$

$$\dot{p}_{\text{laser}}(t) = -[\gamma - c\sigma_{21}n_2(t)]p_{\text{laser}}(t) \tag{8.1b}$$

where we have again made the adiabatic assumptions $n_1 = n_3 = 0$. Also, remember that the loss rate $\gamma = \tau_{\text{photon}}^{-1}$ is the inverse of the photon lifetime in the resonator.

To simplify the solution of these coupled differential equations, we introduce the following dimensionless quantities:

$$\begin{aligned}
\tau &= \gamma t && \text{dimensionless time} \\
s_{21} &= \frac{S_{21}}{\gamma} && \text{dimensionless spontaneous emission rate} \\
w_{\text{pump}} &= \frac{W_{\text{pump}}}{\gamma} && \text{dimensionless pump rate} \\
w_{\text{th}} &= \frac{W_{\text{th}}}{\gamma} && \text{dimensionless threshold pump rate} \\
\nu_2(t) &= \frac{n_2(t)}{n} && \text{fractional inversion} \\
\pi_{\text{laser}}(t) &= \frac{p_{\text{laser}}(t)}{n} && \text{scaled laser photon number} \\
\nu_{\text{th}} &= \frac{\gamma}{cn\sigma_{21}} && \text{fractional threshold inversion}
\end{aligned} \tag{8.2}$$

With these, the differential equations of Equation (8.1) depend only on three independent dimensionless parameters $(\nu_{\text{th}}, s_{21}, w_{\text{pump}})$:

$$\dot{\nu}_2(\tau) = -[\pi_{\text{laser}}(\tau)/\nu_{\text{th}} + s_{21}]\nu_2(\tau) + w_{\text{pump}}[1 - \nu_2(\tau)] \tag{8.3a}$$

$$\dot{\pi}_{\text{laser}}(\tau) = -[1 - \nu_2(\tau)/\nu_{\text{th}}]\pi_{\text{laser}}(\tau) \tag{8.3b}$$

In section 3.6 we studied the stationary (equilibrium) solutions $\dot{\nu}_2 = \dot{\pi}_{\text{laser}} = 0$ of these differential equations:

- *Below threshold:*

$$\pi_{\text{laser}} = 0 \tag{8.4a}$$

$$\nu_2 = \frac{w_{\text{pump}}}{w_{\text{pump}} + s_{21}} \tag{8.4b}$$

- *Above threshold:*

$$\pi_{\text{laser}} = w_{\text{pump}} \cdot (1 - \nu_{\text{th}}) - \nu_{\text{th}}s_{21} = (w_{\text{pump}} - w_{\text{th}}) \cdot (1 - \nu_{\text{th}}) \tag{8.5a}$$

$$\nu_2 = \nu_{\text{th}} \tag{8.5b}$$

- *Threshold:* $w_{\text{th}} = \frac{s_{21}}{1/\nu_{\text{th}} - 1}$

8.1 Dynamics: switching a laser on

Outside of equilibrium, the differential equations in Equation (8.1) or Equation (8.3) cannot be solved analytically. We look at a few special cases numerically.

For all simulations, we set

- $W_{\text{pump}} = 2W_{\text{th}}$: we pump at twice the threshold pump power. Implying $w_{\text{pump}} = 2 \cdot \frac{s_{21}}{1/\nu_{\text{th}}-1}$.
- $\lim_{t\to\infty} n_2(t) = 0.1n$: at equilibrium there is a small population inversion. Implying $\nu_{\text{th}} = 0.1$.
- $n_2(0) = 0$: no population inversion at the beginning of the simulation. Implying $\nu_2(0) = 0$.
- $p_{\text{laser}}(0) = 10^{-6} \cdot \lim_{t\to\infty} p_{\text{laser}}(t)$: very small photon population at the beginning of the simulation. Implying $\pi(0) = 10^{-6} \cdot (w_{\text{pump}} - w_{\text{th}}) \cdot (1 - \nu_{\text{th}}) = 10^{-6} \cdot [w_{\text{pump}} - (w_{\text{pump}} + s_{21})\nu_{\text{th}}]$.

8.1.1 Switching on a low-efficiency laser

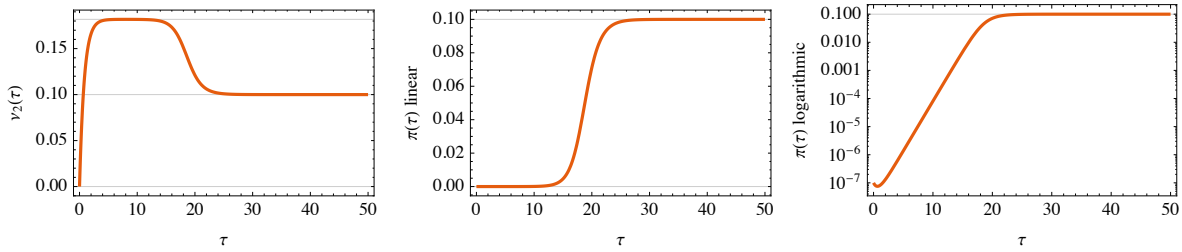

Figure 8.1: Dynamics of switching on a low-efficiency laser, by numerical solution of Equation (8.3). The parameters are $s_{21} = 1$, $\nu_{\text{th}} = 0.1$, $w_{\text{pump}} = 2/9$; the initial conditions are $\nu_2(0) = 0$, $\pi(0) = 10^{-7}$. The inversion builds up on a time scale $\Delta\tau_{\text{inversion}} \approx 0.8$ to a quasi-stationary level $\nu_2 \approx w_{\text{pump}}/(w_{\text{pump}} + s_{21})$; the photon population builds up exponentially on the time scale $\Delta\tau_{\text{laser}} \approx 1.2$ (starting from a very small level) and depletes the inversion to its equilibrium value ν_{th}. This is the regime in which continuous-wave (cw) lasers usually operate.

See Figure 8.1: for large s_{21} the inversion builds up very fast while the photon population builds up much more slowly. To describe the build-up of the inversion at small times, we approximate Equation (8.3)a as

$$\dot{\nu}_2(\tau) \approx -s_{21}\nu_2(\tau) + w_{\text{pump}}[1 - \nu_2(\tau)] \tag{8.6}$$

with the solution

$$\nu_2(\tau) \approx \frac{w_{\text{pump}}}{w_{\text{pump}} + s_{21}} \cdot \left(1 - e^{-(w_{\text{pump}}+s_{21})\tau}\right) \tag{8.7}$$

We see that within a time $\Delta\tau_{\text{inversion}} \sim (w_{\text{pump}} + s_{21})^{-1}$ the inversion builds up to a stationary value of $\nu_2 \approx w_{\text{pump}}/(w_{\text{pump}} + s_{21})$, which is larger than the equilibrium value of ν_{th}, Equation (8.5)b. This excess inversion then allows the photon population to build up: Equation (8.3)b is, assuming constant $\nu_2 = w_{\text{pump}}/(w_{\text{pump}} + s_{21})$,

$$\dot{\pi}_{\text{laser}}(\tau) \approx \left(\frac{w_{\text{pump}}}{w_{\text{pump}} + s_{21}}/\nu_{\text{th}} - 1\right) \pi_{\text{laser}}(\tau) \tag{8.8}$$

with the exponential solution

$$\pi_{\text{laser}}(\tau) \approx \pi_{\text{laser}}(0) \cdot e^{\left(\frac{w_{\text{pump}}}{w_{\text{pump}}+s_{21}}/\nu_{\text{th}}-1\right)\tau} \tag{8.9}$$

The time scale for building up the laser power is therefore $\Delta\tau_{\text{laser}} \sim \left(\frac{w_{\text{pump}}}{w_{\text{pump}}+s_{21}}/\nu_{\text{th}} - 1\right)^{-1}$, starting (usually) from a very small initial population.

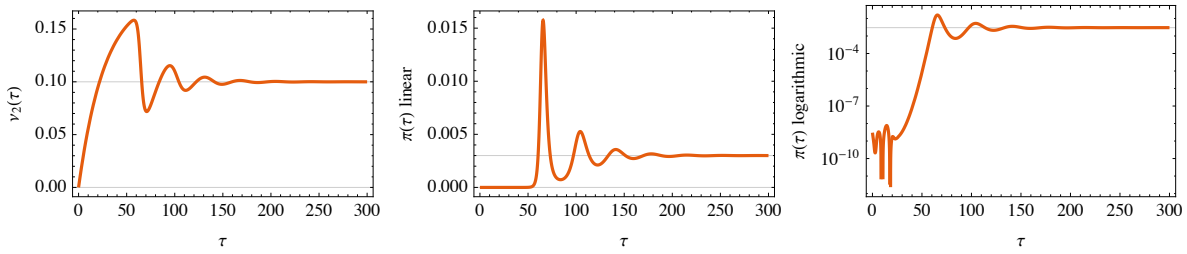

Figure 8.2: Dynamics of switching on a high-efficiency laser, by numerical solution of Equation (8.3). The parameters are $s_{21} = 0.03$, $\nu_{\text{th}} = 0.1$, $w_{\text{pump}} = 1/150$; the initial conditions are $\nu_2(0) = 0$, $\pi_{\text{laser}}(0) = 3 \times 10^{-9}$. The inversion builds up on a slow time scale $\Delta\tau_{\text{inversion}} \approx 27$; the photon population builds up on the much faster time scale $\Delta\tau_{\text{laser}} \approx 1.2$ and periodically over-depletes the inversion, leading to a pulsed laser output.

8.1.2 Switching on a high-efficiency laser

See Figure 8.2: for small s_{21} the inversion builds up more slowly than the photon population; transient laser pulsing ("ringing") results from the periodic over-depletion of the inversion. The duration of the first pulse is on the order of $\Delta\tau_{\text{pulse}} \sim \Delta\tau_{\text{laser}} \sim \left(\frac{w_{\text{pump}}}{w_{\text{pump}}+s_{21}}/\nu_{\text{th}} - 1\right)^{-1}$ given above.

8.2 Q-Switching

Switching an entire laser on and off, particularly its pump w_{pump}, is difficult to do within a short amount of time. To generate short laser pulses, an alternative to subsection 8.1.2 is usually used.

Assume that the laser resonator contains a special element, called a *Q-switch*, which can modify the losses: it can be either in a low-loss state, $\gamma = \gamma_0$, or in a high-loss state, $\gamma \to \infty$ (or at least such a large value that the laser is below threshold). This switch can usually change its state within very short amounts of time: nanoseconds or even shorter.

8.2.1 Q-switch in the high-loss state

For sufficiently large γ (when the Q-switch is in the high-loss state) the laser is below threshold and is described approximately by the differential equation

$$\begin{aligned} \dot{\nu}_2(\tau) &\approx -s_{21}\nu_2(\tau) + w_{\text{pump}}[1 - \nu_2(\tau)] \\ &\Rightarrow \nu_2(\tau) \approx \nu_2(0) \cdot e^{-(s_{21}+w_{\text{pump}})\tau} + \frac{w_{\text{pump}}}{s_{21} + w_{\text{pump}}}\left[1 - e^{-(s_{21}+w_{\text{pump}})\tau}\right] \qquad (8.10\text{a}) \\ \pi_{\text{laser}}(\tau) &\approx 0 \qquad (8.10\text{b}) \end{aligned}$$

leading to a stationary state of $\nu_2 \approx \frac{w_{\text{pump}}}{s_{21}+w_{\text{pump}}}$ and $p \approx 0$ after a buildup time of $\Delta t_{\text{inversion}} \sim (W_{\text{pump}} + S_{21})^{-1}$. This stationary state is independent of the exact value of γ and even persists in the limit $\gamma \to \infty$. Keep in mind that π_{laser} is never exactly zero because of spontaneous emission.

8.2.2 Q-switch in the low-loss state

Once the above equilibrium has been reached, we abruptly switch the Q-switch to its low-loss state $\gamma = \gamma_0$ and bring the laser above its threshold. Assuming a high-efficiency situation, we solve the differential Equation (8.3) in the same was as in subsection 8.1.2, but this time using as initial conditions the stationary state of subsection 8.2.1: $\nu_2(\tau = 0) = \frac{w_{\text{pump}}}{s_{21}+w_{\text{pump}}}$.

There is no need for the switching process to be fast; it may be significantly longer than both the buildup timescale $\Delta\tau_{\text{laser}}$ and the resonator round-trip time.

See Figure 8.3: after "closing the Q-switch" (*i.e.*, switching it to low-loss mode), the laser light builds up exponentially and generates a series of light pulses. The timing of the first light pulse depends on the

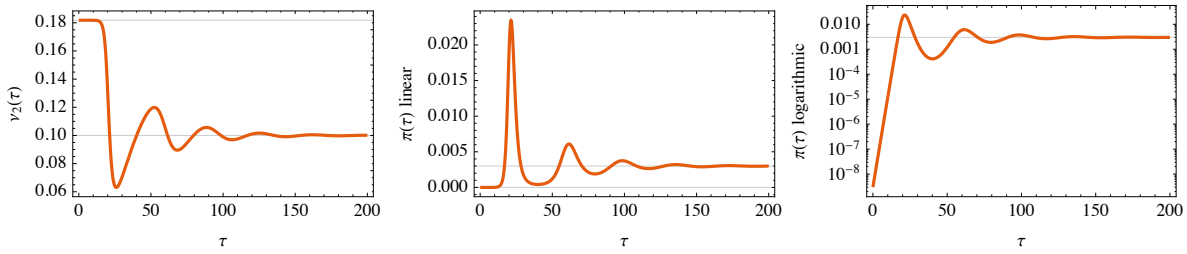

Figure 8.3: Dynamics of Q-switching a high-efficiency laser, by numerical solution of Equation (8.1). The parameters are $s_{21} = 0.03$, $\nu_{\text{th}} = 0.1$, $w_{\text{pump}} = 1/150$ as in Figure 8.2; the initial conditions are $\nu_2(0) = \frac{w_{\text{pump}}}{s_{21}+w_{\text{pump}}} = 0.18$, $\pi(0) = 3 \times 10^{-9}$. The same pulses as in Figure 8.2 are observed, but with larger intensity and more controlled timing.

exact amount of light present in the resonator mode at the time of closing the Q-switch, which can come from spontaneous emission (fluctuates!) or from injection-seeding a weak but stable external laser beam.

If the Q-switch is re-opened after the first pulse (around $\tau = 40$ in this example), then only a single pulse is generated and exits through the output coupler. Again, the duration of the first pulse is on the order of $\Delta\tau_{\text{pulse}} \sim \Delta\tau_{\text{laser}} \sim \left(\frac{w_{\text{pump}}}{w_{\text{pump}}+s_{21}}/\nu_{\text{th}} - 1\right)^{-1}$. Pulses of few nanoseconds duration can be generated in this way.

Example: Q-switched Nd:YAG laser

The laser medium is 'charged' with energy within $\sim 100\,\mu$s, while the 'discharge' takes only $\sim 10\,$ns by laser pulse $\Rightarrow$ peak power $\gg$ pump power.

Typical laser pumped by flash lamps has a peak power of

$$\hat{P} \sim 1\,\text{J}/10\,\text{ns} = 100\,\text{MW} \tag{8.11}$$

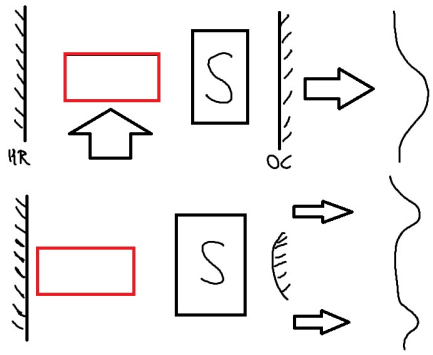

Figure 8.4: Typical experimental realizations of a Q-switched laser. S stands for the saturable absorber in the case of passive Q-switching or for the modulator in the case of active Q-switching. The bottom scheme shows an instable resonator built with one plane and one convex highly reflecting mirrors.

8.2.3 Passive Q-switching with a saturable absorber

A saturable absorber is a material, placed inside the optical resonator, with an absorption that depends on the light intensity in the resonator. As long as there is very little light in the resonator, the absorber introduces a large loss ("the Q-switch is off", subsection 8.2.1) and the laser is below threshold.

When the inversion in the active medium reaches large values, spontaneous emission starts to become so intense that the absorber becomes saturated. This can most easily be visualized (and realized) by an effective 2-level system: by pumping population from the ground into the excited state, the rate of stimulated emission starts to reach the rate of absorption and the absorber becomes transparent. As a result, the loss is reduced dramatically and the Q-switch is closed (subsection 8.2.2).

Specifically, the intensity-dependent absorption coefficient of the saturable absorber is

$$\alpha(I) = \frac{\alpha_0}{1 + I/I_S} \tag{8.12}$$

where I_S is the saturation intensity. Mostly dye solutions are used:

+ broad absorption bands

+ high α_0, giving good lasing suppression

○ $p_S \sim 5 \times 10^{11}\,\mathrm{W/m^2}$

– photochemically instable

Passive Q-switching leads to automatic pulsed operation of the laser, emitting short laser pulses in a more-or-less regular pattern. A big disadvantage of this technique is that the pulses cannot be externally triggered, since they occur spontaneously.

There are applications, however, where pulse regularity is not required, for example in laser cutting.

8.2.4 Active Q-switching

Active Q-switches have the great advantage that they allow for a precise control over the time at which pulses occur. Specific techniques include

- Acousto-optic modulation: An ultrasonic acoustic wave inside a crystal Bragg-deflects the intra-cavity mode. By rapidly switching this acoustic wave on or off, the Q-switch is operated. Sub-microsecond switching time.

- Electro-optic modulation (Pockels effect): A strong electric field rotates the polarization of the intra-cavity mode. By using other polatization-dependent elements (section 7.7) this allows Q-switching. Few-nanosecond switching time.

Most active Q-switches do not absorb in the high-loss state, but rather deviate the beam out of the resonator. This property is often used to out-couple the useable laser beam (instead of through an output coupling end-mirror). Upon re-opening the Q-switch (when the buildup of the first pulse is complete, see Figure 8.3), the entire light energy present in the resonator is deflected and becomes the output beam within a single cavity round-trip. In this way, even shorter laser pulses of $\Delta t \sim 2L/c$ are generated (as long as the Q-switching time is smaller than $2L/c$).

8.3 Mode locking

Mode locking is a method for producing femtosecond ($1\,\mathrm{fs} = 10^{-15}\,\mathrm{s}$) laser pulses. The laser pulse is much shorter than the cavity: $\Delta t \ll 2L/c$ (see subsection 8.2.4 for comparison with a Q-switched laser).

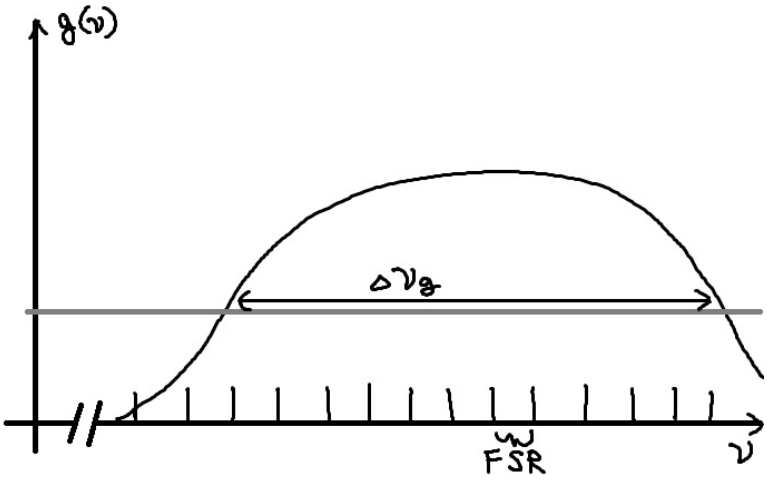

Figure 8.5: For a broad gain profile $g(\nu)$ several modes that are supported by the resonator can participate in lasing.

8.3.1 Principle

Since $c \cdot \Delta t \ll 2L$ we must have $\Delta\nu \gg \Delta\nu_{\text{FSR}} = \frac{c}{2L}$ (see subsection 4.1.1): the laser must operate simultaneously on many longitudinal modes. In order to generate short pulses, we need simultaneous lasing of many longitudinal modes with *fixed phase relations*.

For this we need a broad gain profile $g(\nu)$ with a width $\Delta\nu_g \gg \Delta\nu_{\text{FSR}}$; see Figure 8.5.

For many resonators, $\Delta\nu_{\text{FSR}} = \frac{c}{2L}$ (see section 7.6). In general, we assume that the ℓ^{th} mode has a frequency $\nu_\ell = \nu_0 + \ell \cdot \Delta\nu_{\text{FSR}}$, that is, we assume that the spectrum of the resonator is linear and that there are no transverse excitations ($m = n = 0$; spatial mode filtering as in section 7.7). The electric-field amplitude (in a given polarization direction) in the resonator can be written as a sum over longitudinal modes,

$$\mathcal{E}(\vec{r}, t) = \sum_{\ell=0}^{\infty} c_\ell \mathcal{E}_\ell(\vec{r}) e^{2\pi i \nu_\ell t} \tag{8.13}$$

where the $\mathcal{E}_\ell(\vec{r})$ are the mode functions (for example, Equation (7.12) with specific beam parameters) and the c_ℓ are the amplitudes (every mode can have a different amplitude). Naturally, only those modes where significant gain is available can have a nonzero c_ℓ. (The mathematical form of this decomposition must look familiar to you from quantum mechanics.)

Inserting $\nu_\ell = \nu_0 + \ell \cdot \Delta\nu_{\text{FSR}}$ into Equation (8.13), we notice that

$$\begin{aligned}
\mathcal{E}(\vec{r}, t + \Delta\nu_{\text{FSR}}^{-1}) &= \sum_{\ell=0}^{\infty} c_\ell \mathcal{E}_\ell(\vec{r}) e^{2\pi i(\nu_0 + \ell\cdot\Delta\nu_{\text{FSR}})(t + \Delta\nu_{\text{FSR}}^{-1})} \\
&= \sum_{\ell=0}^{\infty} c_\ell \mathcal{E}_\ell(\vec{r}) e^{2\pi i(\nu_0 + \ell\cdot\Delta\nu_{\text{FSR}})t} \cdot e^{2\pi i \nu_0/\Delta\nu_{\text{FSR}}} \cdot e^{2\pi i \ell} \\
&= e^{2\pi i \nu_0/\Delta\nu_{\text{FSR}}} \cdot \mathcal{E}(\vec{r}, t)
\end{aligned} \tag{8.14}$$

since $e^{2\pi i \ell} = 1$ when $\ell \in \mathbb{Z}$. This means that the magnitude of the electric field is periodic, with period $T_{\text{R}} = \Delta\nu_{\text{FSR}}^{-1} = 2L/c$ equal to the resonator round-trip time:

$$\|\vec{\mathcal{E}}(\vec{r}, t + T_{\text{R}})\| = \|\vec{\mathcal{E}}(\vec{r}, t)\| \tag{8.15}$$

Intuitively, the shape of the electric-field intensity bounces back and forth between the two mirrors and repeats periodically; see Figure 8.6.

Let's make a concrete example: assuming constant coefficients over a finite range of ℓ-values,

$$c_\ell = \begin{cases} c & \text{if } \ell_{\text{min}} \leqslant \ell \leqslant \ell_{\text{max}} \\ 0 & \text{otherwise} \end{cases} \tag{8.16}$$

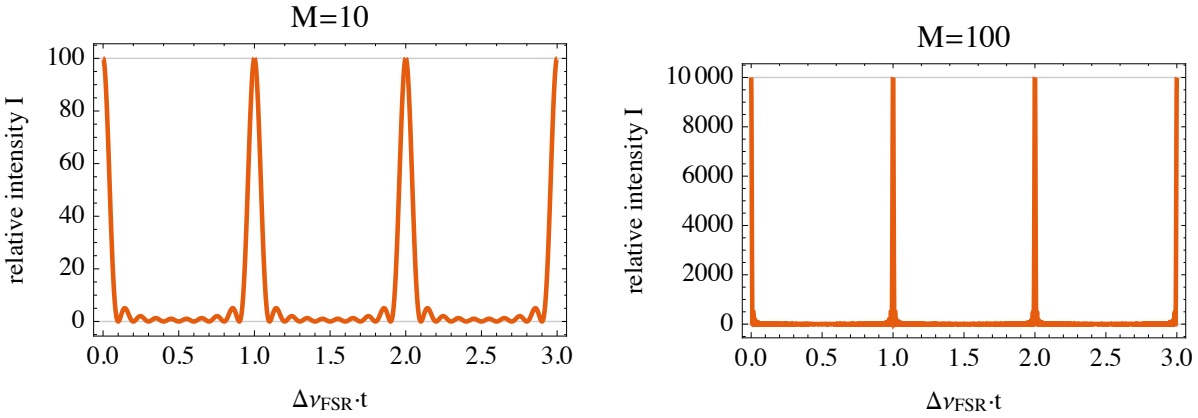

Figure 8.6: Scaled intensity $I(t)$ from Equation (8.18) for $M = 10$ (left) and 100 (right). Sharp pulses separated by the round-trip time $T_R = \Delta\nu_{FSR}^{-1}$ are apparent, with FWHM $\Delta t_{pulse} \approx 0.89 T_R/M$. The peak intensity scales as M^2; the average intensity scales as M.

as well as (for simplicity) equal mode functions $\mathcal{E}_\ell(\vec{r}) \approx \mathcal{E}(\vec{r})$, we find the electric field component from Equation (8.13):

$$\mathcal{E}(\vec{r},t) = c\cdot\mathcal{E}(\vec{r})\cdot\sum_{\ell=\ell_{min}}^{\ell_{max}} e^{2\pi i(\nu_0+\ell\cdot\Delta\nu_{FSR})t} = c\cdot\mathcal{E}(\vec{r})\cdot e^{2\pi i\left(\nu_0+\Delta\nu_{FSR}\cdot\frac{\ell_{min}+\ell_{max}}{2}\right)t}\cdot\frac{\sin(M\cdot\pi\Delta\nu_{FSR}t)}{\sin(\pi\Delta\nu_{FSR}t)} \tag{8.17}$$

where $M = \ell_{max} - \ell_{min} + 1$ is the number of active modes in the sum. Assuming only one polarization, the light-field intensity in the resonator (as well as the laser intensity through the output coupler mirror) is

$$I(t) \propto \|\vec{\mathcal{E}}(t)\|^2 \propto \frac{\sin^2(M\pi\Delta\nu_{FSR}t)}{\sin^2(\pi\Delta\nu_{FSR}t)} \tag{8.18}$$

which represents a series of pulses, separated by the round-trip time T_R, each with a full width at half maximum (FWHM) of $\Delta t_{pulse} \approx 0.89 T_R/M$, see Figure 8.6. The more laser modes are involved and phase-locked in the resonator (larger M), the shorter and more intense the pulses become. The peak intensity is $I_{max} \propto M^2$; but the mean intensity (averaged over one round-trip time) scales only linearly with the number of involved modes $\langle I\rangle \propto M$.

We see that in order to generate very short laser pulses, we need a coherent superposition of many laser modes (large M). A more careful calculation shows that the simple form of Equation (8.16) is not required for short pulses; almost any *coherent* sum of a broad range of modes will generate short pulses. For example, a Gaussian profile

$$c_\ell = c_0\cdot e^{-\frac{(\ell-\ell_c)^2}{2\Delta\ell^2}} \tag{8.19}$$

will also generate short pulses, with approximate Gaussian shape of FWHM $\Delta t_{pulse} \approx 0.27 T_R/\Delta\ell$.

Examples:

1) HeNe at $\lambda = 632\,\text{nm}$, $\Delta\nu_{gain} = 1.5\,\text{GHz}$, $L = 0.5\,\text{m} \Rightarrow \Delta\nu_{FSR} = \frac{c}{2L} = 300\,\text{MHz}$, $M \approx 6$:

$$\Delta t_{pulse} \approx \frac{0.89 T_R}{M} \approx 0.5\,\text{ns} \tag{8.20}$$

2) Ti:Al_2O_3 over a range $\lambda \in [650\,\text{nm}, 950\,\text{nm}]$, $L = 0.5\,\text{m} \Rightarrow \Delta\nu_{FSR} = \frac{c}{2L} = 300\,\text{MHz}$, $\Delta\nu_{gain} = \frac{c}{\lambda_{min}} - \frac{c}{\lambda_{max}} \approx 1.5\times10^{14}\,\text{Hz}$, $M \approx 5\times10^5$:

$$\Delta t_{pulse} \approx \frac{0.89 T_R}{M} \approx 6\,\text{fs} \tag{8.21}$$

8.3.2 The role of coherence

What is the role of coherence in Equation (8.13)? Let's modify the example of Equation (8.16) into an incoherent sum,

$$c_\ell = \begin{cases} c \cdot e^{i\varphi_\ell} & \text{if } \ell_{\min} \leqslant \ell \leqslant \ell_{\max} \\ 0 & \text{otherwise} \end{cases} \tag{8.22}$$

with the complex phases φ_ℓ fluctuating randomly in the sense that over long measurement times, we have $\langle e^{i\varphi_\ell} \rangle = 0$ and $\langle e^{-i\varphi_\ell} \cdot e^{i\varphi_{\ell'}} \rangle = \delta_{\ell,\ell'}$. In this way, the phase relationship between any two modes becomes indeterminate (incoherent).

The resulting intensity is no longer pulsed in the way of Figure 8.6. On average (averaging over many periods), the intensity become time-independent,

$$\begin{aligned} \langle |\mathcal{E}(\vec{r},t)|^2 \rangle &= \left\langle \left[\sum_{\ell=0}^{\infty} c_\ell^* \mathcal{E}_\ell^*(\vec{r}) e^{-2\pi i \nu_\ell t} \right] \left[\sum_{\ell'=0}^{\infty} c_{\ell'} \mathcal{E}_{\ell'}(\vec{r}) e^{2\pi i \nu_{\ell'} t} \right] \right\rangle \\ &= \sum_{\ell,\ell'=0}^{\infty} \langle c_\ell^* c_{\ell'} \rangle \mathcal{E}_\ell^*(\vec{r}) \mathcal{E}_{\ell'}(\vec{r}) e^{2\pi i(\nu_{\ell'} - \nu_\ell)t} = c^2 \sum_{\ell,\ell'=\ell_{\min}}^{\ell_{\max}} \langle e^{-i\varphi_\ell} \cdot e^{i\varphi_{\ell'}} \rangle \mathcal{E}_\ell^*(\vec{r}) \mathcal{E}_{\ell'}(\vec{r}) e^{2\pi i(\nu_{\ell'} - \nu_\ell)t} = c^2 \sum_{\ell=\ell_{\min}}^{\ell_{\max}} |\mathcal{E}_\ell(\vec{r})|^2. \end{aligned} \tag{8.23}$$

We conclude that a well-determined phase relationship between the modes (a "mode lock") is required in order to generate fast pulses.

8.3.3 Experimental realizations

How can such a "mode lock" be achieved? There are several common techniques, all based on mode competition set up such that the lowest loss is achieved if the laser mode has the highest intensity (*i.e.*, the shortest duration). Initial random phase fluctuations will be amplified selectively; eventually, the short pulse will win the mode competition.

Active mode coupling: similar to active Q-switching (subsection 8.2.4). The resonator quality is modulated periodically with a period exactly equal to the cavity round-trip time T_R. A short wavepacket will develop that traverses the Q-switch exactly at the moment of minimum loss; all other resonator-mode combinations experience more loss.

In practice, it is difficult to synchronize the Q-switch exactly with the round-trip time.

Passive mode coupling: similar to passive Q-switching (subsection 8.2.3). A saturable absorber can be used to transmit light only (by bleaching the medium) if it comes with high intensity, *i.e.*, as a mode-coupled pulse. As with active mode coupling, the pulse with highest intensity wins the mode competition. There is no need for active synchronization; however, the absorber must have a switching time (recovery time) much faster than T_R.

Typical absorber materials are dye solutions for mode-coupled dye lasers. An important setup used in the 1980-90s is the "colliding pulse" arrangement, where two ultrashort pulses counterpropagate inside a ring resonator, passing simultaneously through the absorber (a dye jet) from two sides. Disadvantage: difficult to set up.

Passively mode-locked solid-state lasers can be constructed with a SESAM (semiconductor saturable absorber mirror), which is a complex thin-film reflector whose parameters (saturation intensity, recovery time) can be controlled very precisely through the growth of its nanostructured layers.

Kerr lens mode locking (KLM): This dominant technique in use today works by self-focusing in a non-linear optical medium via the Kerr effect (see Figure 8.7). At high light intensities $I \gtrsim 10^{20}\,\mathrm{W/m^2}$, the index of refraction of any medium changes with the intensity as $n(I) = n_0 + n_2 I$, and a light beam with inhomogeneous transverse intensity profile such as a Gaussian beam transforms the medium into a "gradient-index lens," thus self-focusing the beam. When adding an aperture to the arrangement, higher intensities I (mode-locked operation) will be favored and *cw* operation will be suppressed.

The advantage of the Kerr effect over passive mode-locking (above) is that the switching/recovery time of a Kerr lens is very small (electronic response time of the crystal).

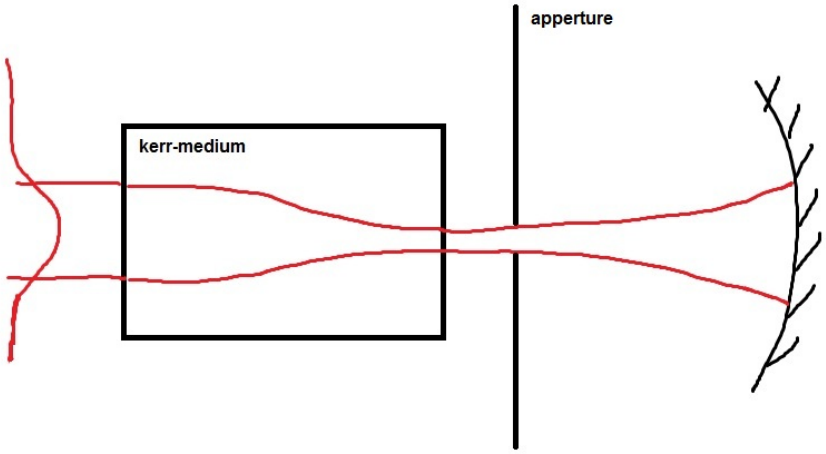

Figure 8.7: An experimental realization of a passive mode coupling mechanism: inserting a Kerr medium into the resonator in combination with an aperture. Only a high-intensity pulse experiences low loss. In the case of a Ti:Al_2O_3 laser the active medium itself shows a sufficient Kerr nonlinearity that can be used for mode coupling (mode locking).

8.4 Short-pulse amplification: CPA

For many experiments, we want to generate laser pulses that are so intense their electric field reaches the atomic field scale

$$E_{\text{atom}} = \frac{e}{4\pi\epsilon_0 a_0^2} \approx 5 \times 10^{11}\,\text{V/m}. \tag{8.24}$$

As an example, a laser pulse of duration $\Delta t_{\text{pulse}} \sim 10\,\text{fs}$ with pulse energy $W_{\text{pulse}} \sim 1\,\text{mJ}$ and a focal waist radius of $w_0 \sim 10\,\mu\text{m}$ has an intensity of $I_{\text{pulse}} = W_{\text{pulse}}/(\pi w_0^2 \cdot \Delta t_{\text{pulse}}) \sim 3 \times 10^{20}\,\text{W/m}^2$, corresponding to a peak electric field strength of $E = \sqrt{2 \cdot I_{\text{pulse}} \cdot Z_0} \sim 5 \times 10^{11}\,\text{V/m}$, with $Z_0 = \sqrt{\mu_0/\epsilon_0} = 377\,\Omega$ the impedance of free space (remember that $I_{\text{rms}} = \frac{U_{\text{peak}}^2}{2Z}$ for an oscillating field).

When we generate such intense laser pulses, hitting any surface is thus very likely to cause ionization, material degradation, and strong non-linear effects. The problem with generating such pulses is therefore that their high intensity damages the laser itself.

The solution is to generate short pulses with low intensity in an "oscillator" (see section 8.3) and amplifying them after the resonator, making sure that the amplified pulses never touch a solid surface (mirror, gain crystal, etc.). This is done by first stretching the weak pulse in time, so that it becomes many orders of magnitude longer and thus less intense; then amplifying the stretched pulse; and finally re-compressing the amplified pulse into a short intense pulse.

In such a *Chirped Pulse Amplifier* (CPA) the stretching and compressing is done by making the path-length wavelength-dependent without making the beam path wavelength-dependent, using a clever combination of lenses and gratings (see Figure 8.8). In the stretched pulse, the different colors composing the pulse arrive at different times (the pulse is "chirped") but still maintain a fixed phase relationship (as in, *e.g.*, Equation (8.16)).

Typical example of what can be achieved with a CPA: $t_{\text{pulse}} \sim 100\,\text{fs}$, $W_{\text{pulse}} \sim 10\,\text{mJ}$, repetition rate $f \sim 1\,\text{kHz}$ (meaning that not every pulse from the oscillator is amplified, but only one every millisecond) $\Rightarrow$ average power $\langle P \rangle = W_{\text{pulse}} \cdot f = 10\,\text{W}$, peak power $\hat{P} = W_{\text{pulse}}/t_{\text{pulse}} = 100\,\text{GW}$, which is approximately the output power of 100 nuclear power plants (but only for 100 fs).

8.4.1 Pulse stretching with a frequency-dependent phase shift

To show the effect of pulse stretching quantitatively, we look at a Gaussian laser pulse of central frequency ω_0 around time $t = 0$ with time-dependent electric field

$$\mathcal{E}(t) = \mathcal{E}_0 \cdot e^{-i\omega_0 t} \cdot e^{-\left(\frac{t}{2\tau}\right)^2} \tag{8.25}$$

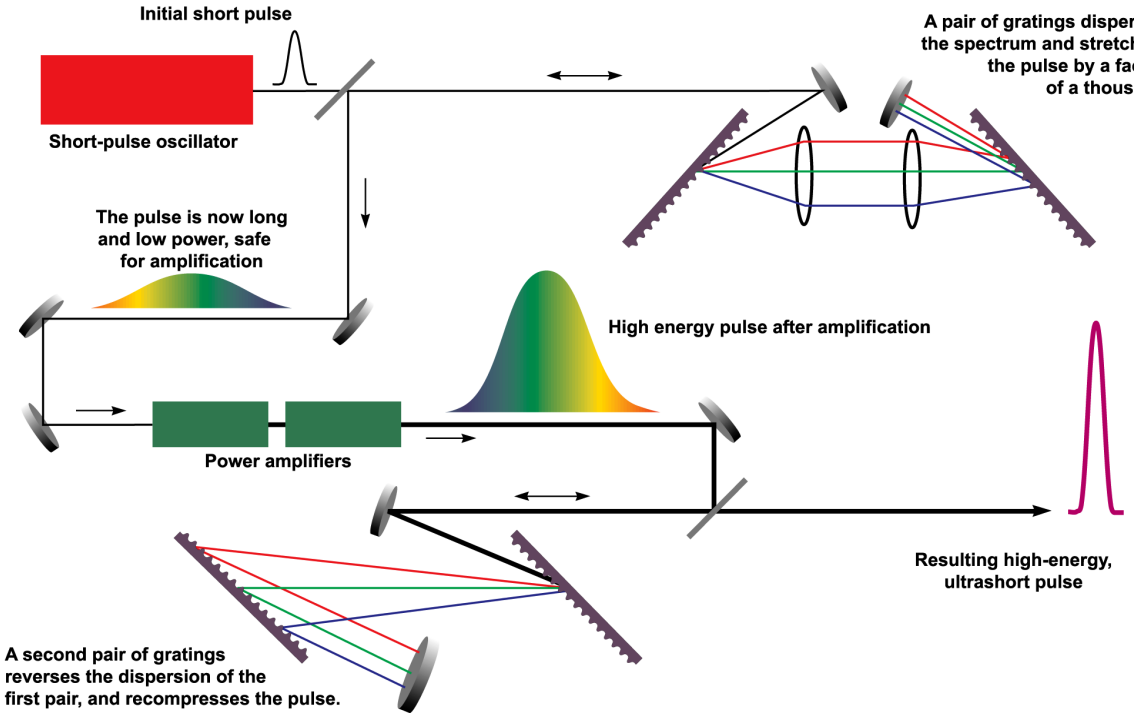

Figure 8.8: Schematic of a chirped pulse amplifier. Each combination of two lenses and two gratings introduces a wavelength-dependent path length without displacing the beam. In the stretched pulse, the different colors composing the beam arrive at different times. Source: https://en.wikipedia.org/wiki/Chirped_pulse_amplification.

This pulse has a time-dependent intensity $I(t) \propto |\mathcal{E}(t)|^2 \propto e^{-\frac{t^2}{2\tau^2}}$ and thus a temporal FWHM of $\Delta t = \tau \cdot 2\sqrt{2\ln(2)} \approx 2.35\tau$. The Fourier transform of this electric field is

$$\tilde{\mathcal{E}}(\omega) = \frac{1}{\sqrt{2\pi}} \int_{-\infty}^{\infty} \mathcal{E}(t) \cdot e^{i\omega t} dt = \mathcal{E}_0 \cdot \tau\sqrt{2} e^{-(\omega-\omega_0)^2\tau^2} \tag{8.26}$$

with a frequency-dependent intensity $\tilde{I}(\omega) \propto |\tilde{\mathcal{E}}(\omega)|^2 \propto e^{-2(\omega-\omega_0)^2\tau^2}$ and thus a frequency FWHM of $\Delta\omega = \sqrt{2\ln(2)}/\tau \approx 1.18/\tau$. Notice that $\Delta\omega \cdot \Delta t = 4\ln(2)$ saturates the Heisenberg uncertainty relation.

Now we introduce a frequency-dependent phase factor $e^{i\varphi(\omega)}$ in Equation (8.26), generated for example with the chromatic elements of Figure 8.8. By series-expanding $\varphi(\omega) \approx \varphi(\omega_0) + (\omega-\omega_0)\varphi'(\omega_0) + \frac{1}{2}(\omega-\omega_0)^2\varphi''(\omega_0)$ to second order around the central pulse frequency ω_0 and assuming that $\Delta\omega$ is sufficiently small, the frequency-dependent electric field of Equation (8.26) becomes

$$\tilde{\mathcal{E}}'(\omega) = e^{i[\varphi(\omega_0)+(\omega-\omega_0)\varphi'(\omega_0)+\frac{1}{2}(\omega-\omega_0)^2\varphi''(\omega_0)]} \cdot \mathcal{E}_0 \cdot \tau\sqrt{2} e^{-(\omega-\omega_0)^2\tau^2} \tag{8.27}$$

and the corresponding real-time pulse is

$$\begin{aligned} \mathcal{E}'(t) &= \frac{1}{\sqrt{2\pi}} \int_{-\infty}^{\infty} \tilde{\mathcal{E}}'(\omega) \cdot e^{-i\omega t} dt \\ &= \mathcal{E}_0 \cdot \frac{\tau}{\sqrt{\tau^2 - \frac{i}{2}\varphi_2}} \cdot e^{-\frac{t^2 + (2\omega_0\varphi_2 - 2\varphi_1 + 4i\omega_0\tau^2)t + \varphi_1^2 - 2\varphi_0\varphi_2 - 4i\varphi_0\tau^2}{4\tau^2 - 2i\varphi_2}} \end{aligned} \tag{8.28}$$

where we have abbreviated $\varphi_0 = \varphi(\omega_0)$, $\varphi_1 = \varphi'(\omega_0)$, $\varphi_2 = \varphi''(\omega_0)$. The intensity profile of this pulse is

$$I'(t) \propto |\mathcal{E}'(t)|^2 = \frac{|\mathcal{E}_0|^2}{\sqrt{1 + \left(\frac{\varphi_2}{2\tau^2}\right)^2}} \cdot e^{-\frac{(t-\varphi_1)^2}{2\tau^2 + \frac{\varphi_2^2}{2\tau^2}}} \tag{8.29}$$

which is still Gaussian but centered at φ_1 (instead of zero) and with a FWHM of

$$\Delta t' = \tau \cdot 2\sqrt{2\ln(2)} \cdot \sqrt{1 + \left(\frac{\varphi_2}{2\tau^2}\right)^2} = \Delta t \cdot \sqrt{1 + \left(\frac{4\ln(2) \cdot \varphi_2}{\Delta t^2}\right)^2} \tag{8.30}$$

We conclude that the series coefficients of the phase factor $\varphi(\omega)$ have the following effects:

- $\varphi_0 = \varphi(\omega_0)$ is a global phase factor and has no effect on the pulse profile.
- $\varphi_1 = \varphi'(\omega_0)$ shifts the Gaussian pulse in time.
- $\varphi_2 = \varphi''(\omega_0)$ increases the pulse duration according to Equation (8.30).
- Higher-order terms in the series-expansion of $\varphi(\omega)$ around ω_0 have effects that distort the pulse shape away from a Gaussian ("non-linear chirp").

8.5 Generation of ultrashort pulses

The fundamental limit for the pulse length is the *Fourier limit* (analogous to the Heisenberg uncertainty relation; see subsection 8.4.1)

$$\Delta\nu \cdot \Delta t \geqslant \frac{4\ln(2)}{\pi} \approx 0.88 \tag{8.31}$$

expressed here in terms of the full widths at half-maximum. For example for a Ti:Al_2O_3 laser with $\lambda = 650 - 950\,\text{nm} \rightarrow \Delta\nu = 1.5 \times 10^{14}\,\text{Hz} \Rightarrow \Delta t \sim \frac{1}{\Delta\nu} \sim 7\,\text{fs}$.

The main technical problem for reaching this limit is the control of the *group velocity dispersion* (GVD, chromatic dispersion) of optical elements. When the index of refraction $n(\nu)$ is frequency-dependent, the resonator round-trip time becomes frequency-dependent since the propagation time through an element of length L is

$$t(\nu) = L \cdot \frac{n(\nu)}{c}. \tag{8.32}$$

Inside the resonator the light pulses pass through the optical elements (*e.g.*, the active medium itself) many times, and even small dispersion effects add up to significant distortions. Therefore, GVD has to be compensated using elements with opposite dispersion (prisms, gratings, *chirped mirrors*).

8.5.1 Group velocity dispersion (GVD)

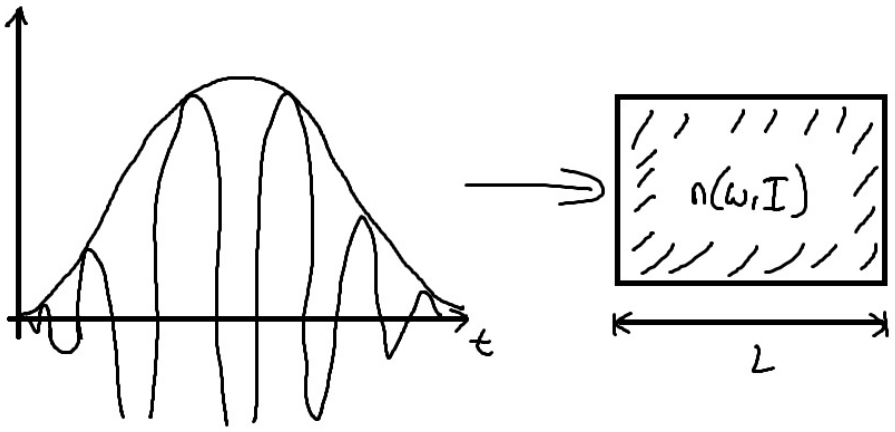

Figure 8.9: A pulse entering a medium with refractive index $n(\omega, I)$

Consider a pulse as shown in Figure 8.9, passing through a medium of length L and with a dispersion relation $k(\omega)$. As a result, light of frequency ω will experience a phase factor of $e^{ik(\omega)\cdot L}$ during the

passage through this medium, corresponding to the situation of subsection 8.4.1 with $\varphi(\omega) = k(\omega) \cdot L$. Series-expansion of $\varphi(\omega)$ to second order:

$$\varphi(\omega) = k(\omega) \cdot L \approx \underbrace{k(\omega_0) \cdot L}_{\varphi_0} + (\omega - \omega_0) \cdot \underbrace{k'(\omega_0) \cdot L}_{\varphi_1} + \frac{1}{2}(\omega - \omega_0)^2 \cdot \underbrace{k''(\omega_0) \cdot L}_{\varphi_2}. \tag{8.33}$$

We conclude that a fast laser pulse will be stretched/compressed if $\varphi_2 = k''(\omega_0) \cdot L \neq 0$, that is, if the second derivative $k''(\omega_0)$ is nonzero. The quantity $\varphi_2 = k''(\omega_0) \cdot L$ is called the *group delay dispersion* (GDD) of an optical element, usually given in units of fs^2.

The *group velocity* is defined in the usual way as

$$v_g(\omega) = \frac{1}{k'(\omega)} \approx \frac{1}{k'(\omega_0)} - (\omega - \omega_0) \cdot \frac{k''(\omega_0)}{[k'(\omega_0)]^2}. \tag{8.34}$$

We see that when $k''(\omega_0) \neq 0$ the group velocity is frequency-dependent: *group velocity dispersion* (GVD).

A simple formula for the quantification of the GVD is

$$k''(\omega) = \frac{\mathrm{d}}{\mathrm{d}\omega} k'(\omega) = \frac{\mathrm{d}}{\mathrm{d}\omega} \frac{1}{v_g(\omega)}. \tag{8.35}$$

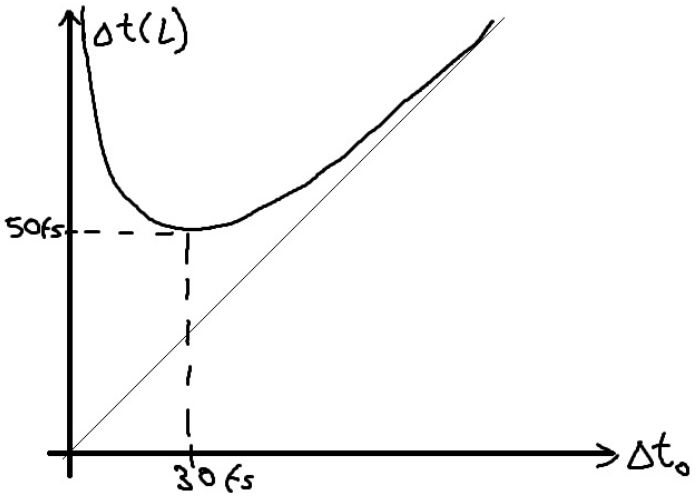

Figure 8.10: Temporal broadening of an ultrashort laser pulse due to group-velocity dispersion of the optical medium as a function of the pulse length of the initial pulse. The absolute values of input pulse length (horizontal axis) and output pulse length (vertical axis) are given for a quartz plate of length $L = 1\,\mathrm{cm}$. See Equation (8.30).

Example

Quarz plate, $L = 1\,\mathrm{cm}$, $\frac{\mathrm{d}^2 n}{\mathrm{d}\lambda^2}(800\,\mathrm{nm}) = 0.04\,\mu\mathrm{m}^{-2}$

$$k'' = \frac{\mathrm{d}^2 k}{\mathrm{d}\omega^2} = \frac{\mathrm{d}^2}{\mathrm{d}\omega^2} \frac{\omega \cdot n(\frac{2\pi c}{\omega})}{c} = \frac{\lambda^3 n''(\lambda)}{2\pi c^2} = 3.6 \times 10^{-26}\,\mathrm{s}^2/\mathrm{m}$$
$$k'' \cdot L = 360\,\mathrm{fs}^2 \tag{8.36}$$

A typical setup for a dispersion compensation is shown in Figure 8.11

8.5.2 Self phase modulation (SPM)

At high intensities, the Kerr effect makes the index of refraction depend not only on the frequency, but also on the intensity I:

$$\boxed{n(\omega, I) = n_0(\omega) + n_2(\omega) \cdot I(t)} \tag{8.37}$$

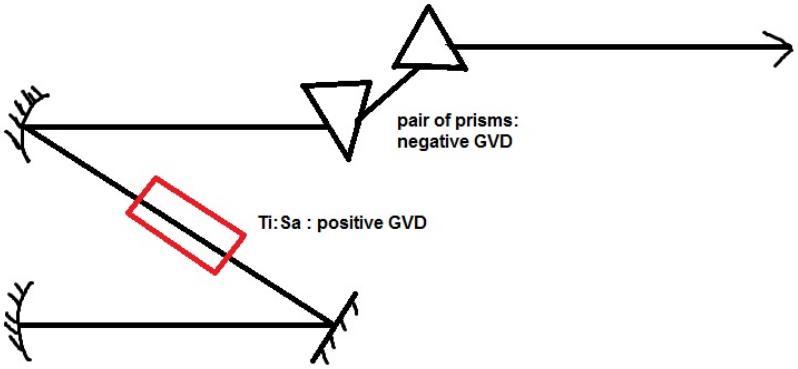

Figure 8.11: Example for a compensation of GVD. The combination of all optical elements gives a total of $\varphi_2 \approx 0$.

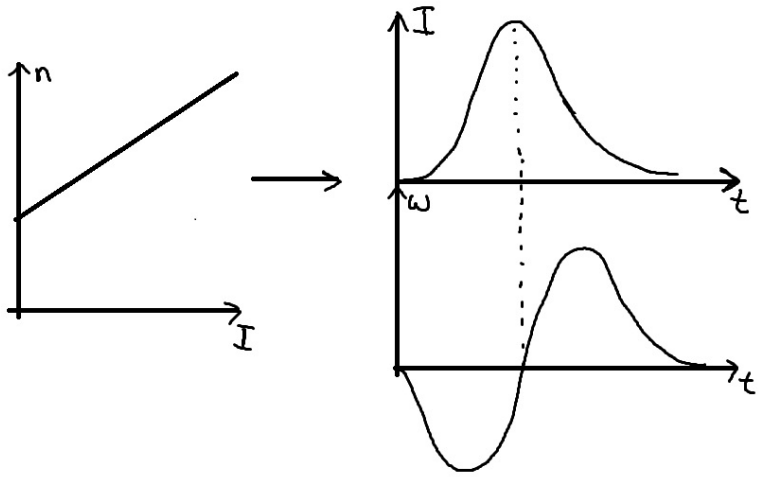

Figure 8.12: Right panel: temporal behaviour of the frequency ω in a pulse that has a Gaussian intensity distribution. Assuming $n_2 > 0$ (left panel).

Usually, the ω-dependence of n_2 can be neglected.

As a result, the phase of the electric field of a short laser pulse depends on the intensity $I(t)$:

$$\varphi = kz - \omega_0 t = \frac{\omega_0}{c} n \cdot z - \omega_0 t = \omega_0 \left(\frac{n_0(\omega_0)}{c} \cdot z - t \right) + n_2 \frac{\omega_0}{c} \cdot z \cdot I(t) \tag{8.38}$$

Assuming $n_2 > 0$ (usually correct): since $\omega = -\frac{\partial \varphi}{\partial t} = \omega_0 - n_2 \frac{\omega_0}{c} z \frac{\partial I}{\partial t}$, at the rising edge of the pulse ($\frac{\partial I}{\partial t} > 0$) the frequency ω is reduced ("red-shifted"), while at the falling edge ($\frac{\partial I}{\partial t} < 0$) the frequency is increased ("blue-shifted"). This effect gives rise to spectral broadening and a chirped pulse (see Figure 8.12):

Spectral broadening: As the output pulse has a broader spectrum than the input pulse (as opposed to GVD, which does not influence the spectral width), while still being fully phase-coherent between the different spectral components and having a similar temporal profile, SPM can be used to access broader wavelength ranges without sacrificing pulse quality. Shortening a laser pulse can be done in this way.

Pulse chirping: The chirp of an SPM pulse can be compensated with GVD elements (subsection 8.5.1) and must be taken into account when designing a GVD-free resonator.

Typical setups:

Intra-cavity: In addition to the setup shown in Figure 8.11 a glass plate (for example) is placed in the cavity for SPM. This broadens the spectrum of the light within the cavity, giving rise to shorter laser pulses when properly corrected with GVD elements.

Extra-cavity: Elements with a strong Kerr nonlinearity can be used to convert narrow-band pulses into very wide-band pulses spanning more than an octave of frequencies ($\rightarrow$ optical frequency comb). In order to achieve strong nonlinear interaction with the medium, the medium has to be very long, for example a specially crafted optical fiber. The negative dispersion after the fiber for pulse compression is obtained by a pair of gratings $\Rightarrow \Delta t_{\text{pulse}} \lesssim 10\,\text{fs}$; "single-pulse" lasers where the electric field only performs one full oscillation.

Nonlinear Optics

Frank Kuehnemann

July 20, 2017

Abstract

General information
References:
Boyd: Nonlinear Optics - A textbook for (at least) a one-semester course. We use it here so you can go further, if you want.
Saleh/Teich: Fundamentals of Photonics. Chapter 21: Nonlinear Optics (N. Bloembergen)

Chapter 9

Nonlinear Optical Susceptibility

9.1 Polarization

Fundamental processes for light interaction with matter:
1) Absorption of radiation (if incident wave excites a resonance/transition in the medium)
2) Polarization of the medium.
In both cases, the interaction can involve electrons or the core ions.
In *linear* interaction, the response of the medium is proportional to the light intensity. If the light field is strong enough (i.e., comparable to the internal fields), the response of the medium show a nonlinear dependnece on the incident light field. Induced dipole moments in the material $\rightarrow$ dipole moment per unit volume, i.e. polarization $P(t)$. In the linear case

$$\tilde{P}(t) = \epsilon_o \chi^{(1)} \tilde{E}(t). \tag{9.1}$$

with ϵ_o the permittivity of free space and $\chi^{(1)}$ the susceptibility of the material. The $\tilde{}$ over any variable indicates a rapidly changing quantity as it is the case for the high-freuqnecy light fields.

In the nonlinear case, the dependence of the polarization on the (light) electric field is expressed as a power series in $\tilde{E}(t)$

$$\tilde{P}(t) = \epsilon_o(\chi^{(1)}\tilde{E}(t) + \chi^{(2)}\tilde{E}^2(t) + \chi^{(3)}\tilde{E}^3(t) + ...). \tag{9.2}$$

In general, $\tilde{P}(t)$ and $\tilde{E}(t)$ will be vectors, $\chi^{(1)}$a second-rank tensor, $\chi^{(2)}$ a third-rank tensor and so on. For the time being, the derivations will be limited to the scalar case. In addition, $\tilde{P}(t)$ is assumed to depend only on the instantaneous field strength, i.e. the material is considered to be loss-less and dispersion-less (and χ will be considered a frequency-independent constant). The latter two assumptions will be dropped at a later stage.

Equation 9.2 can be rewritten as the sum of linear, second-order and third-order polarizations

$$\tilde{P}(t) = \tilde{P}_1(t) + \tilde{P}_2(t) + \tilde{P}_3(t) + ... \tag{9.3}$$

We will see later, that there is a fundamental difference between second-order $\chi^{(2)}$ and third-order $\chi^{(3)}$ nonlinearities.

The polarization approach used here is of value for two reasons: (I) at frequencies well below all resonances in the medium, the polarization properly describes the response of the medium to the applied (light) field. (II) A time-varying polarization is connected with moving/accelerated charges which will serve as sources for new components of the field (i.e., frequency conversion processes).

9.2 Symmetry consideration for the nonlinear effects

The third-order term $\chi^{(3)}$ can be considered as an "ubiquitous" term present in all materials, only the magnitude depending on the considered material and the frequencies. In order for the second-order term $\chi^{(2)}$ to be diffeernt from zero, the crystal must possess a non-centro-symmetric structure. That measn, that anlong at least direction in the crystal, the crystal must look "different" upon inversing that axis. As a consequence, the potential (e.g. for the electronic polarization) will be asymmetric along that direction.

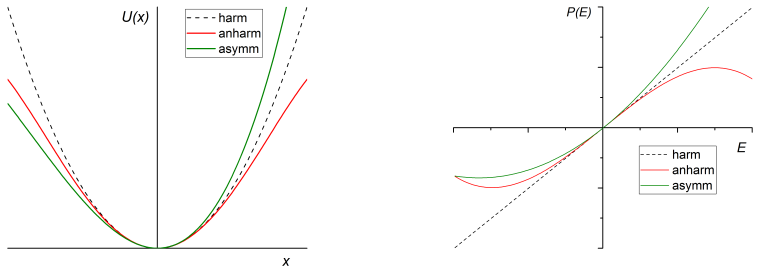

(a) Potential (b) Polarization

Figure 9.1: Types of potentials and resulting polarizations

Figure 9.1(a) showsas comparison a simple harmonic potential (harm - which is necessarily symmetric with respect to inversion), an anharmonic, but symmetric potential (anharm) and an asymmetric potential. If charges are moved in these potentials, this gives rise to the induced polarizations as a function of the incident electric field as plotted in fig. 9.1(b).

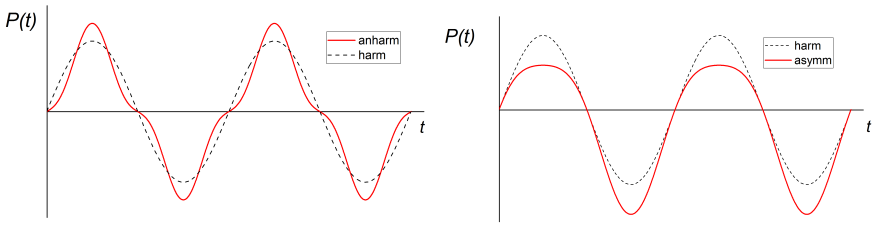

(a) Symmetric nonlinear polarization (b) Asymmetric nonlinear polarization

Figure 9.2: Time dependence of the polarization

If now a simple sinusoidal wave is driving the polarization, this will lead to a time dependence of the polarization as sketched schematically in fig. 9.2 (a) and (b) for the symmetric and asymmetric case, respectively.

How ist this related to crystal symmetry? Let's assume a crystal possessing a centro-symmetric structure and consider the most simple case of second-order polarization and an excitation by a sinusoidal wave, i.e.

$$\tilde{P}^{(2)}(t) = \epsilon_0 \chi^{(2)} \tilde{E}^2(t) \text{ with....} \tilde{E}(t) = cos(\omega \cdot t). \tag{9.4}$$

Changing the sign of E is now simply equivalent to inverting the respective direction in the crystal. Because of the symmetric potential, this should result in a chnage of sign of P (see figure 9.1(b)). Using the above equations, one finds for the second-order polarization

$$-\tilde{P}(t) = \epsilon_0 \chi^{(2)} \left[-\tilde{E}(t)\right]^2 = \epsilon_0 \chi^{(2)} \tilde{E}(t)^2 \tag{9.5}$$

Comparison with eq. 9.4 yields $\tilde{P}(t) = -\tilde{P}(t) = 0$ and hence $\chi^2 = 0$ for any centrosymmetric crystal.

9.3 Description of nonlinear optical processes

At this stage, a basic overview of different processes is given. Some of them will be discussed later in more detail. In the following, we will consider the nonlinear optical materials exposed to plane monochromatic waves propagating in z direction which are described as

$$\tilde{E}(t) = E(z) \cdot e^{-i\omega t} + c.c. \text{ with } E(z) = \frac{1}{2} A e^{ikz} \tag{9.6}$$

9.3.1 Second harmonic generation

For the second-order nonlinearity on gets

$$\begin{aligned}\tilde{P}^{(2)}(t) = \epsilon_0\chi^{(2)}\tilde{E}^2(t) = \epsilon_0\chi^{(2)}(E(z)\cdot e^{-i\omega t} + E^*(z)\cdot e^{i\omega t})^2 \\ = 2\epsilon_0\chi^{(2)}EE^* + (\epsilon_0\chi^{(2)}E^2e^{-2i\cdot\omega\cdot t} + c.c.)\end{aligned} \tag{9.7}$$

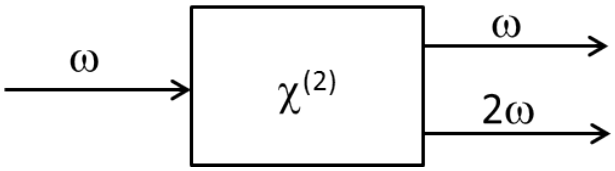

Figure 9.3: Basic scheme of second-harmonic generation

As a results, one has a polarization at twice the initial frequency and a term with zero time dependence, i.e. a constant electric field across the material. The polarization at the doubled frequency will give rise to the second-harmonic generation (SHG) from the medium. The most prominent exmaple for such a source is the green laser pointer. Here, the radiation of a Nd:YAG laser at 1064 nm is frequency-doubled to yield green light at 532 nm. In a photon-framework, it can be understood as the annihilation of two 1064-nm photons and the creation of a 532-nm photon.

9.3.2 Sum and difference frequency generation

Now let's assume that wto waves with frequencies ω_1 and ω_2 are acting on the medium, i.e.

$$\tilde{E}(t) = E_1(z)\cdot e^{-i\omega_1 t} + E_2(z)\cdot e^{-i\omega_2 t} + c.c. \tag{9.8}$$

Considering again the second-order nonlinear polarization $\tilde{P}^{(2)}(t) = \epsilon_0\chi^{(2)}\tilde{E}^2(t)$ one gets

$$\begin{aligned}\tilde{P}^{(2)}(t) = \epsilon_0\chi^{(2)}[E_1^2\cdot e^{-i\cdot 2\omega_1 t} + E_2^2\cdot e^{-i\cdot 2\omega_2 t} + 2E_1E_2e^{-i(\omega_1+\omega_2)t} + \\ 2E_1E_2^*e^{-i(\omega_1-\omega_2)t} + c.c.] + 2\epsilon_0\chi^{(2)}[E_1E_1^* + E_2E_2^*]\end{aligned} \tag{9.9}$$

As a result, one has in total four different conversion processes (sum and difference frequency generation and the SHG of waves one and two). It shall already be mentioned here, that in real situations one of the four processes will dominate, controlled by the phase-matching condition which is relevant for all materials due to dispersion.

Sum frequency generation (SFG) is pretty similar to SHG, except that two photons at different frequencies are annihilated to generate the SFG photon.

In difference frequency generation (DFG) with the input of ω_3 ands ω_2 one takes a photon at the highest frequency (denoted ω_3) to generate one photon at frequency ω_1 As we will see later in more detail, energy conservation requires

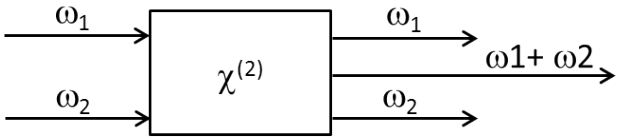

Figure 9.4: Basic scheme of sum-frequency generation

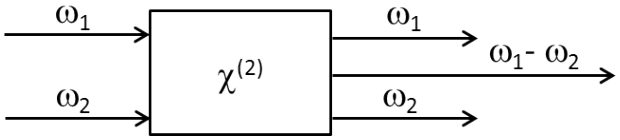

Figure 9.5: Basic scheme of difference-frequency generation

that this is connected with the generation of a photon ω_2 , i.e. DFG also results in an amplification of ω_2.

The latter process is called "optical parametric amplification" (OPA). "Parametric" indicates, that the amplification process is not associated with any net deposition of energy in the material. Only virtual levels are involved. Before and after the process, the medium is in the same state. This is in contrast to the amplification of a light wave in a LASER ("Light *amplification* by stimulated emission of radiation") where energy is deposited in the medium after the absorption-emission process.

9.3.3 Optical parametric oscillation

If only wave ω_3 is provided, one may still observe the emission of photons with ω_2 and ω_1, albeit with extremely low probability. Without any "seed" wave ω_2, the choice of frequencies seems arbitrary, as long as energy conservation is observed. It will be shown later, that the actual frequencies of the two photons will be determined by the phase-matching conditions. The process is called optical parametric generation (OPG) or spontaneous parametric down conversion (SPDC). Despite the low photon yield, it is an essential concept for the generation of "entangled" photons for quantum communication, quantum cryptography, and the like. In the Laser, amplification can be turned into an self-sustaining oscillation (what we know as the actual "laser") by providing feedback through mirrors. Something similar is possible here: Using feedback via mirrors, OPA can be turned into optical parametric oscillation (OPO). This can start, as in the laser, without providing any external "seed" photons of frequency ω_2.

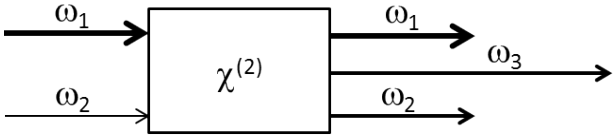

Figure 9.6: difference-frequency generation as optical parametric amplification

9.3.4 Third-order nonlinearities

Let's start again with the general expression

$$\tilde{P}^{(3)}(t) = \epsilon_0 \chi^{(3)} \tilde{E}^3(t) \tag{9.10}$$

In analogy to the second-order case one can deduce, that with three incident waves with different frequencies $E_1(\omega_1)$, $E_2(\omega_2)$ and $E_3(\omega_3)$ one may observe waves containing frequencies ω_1, ω_2, ω_3, third harmonics $3\omega_1$, $3\omega_2$, $3\omega_3$ as well as various linear (sum- and difference) combinations of the three frequencies.

For the sake of simplicity we will consider in more detail only the case of a single incident wave with frequency ω. Inserting the wave function 9.6 into equation 9.10, one gets, in addition to the generation of the wave at 3ω, a nonlinear contribution at the fundamental frequency

$$P^{(3)}(\omega) = 3 \cdot \epsilon_0 \cdot \chi^{(3)}(\omega) \left|E(\omega)\right|^2 \cdot E(\omega) \tag{9.11}$$

The nonlinear refractive index

The resulting total (linear plus nonlinear) polarization at frequency ω is hence given as

$$\begin{aligned} P^{tot}(\omega) = \epsilon_0 \cdot \chi^{(1)} \cdot E(\omega) + 3 \cdot \epsilon_0 \cdot \chi^{(3)}(\omega) \left|E(\omega)\right|^2 \cdot E(\omega) \\ = \epsilon_0 \cdot \chi^{eff} \cdot E(\omega) \end{aligned} \tag{9.12}$$

with

$$\chi^{eff} = \chi^{(1)} + 3\chi^{(3)}(\omega) \left|E(\omega)\right|^2 \tag{9.13}$$

The susceptibility χ is related to the order quantities describing the material properties. In general, one would find $(n + i \cot \kappa)^2 = 1 + \chi$. Since we assumed the loss-less case (i.e. the imaginary part κ of the complex refractive index to be zero), one gets

$$n^2 = 1 + \chi = \frac{\epsilon}{\epsilon_0}. \tag{9.14}$$

The nonlinear refractive index n_2 is introduced through

$$n_{\text{tot}} = n_0 + n_2 \cdot I \tag{9.15}$$

with the linear (low-intensity) refractive index n_0 and the time-averaged field intensity I of the optical field. in a medium with (linear) refractive index n_0 it is related to the electric field of the light wave through

$$I = 2n_0\epsilon_0 c\,|E(\omega)|^2 \tag{9.16}$$

Inserting eq.(9.16) into eq. (9.15), squaring it and comparing it with eq.(9.14) yields

$$[n_0 + n_2 \cdot I]^2 = 1 + \chi^{(1)} + 3\chi^{(3)}(\omega)\frac{1}{2n_0\epsilon_0 \cdot c} \cdot I \tag{9.17}$$

When comparing both sides of the equation, only the terms linear in I are kept, since the nonlinear contribution to n is considered to be a small one. Hence one gets

$$n_0^2 + 2n_0 n_2 I = (1 + \chi^{(1)}) + 3\chi^{(3)}(\omega)\frac{1}{2n_0\epsilon_0 \cdot c} \cdot I \tag{9.18}$$

and with $n_0^2 = (1 + \chi^{(1)})$ one gets

$$2n_0 n_2 I = 3\chi^{(3)}(\omega)\frac{1}{2n_0\epsilon_0 \cdot c} \cdot I \tag{9.19}$$

or finally

$$n_2 = \frac{3}{4}\frac{1}{n_0^2\epsilon_0 \cdot c}\chi^{(3)}(\omega) \tag{9.20}$$

For electronic excitation, the nonlinear refractive index n_2 is at the order of 10^{-16} to 10^{-14} $\frac{cm^2}{W}$. As a result, it requires laser field intensities well above $1\frac{GW}{cm^2}$ to cause noticeable chnages in the refactive index. Such (and higher) intensities are achieved, first of all, with pulsed lasers.